Hochschule für Angewandte Wissenschaften Hamburg
Department Maschinenbau und Produktion

Analysis of Parameters for the Acceleration of Unsteady Simulations with the DLR-Tau Code

Thesis Project for the Degree of Master of Engineering
in Computation and Simulation of Mechanical Systems
in collaboration with the German Aerospace Center (DLR)

Carlos Omar Márquez Gutiérrez
Mat.Nr. 1876040

Tutors:
Prof. Dr.-Ing. Peter Wulf
Dipl.-Ing. Arne Stürmer

July 2008

Abstract

In this CFD study, the variation of the parameters of the dual time-stepping method implemented in the DLR-Tau Code for the computation of unsteady simulations are investigated. Two dimensional and three dimensional cases were calculated to find the best combination of parameters for the acceleration of the simulations in terms of calculation time. With the 2-D Cases (Pitching oscillation of a NACA 0012 airfoil and laminar flow over a circular cylinder), it could be proven, that by using a variation of the time steps from a *quick* parameter setting to an *accurate* setup, a reduction of almost 50% in the calculation time is achievable without observing a major impact on the accuracy of the relevant force coefficients versus the use of a constant time step with a considerable number of inner iterations. Furthermore, advantages of the initialization of the flow through a steady-state simulation can be observed especially for the circular cylinder case. The experiences gained from the 2-D cases were applied to the 3-D cases (Pitching oscillation of a transport aircraft configuration DLR-F12 and a rotating installed AGARD propeller). The results obtained for the 3-D Cases are in agreement with those of the 2-D Cases, as a reduction of the calculation time by almost 50% could be achieved. Analogous to the cylinder case, the installed propeller case shows the advantages of the initialization of the flow with a steady-state simulation, which leads to a notable acceleration of the convergence.

Contents

List of Figures

List of Tables

List of Abbreviations

AGARD	Advisory Group for Aerospace Research and Development
AIAA	American Institute of Aeronautics and Astronautics
AMD	Advanced Micro Devices
AUSM	Advection Upstream Splitting Method
CAD	Computer Aided Design
CFD	Computational Fluid Dynamics
CFL	Courant Friedrichs Lewy number
CV	Control Volume
DES	Detached Eddy Simulation
EARSM	Explicit Algebraic Reynolds Stress Model
FDM	Finite Difference Method
FEM	Finite Element Method
FLOPS	Floating point Operations Per Second
FVM	Finite Volume Method
GARTEUR	Group for Aeronautical Research and Technology in Europe
GCL	Geometric Conservation Law
HPC	High Performance Computing
HTP	Horizontal Tail Plane
IGES	Initial Graphics Exchange Specification
LES	Large Eddy Simulation
MPI	Message Passing Interface
NACA	National Advisory Committee for Aeronautics
NATO	North Atlantic Treaty Organization
NS	Navier-Stokes
uRANS	unsteady Reynolds-Averaged Navier-Stokes equations
VTP	Vertical Tail Plane
WTT	Wind Tunnel Test

List of Symbols

Arabic symbols:

A	reference area, [m]
b	wingspan [m]
c	reference chord length, [m]
C_D	aerodynamic drag coefficient = $D/(q_\infty \cdot A)$, [-]
C_L, C_N	aerodynamic lift coefficient = $L/(q_\infty \cdot A)$, [-]
C_m	aerodynamic moment coefficient = $M/(q_\infty \cdot A \cdot c)$, [-]
c_P	pressure coefficient = $(p - p_\infty)/q_\infty$, [-]
c_p	specific heat capacity at constant pressure, [J/(molK)]
c_v	specific heat capacity at constant volume, [J/(molK)]
C_T	propeller thrust coefficient = $T/(\rho \cdot n^2 \cdot d^4)$, [-]
C_y	propeller lateral force coefficient = $F_y/(\rho \cdot n^2 \cdot d^4)$, [-]
C_z	propeller lift coefficient = $L/(\rho \cdot n^2 \cdot d^4)$, [-]
d	diameter, [m]
D	drag force, [N]
e	internal energy, [J]
E_t	total energy inside the control volume, [J]
f	oscillation frequency, [Hz]
J	advance ratio = $U_\infty/(n \cdot d)$, [-]
k	reduced frequency = $\omega \cdot c/U_\infty$, [-]
k_{AGARD}	reduced frequency AGARD = $(\omega \cdot c)/(2 \cdot U_\infty)$, [-]
L	lift force, [N]
M	moment, [Nm]
n	propeller rotational speed, [1/s]
p	pressure, [Pa]
p_∞	free stream pressure, [Pa]
$\dot{q}$	volumetric rate of heat addition per unit mass
$\dot{q}_c$	heat conduction
q_∞	dynamic pressure = $\rho/2 \cdot U_\infty^2$, [Pa]

S	control surface
Sr	Strouhal number, [-]
t	time, [s]
T_s	physical period, [s]
T	thrust, [N]
u, v, w	velocity components in x, y, and z direction, [m/s]
U_∞	free stream velocity, [m/s]
V	velocity, [m/s]
V_t	contravariant velocity, [m/s]

Greek symbols:

α	angle of attack, [°]
α_m	mean pitch amplitude, [°]
α_0	mean incidence, [°]
β_{75}	propeller pitch angle at 75%-radius, [°]
ω	angular velocity, [rad/s]
Ω	control volume
ϕ_S	angle of separation, [°]
τ	non-dimensional time, [-]
σ	CFL number, [-]
σ_n	normal shear stress, $[N/m^2]$
σ_v	viscous shear stress, $[N/m^2]$
ρ	density, $[kg/m^3]$

Motivation

Computational Fluid Dynamics (CFD) has become an established design and analysis tool in aeronautical engineering. Rapid advances in the required computer hardware as well as in the algorithms and methods employed have led to this disciplines wide applicability for a significant amount of the flight regimes of interest in the aerospace industry. Modern CFD codes, such as the DLR TAU-Code [16], have been thoroughly validated through the comparison of numerical results with wind tunnel and flight test data and have achieved a high degree of maturity. The increasing use of CFD in aircraft design allows for relatively quick trade studies on aircraft configuration variations and greatly helps in the optimization of the flight vehicles performance characteristics.

CFD is based on the numerical solution of the Navier-Stokes equations, which are a system of non-linear equations applicable to viscous fluid flows. For the types of flows of interest in aerospace no closed-form solution of these so-called conservation laws are available. Thus an iterative solution approach using so-called computational grids, which discretize the flow domain of interest, is necessary. Due to the aerospace industries push for simulation methods that allow for increasing fidelity and geometric complexity, unstructured CFD methods like the DLR TAU-Code were developed [16]. Thanks to the flexibility of these codes with respect to the types of elements permitted in the computational grid, the previously quite time-consuming process of grid generation for structured CFD methods can be automated to a great extent and high-quality meshes are obtained in a much quicker time-frame. However the algorithms needed to be able to compute flows using these unstructured grids are inherently less efficient than those applicable for structured CFD solvers. Coupled with the desire to analyze more and more complex geometries, this can lead to quite substantial computational costs and turn-around times, making efficient numerical methods and approaches a necessity.

Recently, the simulation of unsteady flow phenomena is becoming progressively more important to the aerospace industry [17], [15]. This trend is driven in part

by the continuously increasing use of numerical methods in aircraft design beyond the hitherto typical design point flight conditions towards the edges of the flight envelope. Here unsteady flow separation phenomena occur, the understanding of which can be vital to improve the off-design performance of flight vehicles. The move towards increasing geometric complexity and fidelity in the simulations also makes the treatment of control surface deflections and maneuvers, both coupled with unsteady flow phenomena, an area that will become an important capability for industry [21]. Furthermore, the recent renewed interest in propeller propulsion for civil aircraft due to this powerplants superior efficiency versus the turbofan leads to the need for an unsteady analysis of the aerodynamics [22], [23].

While an efficient and established time-accurate solution scheme for the CFD simulation of such flows based on the unsteady Reynolds-Averaged Navier-Stokes equations (uRANS) exists in the dual time approach [8], the computational costs of these types of computations are still quite high and typically beyond the turn-around times required in the aerospace industry. Despite the continuous performance improvement of computer hardware and the use of large-scale parallel compute clusters, it is nevertheless essential to develop and establish an efficient approach to unsteady CFD simulations through the use of appropriate algorithms, models and settings [17], [15].

In the scope of this thesis, a number of 2D- and 3D-test cases from literature [12], [18], [19] are numerically investigated to determine an optimal setting of parameters of the dual time stepping scheme as implemented in the DLR TAU-Code with the aim of finding a good balance of computational cost and solution quality.

Tasks

The following tasks are to be performed in this thesis:

1. Familiarization with the CentaurSoft Centaur mesh generation software and the DLR TAU-Code
2. Selection of the preferred 2D- and 3D-test cases for the parameter study from literature
3. Generation of hybrid meshes for the selected 2D- and 3D-test cases
4. Reference uRANS simulations for the selected 2D and 3D-test cases

5. uRANS computations with variations of the relevant parameters of the dual time method

6. Comparison and validation of the numerical results

7. Analysis of the impact of the parameter variation on solution accuracy and computational cost

8. Establishment of guidelines and recommendations for the efficient and accurate CFD simulation of unsteady flows with the DLR TAU-Code

The results of this study are to be documented in a detailed report according to the guidelines set for master theses. The report is to be submitted both in electronic form on a CD or DVD as well as in a form suitable for reproduction and will remain the property of DLR.

Supervising Tutors

Deutsches Zentrum für Luft- und Raumfahrt e.V.
Institut für Aerodynamik und Strömungstechnik, Abt. Transportflugzeuge
Prof. Dr.-Ing. habil. C.-C. Rossow
Dipl.-Ing. A. Stuermer

Hochschule für Angewandte Wissenschaften Hamburg
Department Maschinenbau und Produktion
Prof. Dr.-Ing. Peter Wulf

Duration: 6 months

Introduction

The German Aerospace Centre (DLR) (German: Deutsches Zentrum für Luft- und Raumfahrt e.V.) is the national research center for aeronautics and space flight of the Federal Republic of Germany. Its extensive research and development projects are included in national and international cooperative programs. In addition to its research projects, the DLR is the assigned space agency of Germany bestowing headquarters of german space flight activities and its associates. Its mission is the exploration, application, and assessment of advanced aerodynamics and flow technologies for efficient air and space transportation [33].

The DLR Institute of Aerodynamics and Flow Technology is a leading research institute in the field of aerodynamics/aeroacoustics of airplanes and aerothermodynamics of space vehicles. It has two main sites at Braunschweig and Göttingen and has a division at Cologne. The institute coordinates its efforts with the German/European Aerospace industry and with a large number of universities. It is acting as a link between the basic research at the universities and industrial application. This results in a large number of cooperative national/European research projects [33].

One of the investigation fields of the DLR is the numerical aerodynamic analysis of modern commercial and transport aircraft. For this purpose, a tool for the simulation of the flow phenomena around an aircraft-configuration was developed. The DLR TAU-Code developed in the Institute of Aerodynamics and Flow Technology is a finite-volume Euler/Navier-Stokes solver which allows the simulation of the flow around complex geometric configurations. This code has been thoroughly validated through the comparison of numerical results with wind tunnel and flight test data and has achieved a high degree of maturity [16].

In most fluid dynamics applications, unsteady flow is a natural phenomenon and steady-state modeling is just a simplification of the real physics. As computing power increases, the number and complexity of unsteady flow simulations grows, too. While an efficient and established time-accurate solution scheme for the CFD

simulation of unsteady flows based on the uRANS-equations is implemented in the Tau-Code [8], the computational costs of these types of computations are still quite high and typically beyond the turn-around times required in the aerospace industry. The purpose of the present study is to analyze the parameters for the acceleration of unsteady simulations with the use of the dual time stepping method. The method is based on an implicit scheme which utilizes a pseudo-time step for the temporal discretization. The efficiency of the method depends on the balance between time steps and inner iterations for each step. An optimization of these parameters to reduce the time needed for the calculations is required. In the present Master thesis several 2-D and 3-D configurations are computed with the purpose of finding the best setting of parameters for the optimization of the method.

The first part of this report deals with the theory of the numerical solution of the Navier-Stokes equations. The spatial as well as the temporal discretization of the equations used by the DLR Tau-Code for the calculations in the present investigation are described. These include the integral form of the governing equations for static and moving grids, the Finite Volume Method for the spatial discretization, the Central Difference Scheme including Artificial Dissipation for the calculation of the inviscid fluxes, and the description of the temporal discretization by means of the Dual Time-Stepping Scheme. For all the numerical computations the one-equation Spalart-Allmaras turbulence model with Edwards modification [9] is used. Anyhow, due to the focus of this project on the temporal discretization method, no detailed description of the model is provided here. For more information about the Spalart-Allmaras turbulence model refer to [25] and [6].

The second part involves the investigation of the parameters for the acceleration of unsteady simulations with the evaluation of two standard 2-D cases of unsteady flow, and the insights gained are applied to two 3-D cases. The fist 2-D case is a NACA0012 airfoil with a periodic oscillating movement around the pitch axis located at 25% of the chord. The second case is the analysis of the flow over a blunt body with cylindrical circular area. The third case deals with the calculation of a modern transport aircraft configuration (DLR-F12) simulating a periodic oscillating pitch movement. Finally, the fourth case focuses on the simulation of a rotating AGARD-propeller mounted on a wing section.

Chapter 1

Flow solver and Grid generation

1.1 DLR Tau-Code

The DLR-TAU-Code developed in the Institute of Aerodynamics and Flow Technology is a finite-volume Euler / Navier-Stokes solver working with hybrid, unstructured or structured grids. The code is composed of three independent modules: the preprocessing module, the solver and the grid adaptation module. The preprocessing is decoupled from the solver in order to allow grid partitioning and calculation of the metrics on a different platform than used by the solver. This provides the possibility to run the solver independently, which is in terms of CPU-time requirements the most critical part of the system. Thus it is possible to run large scale calculations also on distributed memory machines with limited memory on each node. The third module is for grid adaptation. It detects regions with insufficient grid resolution and performs local grid refinement. The initial solution is interpolated onto the adapted grid. Although just the preprocessing- and solver modules are used in the present project, a brief description of the three modules including the adaptation module is provided in this chapter.

1.1.1 Preprocessing Module

The governing equations are solved on a dual grid of control volumes, which has to be determined from the initial primary grid.

For multigrid computations, coarse grids are constructed by agglomerating the control volumes of the dual grid in order to create a new grid of coarser control volumes. The coarse grid control volumes can be fused again in order to achieve an

even coarser grid.

For parallel computations the initial grid is partitioned into as many sub-domains as processors will be used. Only a simple initial partitioning is employed, which divides the grids according to the point coordinates. Grid points from neighboring domains connected by edges which have been cut by the partitioning are stored in addition to the points owned by the domain. The variables for these additional points have to be transferred from the corresponding domain. If this is guaranteed by the communication each domain can be computed independently. The communication tables are set up in the preprocessing to ensure this feature.

In order to enable the vectorization of the code in each sub domain a coloring algorithm is used. Looping over the colors, eliminates the possibility that two edges sharing a common endpoint are processed within the same vector; thereby reducing memory bank conflicts.

1.1.2 Flow Solver

The flow solver is a three-dimensional parallel hybrid multigrid code. It is based on a finite volume scheme for solving the Reynolds-averaged Navier-Stokes equations.

The flow variables are stored in the vertices of the initial grid. The temporal gradients are discretized using a multi-step Runge-Kutta scheme. For accelerating the convergence to steady state a local time-stepping concept is employed. The calculation of the inviscid fluxes is performed using either, a central method with scalar or matrix dissipation, or alternatively an AUSM (Advection Upstream Splitting Method) or a Roe type 2nd-order upwind scheme. The gradients of the flow variables are determined by employing a Green-Gauß formula. The viscous fluxes are discretized using central differences.

For turbulence modeling, the Tau-Code provides two classes of turbulence models: The RANS turbulence models and the DES models (coupling RANS in boundary layers and LES in separation regions). Several RANS models with various versions are available: 1-equation turbulence models based on the Spalart-Allmaras model, 2-equation turbulence models based on the Wilcox k-ω model and Explicit algebraic Reynolds stress models (EARSM) based on the k-ω model. Of these models, the 1-equation Spalart-Allmaras model with Edwards modification [9] is used for all the calculations performed in the present study.

The data structure provided by the preprocessing allows to run the solver in several sub-domains in parallel. The only additional work to be performed in mul-

tiprocessor mode is the communication required to update the point-data for the additional points. This communication between the different concurrent processes is carried out using the above mentioned communication tables and the MPI-library. Since this library supports non-blocking sends and receives, all data to be sent is copied into send buffers and all receive/sends are started together. The communication is hidden by an interface routine such that inside the solver only calls of this interface appear in addition.

For time-accurate solutions, a global as well as a dual time-stepping scheme is implemented. The dual time stepping scheme follows the approach of Jameson [14], where the Runge-Kutta scheme is slightly modified in order to avoid instabilities for small physical time-steps. The time discretization can be chosen to be first, second or third order (where a higher order implies increased overhead but also better temporal accuracy).

For moving or deforming meshes, grid speeds are considered in specific flux calculations and reconstruction schemes.

1.1.3 Grid Adaptation Module

The primary grid can be adapted to the flow solution by cell division if a better resolution of the flow field is required in certain regions of the computational domain. The description given in this section concentrates on tetrahedral and prismatic cells.

Either a residual-based error indicator or an indicator based on the equidistribution principle can be used to compute a measure for the necessary grid resolution in the inviscid flow field. The latter indicator (which operates on edges), is however, also used for viscous flows.

The adaptation is only employed on tetrahedral or prismatic elements. While the tetrahedra can be divided along all edges, the prismatic elements are presently refined only on their triangular faces similar to the refinement of tetrahedra. This concept leads to the introduction of new wall-normal grid lines through the whole prismatic layer when a single prismatic element is refined. The new grid lines are defined by the mid points of the refined edges of the affected prismatic elements. The refinement strategy used ensures that the quality of the grid is not degraded by numerous divisions of one edge of a triangle without an according refinement of neighboring edges. Since all points introduced by the algorithm are located on the middle of an edge of the initial grid, interpolating all variables of the flow field solution to the new points linearly along the edge is a straightforward process.

A refinement of the wall-normal grid resolution inside the prismatic layer is presently not implemented in the automatic procedure. It requires the start of an additional program that replaces the old prismatic layers by new ones. Thus the wall-normal marching steps from one cell layer to the next change, eventually also the number of prismatic layers, both depending on the user input. Wall-normal grid lines and the local overall height of all prismatic layers are left unchanged. Thus, also the initial surface triangulation is not affected.

1.2 Centaur Mesh Generation Software

For most of the unstructured grid generation requirements, the DLR uses the software *CentaurSoft* [31]. The system consist mainly of two parts: an interactive program which reads in CAD data in IGES format and performs some CAD cleaning if necessary, and the automatic computation of the complete grid.

Centaur also allows the specification of boundary conditions and element sizes if the user does not prefer the default values [4]. Different parameters control the surface, prismatic and tetrahedral element sizes. A selection of user definable sources offer the possibility to generate grids of the desired density in certain areas.

The first step after the geometry data from the CAD package has been processed (via the CAD conversion engine) is to triangulate the portions of the surface from which prisms will be marched. The surface input file (`*.sin` file) allows the user to change manually the parameters for the surface grid generation if the default values do not satisfy the user requirements. Thus values like for instance the overall stretching ratio, or the element length scale can be manipulated.

The next step after the surface triangulation is to march nodes away from the body surface to create prismatic elements which normally are used in the so called Navier-Stokes meshes. These kind of meshes are used to calculate viscous flows which need an adapted grid at the vicinity of the wall to allow for a good resolution of the boundary layer. They are characterized by a structured prismatic or hexahedral mesh in the vicinity of the wall using an initial marching step size which increases exponentially after each prismatic layer. The parameters for the initial prismatic marching step, the number of prismatic layers and the stretching factor, among other parameters, can be manually modified in the prismatic input file (`*.pin` file).

The remainder of the computational domain (after prisms generation) is filled with tetrahedral elements because of the ease with which these elements fill arbitrary

volumes in a single block; the parameters for the tetrahedral grid generation are defined by the tetrahedral input file (`*.tin` file).

Centaur allows to introduce sources to refine zones which require more resolution of the solution. The source input file (`*.lin` file) is where user defined sources are specified. Sources are used to add nodes to the mesh in either the mesh generation or grid adaptation process, where extra resolution is needed, or where automatic measures (curvature, proximity, and CAD clustering) do not place enough points to adequately resolve the geometry or flow features [31]. The Centaur grid generator allows the user the ability to specify mesh clustering in regions where the mesh would not automatically cluster due to geometric features or in areas where the user would like additional mesh clustering. Both geometric (line, sphere, cylinder, hexahedron) and CAD-based (curve, panel, group) types of sources are supported. The sources can control the clustering either by specifying a length scale in the source region or by specifying an additional amount of clustering relative to the preexisting clustering [31]. Relative sources can also be used to locally coarsen the mesh. Sources can be used to create anisotropic elements in the surface mesh. Anisotropy allows for a smaller number of points to be used in directions where the flow does not vary while allowing for sufficient clustering in the directions with large flow gradients. Sources can also be used to locally control other aspects of the prismatic mesh generation such as stretching and the number of layers [31].

Chapter 2

Governing Equations and Spatial Discretization

CFD methods are based on the fundamental governing equations of fluid dynamics. They are mathematical statements of three fundamental physical principles:

- Mass Conservation ⇒ Continuity equation
- Momentum Conservation ⇒ Momentum equation
- Energy Conservation ⇒ Energy equation

These principles can be modeled in mathematical form with the so called Navier-Stokes (NS) -equations. These equations can be simplified by removing terms describing viscosity to yield the Euler equations. Further simplifications, by removing terms describing vorticity yields the full potential equations. Finally these equations can be linearized to yield the linearized potential equations [32]. For the types of flows of interest in aerospace no closed-form solution of these so-called conservation laws are available. Thus an iterative solution approach using so-called computational grids, which discretize the flow domain of interest, is necessary.

In the present chapter, the NS-equations and the discretization method for the approximation to their solution are described.

2.1 Navier-Stokes Equations

The NS-equations describe a viscous flow where the transport phenomena of friction, thermal conduction, and/or mass diffusion are included. These transport phenom-

ena are dissipative, i.e. they always increase the entropy of the flow [2].

The NS-equations can be represented in differential or integral form in conservation and non-conservation form. The integral form of the equations allows for the presence of discontinuities inside the fixed *Control Volume* (see definition in section 2.3.1). However, the differential form of the governing equations assumes the flow properties are differentiable, hence continuous. This is a strong argument for the integral form of the equations to be considered *more fundamental* than the differential form [2].

The conservation and non-conservation form of the equations lend themselves to the approach using a finite control volume. This can be fixed in space with the fluid moving through it (Conservation form or Euler representation) or the control volume may be moving with the fluid such that the same fluid particles are always inside it (Non-conservation form or Lagrange representation).

2.1.1 Integral Form of the NS- Equations

Continuity Equation

Conservation form

$$\frac{\partial}{\partial t}\iiint_{\Omega}\rho d\Omega + \iint_{S}\rho\vec{V}\cdot d\vec{S} = 0 \tag{2.1}$$

Here $d\Omega$ denotes the control volume and dS the control surface.

Momentum Equation

Conservation form

x- component:

$$\begin{aligned}\frac{\partial}{\partial t}\iiint_{\Omega}(\rho u)d\Omega + \iint_{S}(\rho u\vec{V})\cdot d\vec{S} \\ = \iint_{S}(-p\vec{n}\cdot\vec{i} + \sigma_n\vec{n}\cdot\vec{i} + \sigma_s\vec{m}\cdot\vec{i})dS + \iiint_{\Omega}(\rho f_x)d\Omega\end{aligned} \tag{2.2}$$

y- component:

$$\begin{aligned}\frac{\partial}{\partial t}\iiint_{\Omega}(\rho v)d\Omega + \iint_{S}(\rho v\vec{V})\cdot d\vec{S} \\ = \iint_{S}(-p\vec{n}\cdot\vec{j} + \sigma_n\vec{n}\cdot\vec{j} + \sigma_s\vec{m}\cdot\vec{j})dS + \iiint_{\Omega}(\rho f_y)d\Omega\end{aligned} \tag{2.3}$$

z- component:

$$\begin{aligned}\frac{\partial}{\partial t}\iiint_{\Omega}(\rho w)d\Omega + \iint_{S}(\rho w\vec{V})\cdot d\vec{S} \\ = \iint_{S}(-p\vec{n}\cdot\vec{k} + \sigma_n\vec{n}\cdot\vec{k} + \sigma_s\vec{m}\cdot\vec{k})dS + \iiint_{\Omega}(\rho f_z)d\Omega\end{aligned} \tag{2.4}$$

Here $\vec{n}$ is a unit vector perpendicular to the infinitesimal control surface dS and $\vec{m}$ is a unit vector tangent to the surface and pointing in the direction of the viscous shear stress that acts on the surface. The terms σ_n and σ_s represent the normal shear stress and the viscous shear stress respectively.

Energy Equation

Conservation form

$$\begin{aligned}\frac{\partial}{\partial t}\iiint_{\Omega}E_t d\Omega + \iint_{S}E_t\vec{V}\cdot d\vec{S} = \iiint_{\Omega}(\rho\vec{q} + \rho\vec{f}\cdot\vec{V})d\Omega \\ = \iint_{S}(\dot{\vec{q}_c}\cdot\vec{n} - p\vec{n}\cdot\vec{V} + \sigma_n\vec{n}\cdot\vec{V} + \sigma_s\vec{m}\cdot\vec{V})dS\end{aligned} \tag{2.5}$$

Here $\vec{q}$ denotes the volumetric rate of heat addition per unit mass and $\vec{q_c}$ denotes the heat conduction where:

$$\dot{q}_{c_x} = k\frac{\partial T}{\partial x},\ \dot{q}_{c_y} = k\frac{\partial T}{\partial y} \text{ and } \dot{q}_{c_z} = k\frac{\partial T}{\partial z}$$

E_t represents the total energy inside the control volume

$$E_t = \rho\left(e + \frac{V^2}{2}\right). \tag{2.6}$$

And finally the equation of state for the fluid to relate p, ρ, and e. The most common example is the perfect gas law

$$p = (\gamma - 1)c_v\rho T \tag{2.7}$$

where,

$$e = \quad c_v T \tag{2.8}$$
$$\gamma = \quad \tfrac{c_p}{c_v}. \tag{2.9}$$

The integral form of the NS-equations in conservative form can be summarized as:

$$\frac{\partial}{\partial t}\iiint_{\Omega} \mathbf{W} d\Omega + \iint_{S} \mathbf{F}\cdot\mathbf{n} dS = \iiint_{\Omega} \mathbf{Q} d\Omega \tag{2.10}$$

In Equation 2.10 the *flux density tensor* $\mathbf{F}$ is composed of the fluxes $\mathbf{F}_x$, $\mathbf{F}_y$ and $\mathbf{F}_z$, which include the *viscous* ($\mathbf{F}^v$) and *convective* ($\mathbf{F}^c$) components of the fluxes, $\mathbf{W}$ represents the vector of *conservative variables*, and $\mathbf{Q}$ the *source term* vector

where,

$$\mathbf{W} = \begin{pmatrix} \rho \\ \rho u \\ \rho v \\ \rho w \\ E_t \end{pmatrix}, \tag{2.11}$$

$$\mathbf{F}_x = (\mathbf{F}_x^c - \mathbf{F}_x^v) = \begin{pmatrix} \rho u \\ \rho u^2 + p_x \\ \rho v u \\ \rho w u \\ E_t u + p u \end{pmatrix} - \begin{pmatrix} 0 \\ \tau_{xx} \\ \tau_{xy} \\ \tau_{xz} \\ \dot{q}_{c_x} + u\tau_{xx} + v\tau_{xy} + w\tau_{xz} \end{pmatrix}, \tag{2.12}$$

$$\mathbf{F}_y = (\mathbf{F}_y^c - \mathbf{F}_y^v) = \begin{pmatrix} \rho v \\ \rho uv \\ \rho v^2 + p_y \\ \rho wv \\ E_t v + pv \end{pmatrix} - \begin{pmatrix} 0 \\ \tau_{yx} \\ \tau_{yy} \\ \tau_{yz} \\ \dot{q}_{c_y} + u\tau_{yx} + v\tau_{yy} + w\tau_{yz} \end{pmatrix}, \tag{2.13}$$

$$\mathbf{F}_z = (\mathbf{F}_z^c - \mathbf{F}_z^v) = \begin{pmatrix} \rho w \\ \rho uw \\ \rho vw \\ \rho w^2 + p_z \\ E_t w + pw \end{pmatrix} - \begin{pmatrix} 0 \\ \tau_{zx} \\ \tau_{zy} \\ \tau_{zz} \\ \dot{q}_{c_z} + u\tau_{zx} + v\tau_{zy} + w\tau_{zz} \end{pmatrix}, \tag{2.14}$$

and

$$\mathbf{Q} = \begin{pmatrix} 0 \\ \rho f_x \\ \rho f_y \\ \rho f_z \\ \rho(uf_x + vf_y + wf_z) + \rho\dot{q} \end{pmatrix}. \tag{2.15}$$

2.2 Navier-Stokes Equations for Moving Grids

In certain cases, where for instance fluid-structure interaction is investigated or where store separation is simulated, it is necessary to solve the governing equations on a moving and possibly a deforming grid [3]. Written in time-dependent integral form for a moving and/or deforming control volume Ω with a surface element dS, the NS- equations read

$$\frac{\partial}{\partial t}\iiint_\Omega \mathbf{W} d\Omega + \iint_S (\mathbf{F}_c^M - \mathbf{F}_v) dS = \iiint_\Omega \mathbf{Q} d\Omega, \tag{2.16}$$

where the vector of the convective fluxes $\mathbf{F}_c^M$ becomes on dynamic grids

$$\mathbf{F}_c^M = \mathbf{F}_c - V_t \mathbf{W}, \tag{2.17}$$

with V_t being the contravariant velocity of the face of the control volume. Hence,

$$V_t = n_x \frac{dx}{dt} + n_y \frac{dy}{dt} + n_z \frac{dz}{dt}, \tag{2.18}$$

here n_x, n_y and n_z denote the components of the outward facing unit normal vector of the surface dS. The convective fluxes can be written in the form

$$\mathbf{F}_c^M = \begin{pmatrix} \rho V_t \\ \rho u V_r + n_x p \\ \rho v V_r + n_y p \\ \rho z V_r + n_z p \end{pmatrix}. \tag{2.19}$$

Furthermore, V_r represents the contravariant velocity relative to the motion of the grid,

$$V_r = n_x u + n_y v + n_z w - V_t = V - V_t. \tag{2.20}$$

The viscous fluxes and the source term retain the same forms as in Eq. 2.10.

Thomas and Lombard [26] concluded that beside the conservation of mass, momentum and energy, the so called *Geometric Conservation Law* (GCL) must be satisfied in order to avoid errors induced by deformation of control volumes. In this case the integral form of the GCL reads

$$\frac{\partial}{\partial t} \iiint_{\Omega} d\Omega - \iint_{dS} V_t dS = 0. \tag{2.21}$$

The CGL results from the requirement that the computation of the control volumes or of the grid velocities must be performed in such a way that the resulting numerical scheme preserves the state of a uniform flow, independently of the deformation of the grid [3].

2.3 Spatial Discretization

After choosing the mathematical model, one has to choose a suitable discretization method for the approximation of the differential equations by a system of algebraic equations for the variables at some set of discrete locations in space and time. The most important approaches for this purpose, are the Finite Difference (FDM) ,

Finite Volume (FVM) and Finite Element (FEM) methods. Since the DLR Tau-Code utilizes a FV method due to its suitability for complex geometries as in the aerospace industry, only the FV method is described in this chapter. A detailed explanation of the FD method is given in Reference [2], while information about the FE method can be found in [10].

2.3.1 Finite Volume Method

The Finite Volume Method uses the integral form of the conservation equations as its starting point. The solution domain is subdivided into a finite number of Control Volumes (CVs) , and the conservation equations are applied to each CV. At the centroid of each CV lies a computational node at which the variable values are to be calculated. Interpolation is used to express the variable values at the CV surface in terms of the nodal (CV- center) values. The surface and volume integrals are approximated using suitable quadrature formulae. As a result, one obtains an algebraic equation for each CV, in terms of the CV- center and neighbor nodal values [10].

The surface integrals can be approximated as the sum of integrals over the k number of faces of the CV. In this form, the second term of Eq.(2.10) is approximated as

$$\iint_S f dS = \sum_k \iint_{S_k} f dS_k = \sum_k f_k \Delta S_k, \tag{2.22}$$

where f is the component of the convective or diffusive flux vector in the direction normal to the CV face and S_k the approximation of the k number of face surfaces.

Some terms in the transport equations require integration over the volume of the CV. The simplest second-order accurate approximation is to replace the volume integral by the product of the mean value of the integrand and the CV volume and approximate the former as the value at the CV center:

$$\iiint_\Omega q d\Omega = \overline{q} \Delta\Omega \approx q_p \Omega, \tag{2.23}$$

where q_p stands for the value of q at the CV center. Applying equations (2.22) and (2.23) in (2.10) the approximation of the governing equation can be written as

$$\frac{d}{dt}\mathbf{W} = -\frac{1}{\Omega}\left[\sum_k \mathbf{F}_k \Delta S_k - \mathbf{Q}\Omega\right]. \tag{2.24}$$

The term in brackets on the right-hand side is also generally termed the *residual* of the continuity, momentum and energy equations. Hence Eq. 2.24 can be abbreviated as

$$\frac{d}{dt}\mathbf{W}_i = -\frac{1}{\Omega_i}\mathbf{R}_i. \tag{2.25}$$

2.3.2 Central Difference Scheme

The approximations to the integrals require the values of variables at locations other than the CV centers. To calculate the convective and diffusive fluxes, the value of the conservative variables and its gradients normal to the cell face at one or more locations on the CV surface are needed. They have to be expressed in terms of the nodal values by interpolation [10]. This can be done using the cell-centered scheme, where the fluxes at the face of the CV can be expressed with Equation 2.26 [3],

$$(\mathbf{F}\Delta S)_{i+1/2,j,k} \approx \mathbf{F}(\mathbf{W}_{i+1/2,j,k})\Delta S_{i+1/2,j,k}, \tag{2.26}$$

where the conservative variables at the face $\vec{n}_{i+1/2,j}$ of the CV are defined as the arithmetic average of values at the two adjacent cells, i.e.:

$$\mathbf{W}_{i+1/2,j,k} = \frac{1}{2}\left(\mathbf{W}_{i,j,k} + \mathbf{W}_{i+1,j,k}\right) \tag{2.27}$$

The subscripts (i, j, k) denotes the CV- center, $(i + 1/2, j, k)$ the values at the CV- face, and $(i + 1, j, k)$ represents the values at the neighboring CV- center.

2.3.3 Artificial Dissipation

Since the central scheme would allow for odd-even decoupling of the solution and overshoots at shocks, artificial dissipation has to be added for stability. In this form the artificial dissipation term is added to Eq.(2.26) as follows [3], [14]:

$$(\mathbf{F}\Delta S)_{i+1/2,j,k} \approx \mathbf{F}(\mathbf{W}_{i+1/2,j,k})\Delta S_{i+1/2,j,k} - \mathbf{D}_{i+1/2,j,k} \tag{2.28}$$

The artificial dissipation flux consists of a blend of adaptive second- and fourth-order differences which result from the sum of first- and third-order difference operators.

$$\begin{aligned}\mathbf{D}_{i+1/2,j,k} = \frac{1}{2}\widetilde{\alpha}[&\epsilon^{(2)}_{i+1/2,j,k}(\mathbf{W}_{i+1/2,j,k} - \mathbf{W}_{i,j,k}) \\ &- \epsilon^{(4)}_{i+1/2,j,k}(\mathbf{W}_{i+2,j,k} - 3\mathbf{W}_{i+1,j,k} + 3\mathbf{W}_{i,j,k} - \mathbf{W}_{i-1,j,k})]\end{aligned} \tag{2.29}$$

where $\widetilde{\alpha}$ describes the scaling of dissipation either *scalar dissipation* or *matrix dissipation*. The coefficients $\epsilon^{(2)}_{i+1/2,j,k}$ and $\epsilon^{(4)}_{i+1/2,j,k}$ contain shock switches for the second and fourth order dissipation, and control the amount of dissipation to be added.

Chapter 3

Temporal Discretization

In computing unsteady flows, we have a fourth coordinate direction to consider: *time*. In general the algorithms for computing unsteady flows are of two main types, explicit and implicit. The DLR Tau-Code allows the use of explicit algorithms like the *global time stepping* scheme which is based on the k-step low-storage Runge Kutta scheme (see [14]). Nevertheless explicit methods are subject to severe stability restrictions. This often limits the time step size for stability reasons to values that are much smaller than those required to obtain accuracy, hence leading to a large number of time steps.

Another method for the time discretization, is the implicit *dual time stepping* scheme implemented in the DLR Tau-Code. Implicit methods help to bypass the time step limitations, which is specially important for the simulation of viscous high Reynolds number flows.

3.1 Dual Time-Stepping Scheme

The Time-Stepping Scheme parts from the separation of spatial and temporal discretization of the governing equations. This leads for each CV to a system of coupled ordinary differential equations in time. Recalling Eq. (2.25), the system has to be integrated in time either to obtain a steady-state solution or to reproduce the time history of an unsteady flow. The solution of the equation system for explicit and implicit methods can be derived from a *basic non-linear scheme* [3], which reads

$$\frac{(\Omega\bar{\mathbf{M}})_i}{\Delta t_i}\Delta\mathbf{W}_i^n = -\frac{\beta}{1+\omega}\mathbf{R}_i^{n+1} - \frac{1-\beta}{1+\omega}\mathbf{R}_i^{n+1} + \frac{\omega}{1+\omega}\frac{(\Omega\bar{\mathbf{M}})_i}{\Delta t_i}\Delta\mathbf{W}_i^{n-1} \tag{3.1}$$

where

$$\Delta \mathbf{W}_i^n = \mathbf{W}_i^{n+1} - \mathbf{W}_i^n \tag{3.2}$$

stands for the *update* (correction) of the solution. The superscripts n and $(n+1)$ denote the time levels with n representing the present time t and $(n+1)$ the time $t + \Delta t$ respectively. The parameters β and ω determine the discretization type (explicit or implicit) and temporal accuracy.

The dual time-stepping approach is based on the second- order time accurate version of the basic non-linear scheme in Eq. (3.1). For this purpose $\beta = 1$ and $\omega = 1/2$, hence

$$\frac{3(\Omega\bar{\mathbf{M}})_i^{n+1}\mathbf{W}_i^{n+1} - 4(\Omega\bar{\mathbf{M}})_i^{n}\mathbf{W}_i^{n} + (\Omega\bar{\mathbf{M}})_i^{n-1}\mathbf{W}_i^{n-1}}{2\Delta t} = -\mathbf{R}_i^{n+1}. \tag{3.3}$$

In order to solve the system of non-linear equations, a Newton´s method or a time-stepping methodology can be applied. The time-stepping methodology can be written as

$$\frac{\partial}{\partial t^*}\left(\Omega_i^{n+1}\mathbf{W}_i^*\right) = -\mathbf{R}_i^*\mathbf{W}^* \tag{3.4}$$

where $\mathbf{W}^*$ is the approximation to $\mathbf{W}^{n+1}$ and t^* denotes a *pseudo-time* variable. The unsteady residual is defined as

$$\mathbf{R}_i^*(\mathbf{W}^*) = \mathbf{R}_i(\mathbf{W}^*) + \frac{3}{2\Delta t}(\Omega\bar{\mathbf{M}})_i^{n+1}\mathbf{W}_i^* - \mathbf{Q}_i^*. \tag{3.5}$$

All terms which are constant during the time-stepping are gathered in a source term, i.e.,

$$\mathbf{Q}_i^* = \frac{2}{\Delta t}(\Omega\bar{\mathbf{M}})_i^{n}\mathbf{W}_i^{n} - \frac{1}{2\Delta t}(\Omega\bar{\mathbf{M}})_i^{n-1}\mathbf{W}_i^{n-1}. \tag{3.6}$$

3.1.1 Explicit Multistage Scheme

The concept of explicit multistage schemes (Runge-Kutta) was first presented by Jameson (see [14]). The multistage scheme advances the solution in a number of steps (*stages*) which can be viewed as a sequence of updates according to Eq. (3.4).

An m-stage explicit scheme for the solution of the pseudo-time problem reads:

$$\begin{aligned}
\mathbf{W}_i^{(0)} &= (\mathbf{W}_i^*)^l \\
\mathbf{W}_i^{(1)} &= \mathbf{W}_i^{(0)} - \tfrac{\alpha_1 \Delta t_i^*}{\Omega_i^{n+1}} \mathbf{R}_i^*(\mathbf{W}_i^{(0)}) \\
\mathbf{W}_i^{(2)} &= \mathbf{W}_i^{(0)} - \tfrac{\alpha_2 \Delta t_i^*}{\Omega_i^{n+1}} \mathbf{R}_i^*(\mathbf{W}_i^{(1)}) \\
&\vdots \\
(\mathbf{W}_i^*)^{l+1} &= \mathbf{W}_i^{(0)} - \tfrac{\alpha_m \Delta t_i^*}{\Omega_i^{n+1}} \mathbf{R}_i^*(\mathbf{W}_i^{(m-1)})
\end{aligned} \tag{3.7}$$

where α_k represents the stage coefficients. The stage coefficients can be tuned to increase the maximum time step and to improve the stability for a particular spatial discretization. For consistency, it is only required that $\alpha_m = 1$. Here l denotes the actual and $(l+1)$ the new pseudo-time level, respectively. The time-marching process is started either with $(\mathbf{W}_i^*)^l = \mathbf{W}_i^n$ or with a value extrapolated from previous physical time steps. It is continued until $(\mathbf{W}_i^*)^{l+1}$ approximates $\mathbf{W}_i^{n+1}$ with sufficient accuracy. After that, the next physical time step is conducted. The pseudo-time step Δt^* is computed as

$$\Delta t^* = \sigma \frac{\Delta x}{|\Lambda_c|} \tag{3.8}$$

where $\Delta x / |\Lambda_c|$ represents the time necessary to propagate information over the cell size Δx with the velocity Λ_c. The velocity Λ_c corresponds to the maximum eigenvalue of the convective flux Jacobian. The positive coefficient σ denotes the *CFL number* .

Chapter 4

2-D Cases

4.1 Case 1: Pitching Oscillation of a NACA0012 Airfoil

The first case analyzed is a NACA0012 airfoil (see Fig. 4.1) oscillating in pitch at transonic speed. The airfoil oscillates around the pitch axis located at 25% of the chord. The angle of attack α varies in time according to Eq. (4.1)

$$\alpha(t) = \alpha_m + \alpha_0 sin(2\pi f t), \tag{4.1}$$

where α_m is the mean incidence and α_0 is the pitch amplitude, f represents the frequency and t the time. This expression can be simplified using the DLR Tau-Code definition for the reduced frequency k and the non-dimensional time τ (see [6]), where

$$k = \frac{\omega \cdot c}{U_\infty} \tag{4.2}$$

and

$$\tau = \frac{2 \cdot U_\infty \cdot t}{c}, \tag{4.3}$$

as

$$\alpha(\tau) = \alpha_m + \alpha_0 sin(k\tau). \tag{4.4}$$

Here, c represents the chord length and U_∞ the free stream velocity.

The physical parameters of the simulation are listed below, as they appear in the DLR-Tau script:

Reference Mach number	0.755
Angle of attack α_m	0.0°
Fourier coefficient for rotation pitch α_0	2.51°
Frequency f	62.5 Hz
Reduced frequency for rotation k	0.1628
Reynolds number	$5.5 \cdot 10^6$
Reference Temperature	288.15 K
Prandtl number	0.72
Sutherland constant	110.4
Sutherland reference viscosity	$1.716 \cdot 10^{-5}$

The flow conditions and the oscillation parameters correspond to the parameters used in the experiments described in Case CT5 of the AGARD investigation in Ref. [18]. However, some differences need to be noted for the numerical simulation. The mean angle of attack given in [18] as $\alpha_m = 0.016°$ is approximated to zero. This assumption is also performed in [8] where it was confirmed that this does not have a major influence on the results. The reduced frequency is doubled in order to remain consistent with the oscillation frequency performed in the experiments, whose definition differs from the one implemented in the DLR Tau-Code. The definition of the reduced frequency given in [18] differs from the one given in [6] as follows:

$$k_{AGARD} = \frac{\omega \cdot c}{2 \cdot U_\infty} \tag{4.5}$$

The geometry of the airfoil was taken from the NACA 4-Digit Series definition with a chord length of 101.6 mm.

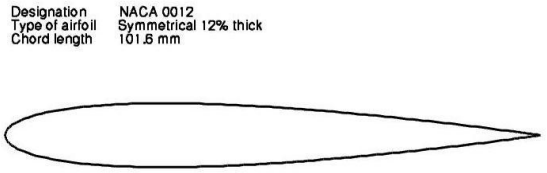

Figure 4.1: NACA0012 airfoil geometry

4.1.1 Grid Generation

The grid generated for the first case is a hybrid grid with structured quadrilateral elements in the vicinity of the wall and unstructured triangles in the far field. The structured grid has an initial layer thickness of 0.0011684 mm with 32 prismatic layers and a stretching factor of 1.2. This yields a maximum Y^+- value of 2.9 at the leading edge and a minimum Y^+- value of 1.0 at the trailing edge of the airfoil (see Fig. 4.2). The complete input files used in *CentaurSoft* for the grid generation are listed in Appendix A.1. The total grid has 26,724 points.

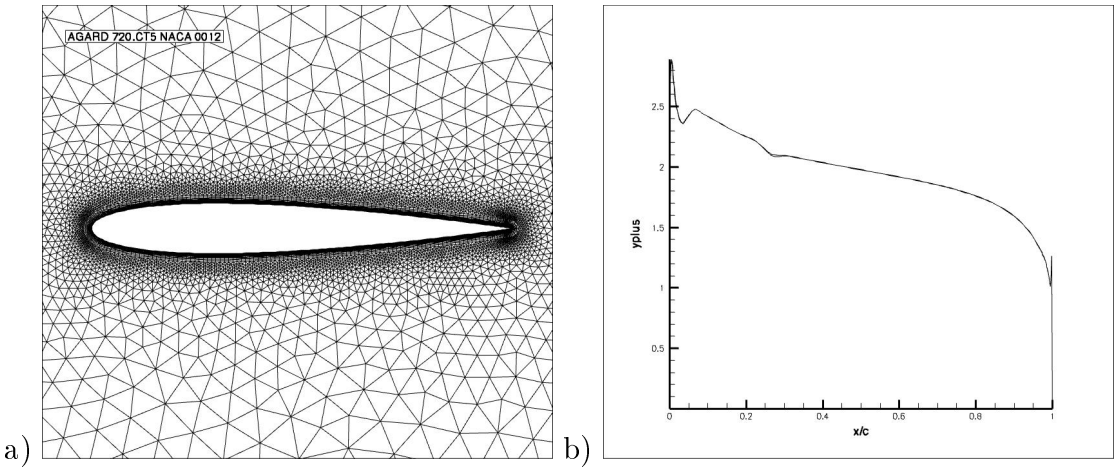

Figure 4.2: a) NACA0012 hybrid mesh, b) Y^+ distribution

4.1.2 Numerical Parameters for the Unsteady Simulations

The purpose of the present investigation, is the acceleration of the simulations by varying the number of physical time steps and the number of inner iterations for each time step. All other numerical parameters are retained unvaried. A central scheme is applied for the convective RANS flux discretization, with scalar dissipation for stability using the values for the coefficients $\epsilon^{(2)} = 1/2$ and $\epsilon^{(4)} = 1/64$. Temporal discretization is done using the dual time stepping scheme in combination with a 3 stage Runge-Kutta scheme. A 3v Multigrid cycle is applied for convergence acceleration and a CFL number of 1.8 for the calculation of the pseudo-time step is set. The run is performed using the 1-Equation turbulence of Spalart-Allmaras with Edwards modification [9]. The numerical solutions are generated based on the DLR TAU-Code version 2007.1.0. The complete setting of parameters used in TAU for the simulation are listed in Appendix A.1.

Unless otherwise specified, the default parameters are used for the computations.

All the calculations were performed on the same Intel Pentium IV Workstation using a 3.00 GHz processor.

4.1.3 Results

The strategy for the parameter analysis is first of all to get a reference solution in order to gauge the quality of the CFD results. For this purpose a reference calculation is performed and compared with the experiments and with previous numerical analysis of a similar case as in Ref. [8] Case 1.1. The first calculation can be considered as the *longest calculation* with 180 physical time steps per period and 150 inner iterations for each step. Furthermore 5 physical cycles are computed in order to achieve the periodic state of the solution. Compared to these results, the simulations employing optimization of the dual-time stepping parameters should not show dramatic changes in the accuracy but in the time needed for the calculation. All the calculations are performed beginning from *scratch*, which means that no initialization of the flow through a steady simulation is performed and farfield conditions are set throughout. For this particular case, an initialization of the flow does not represent a real advantage against the simulation without initialization of the flow beginning with a *restart*. This is observed in Figure 4.3 where the results of a simulation with a steady state initialization of the flow (red line in the figure) is compared with a simulation without initialization of the flow (dashed black line in the figure).

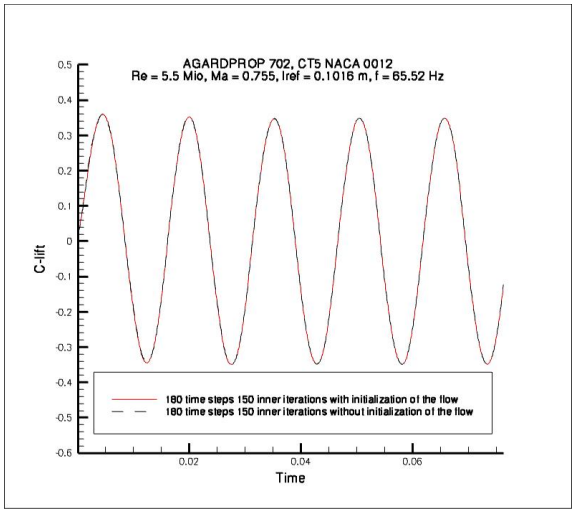

Figure 4.3: NACA 0012 periodic pitching motion with and without initialization of the flow

The results of the simulation show a periodic development of the relevant force coefficients after 4 physical cycles. Figure 4.4 shows the C_N- values which correspond to the lift coefficients plotted as a function of the angle of attack α compared with the experiments and with the available data from [8] for each physical cycle. The results obtained agree reasonably well with the experiments in the last half of the cycle and show slightly greater differences in the first half of the cycle. This is attributed in Ref. [8] to an asymmetry in the experimental setup which was observed through a pronounced deviation of the values from a symmetry line plotted through the Origin at the coordinates (0,0) (see Ref. [8]). The TAU results compared with Ref. [8] show a larger amplitude of the C_N- values which can be attributed to differences in the computational grid. The grid used in the GARTEUR studies had boundary layer resolution adapted for Y^+- values between 0.3 and 1.0, which represents a finer grid in the vicinity of the wall.

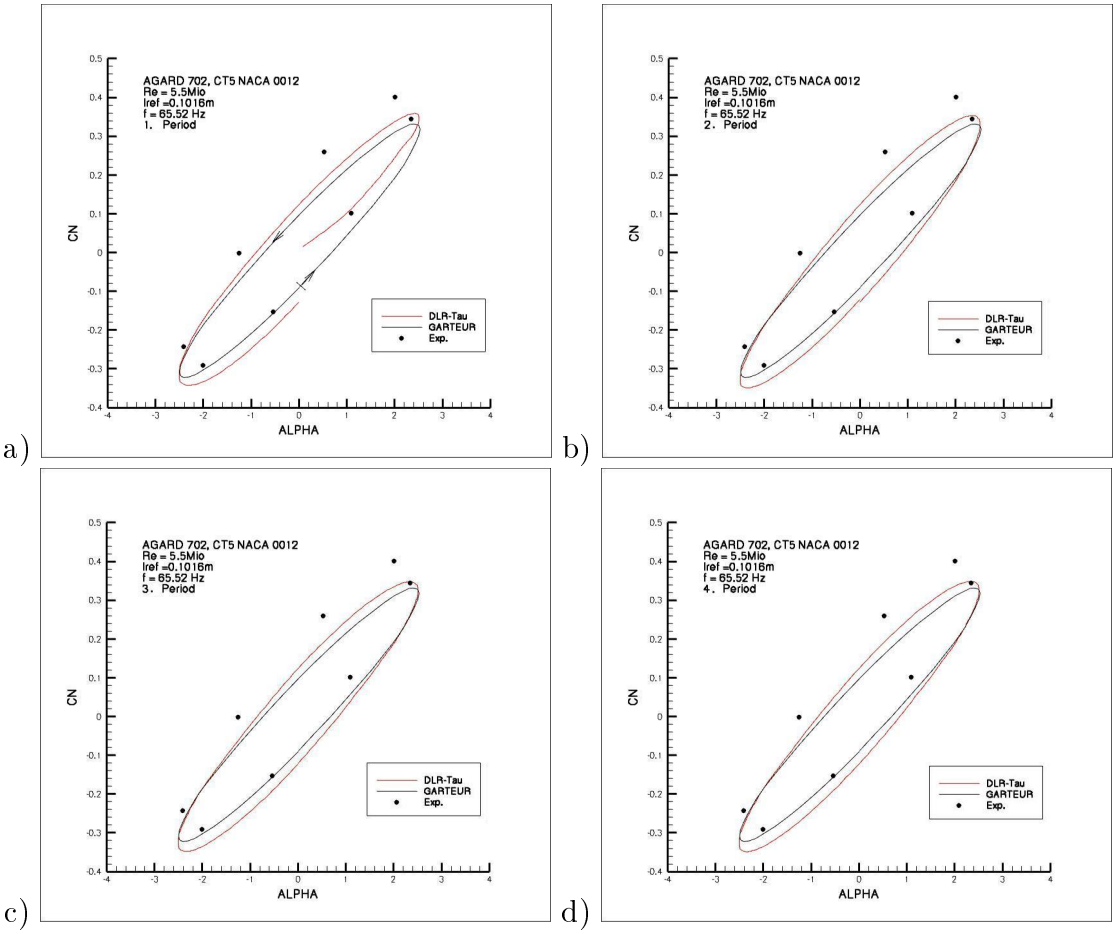

Figure 4.4: C_N-α results compared with Ref. [18] and Ref. [8], *a*) 1st cycle, *b*) 2nd cycle, *c*) 3rd cycle, *d*) 4th cycle

The differences in the amplitude of the lift coefficients can also be found in the inverse c_P distribution after the 5th physical cycle in Figure 4.5. Here, the position

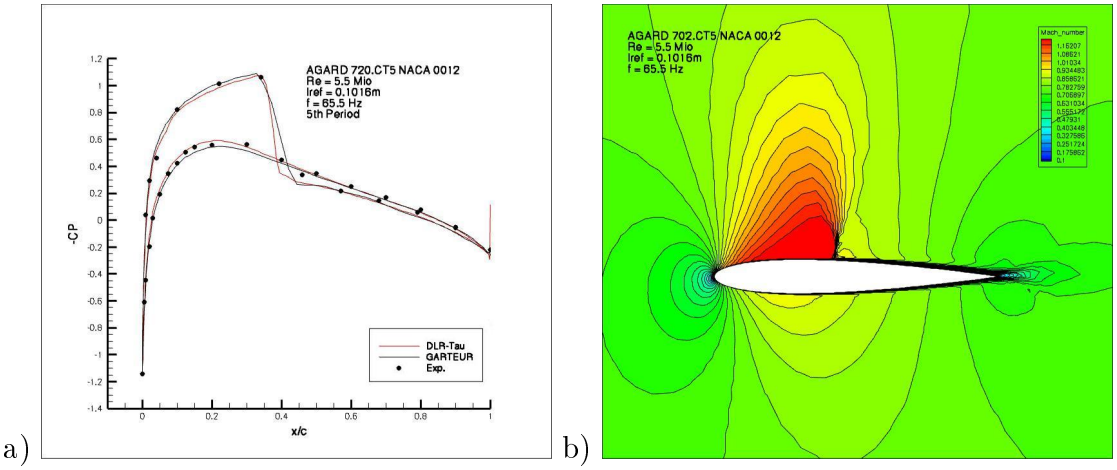

a) b)

Figure 4.5: a) -c_P distribution after 5 physical cycles b) Isotachs showing the position of the shock

of the shock in Ref. [8] appears further downstream than seen in the experiments and the present study.

To ensure that the inner iterations for each physical time step are sufficient, the convergence history of the density and turbulence residuals as function of the number of inner iterations are observed. Figure 4.6 shows the density residuals as red line and the turbulence residuals as black line, as well as the lift convergence history as the blue line for the first quarter of the 4th period. The residuals are reduced by more than one order of magnitude which ensures a sufficient accuracy of the solution [3]. It can also be observed that the lift coefficients converge in each physical time step creating the typical plateaued distribution of the aerodynamic coefficients of an unsteady numerical calculation.

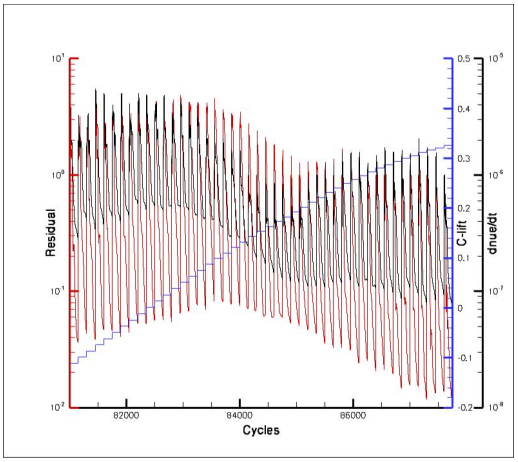

Figure 4.6: NACA 0012 residuals convergence history at the beginning of the 4th Period

For the purpose of the parameter analysis for the acceleration of the simulations with the dual time stepping scheme, the obtained results with these settings show sufficient accuracy, and can thus be taken as a point of reference in the present case.

Variation of the Relevant Parameters of the Dual Time Step Scheme

In addition to the validation results, 3 more simulations are performed with a variation of the physical time steps per period. The parameters used for these simulations are listed in Table 4.1.

	time steps per physical cycle [-]
Variant 1.1	180
Variant 1.2	90
Variant 1.3	45
Variant 1.4	25

Table 4.1: Setting of parameters analyzed for Case 1

The next step of the analysis is to vary the number of inner iterations per time step. For this, the number of inner iterations are varied until convergence of the normalized C_{Nmax}-values as a function of the inner iterations (n) per time step is obtained. The reference setting with $n = 150$ showed a reasonably good convergence of the residuals with a reduction of more than one order of magnitude in each physical time step, and an acceptable agreement with the experiments. In order to get accurate results, this reduction should not be less than one order of magnitude, otherwise the results would not fulfill the stability criteria, and they would be dominated by numerical errors.

Since the real time needed for the calculations depends on the total number of inner iterations, it is expected that by reducing the number of time steps per oscillation period, the time needed for the calculation should be also reduced. This is confirmed when observing Figure 4.7, which shows the CPU-Time as function of the number of inner iterations for each variant. The time for the different variants was normalized by the time $t = 19760.3$ [s], the total runtime of the simulation per Variant 1.1. It can be observed that the time is linearly reduced by decreasing the inner iterations per time step. In Fig. 4.7, Variant 1.4 (black line in the figure) shows the cheapest calculation in time compared with Variant 1.1 (red line in the figure) showing a reduction of the run time of almost 70% at the settings with the largest number of inner iterations. Furthermore it can be observed that even setting

a larger number of inner iterations than the reference, the time necessary for the calculation would be much lower than the one needed for the reference computation.

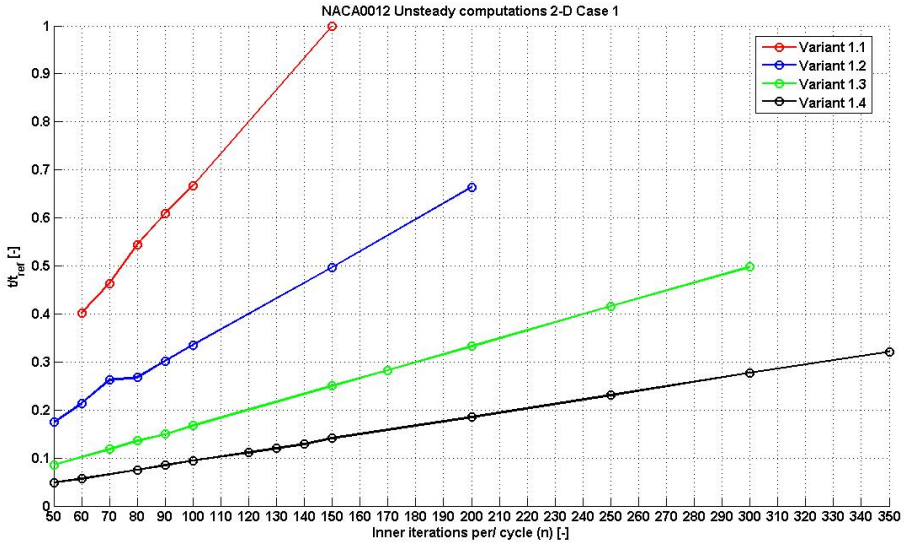

Figure 4.7: CPU- time as function of inner iterations per time step (n)

Figure 4.8 shows the deviation of the C_{Nmax} results for all the computations performed. Here the C_{Nmax}- values are extracted directly from the 5th period of the oscillatory lift distribution and depicted as a function of the inner iterations per time step. For a better analysis of the results, the C_{Nmax}- values are normalized by the $C_{Nmax,ref} = 0.34857$ given in Variant 1.1. Even though Variant 1.4 is the cheapest in terms of time, it delivers the largest difference compared with the other variants. It shows a notable discrepancy in the C_{Nmax}- plot of approximately 2.71%, at the converged values which are achieved at the largest number of inner iterations, compared with the reference.

The C_N-α diagrams for the settings with the largest number of inner iterations are depicted in Fig. 4.9. The largest discrepancy in the coefficients is observed in Variant 1.4, where the amplitude of the oscillatory lift distribution is larger than that obtained in the reference. This can be better observed in Fig. 4.10, where the normalized C_{Nmax}- values as function of the time steps per period for the settings with the largest number of inner iterations are depicted. Here it is clearly seen how the different setting of parameters vary from each other.

The $-c_P$ distribution after 5 cycles do not reveal major differences among the different parameter settings, except for a little fluctuation of the pressure distribution on the suction side at the position of the shock. Here the values obtained differ gradually from one setting to another. The values with the most number of time

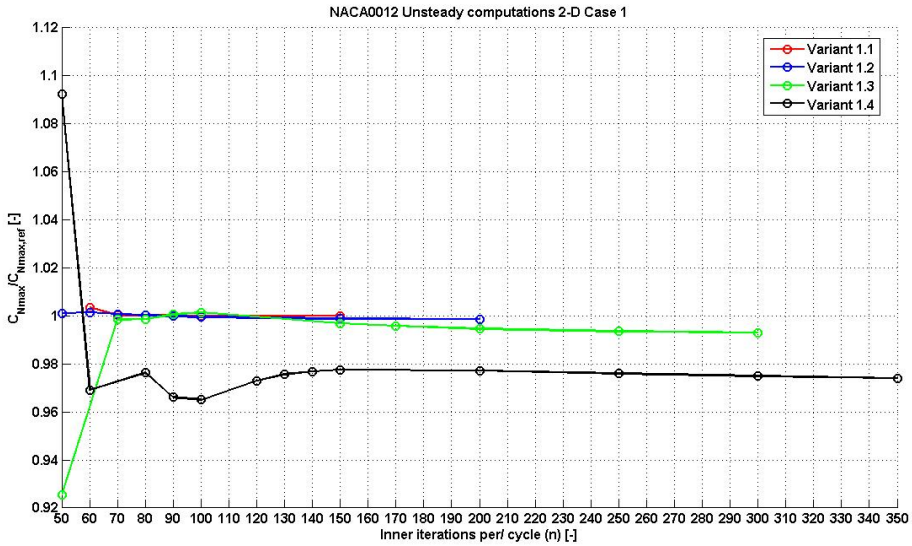

Figure 4.8: C_{Nmax} as function of inner iterations per time step (n)

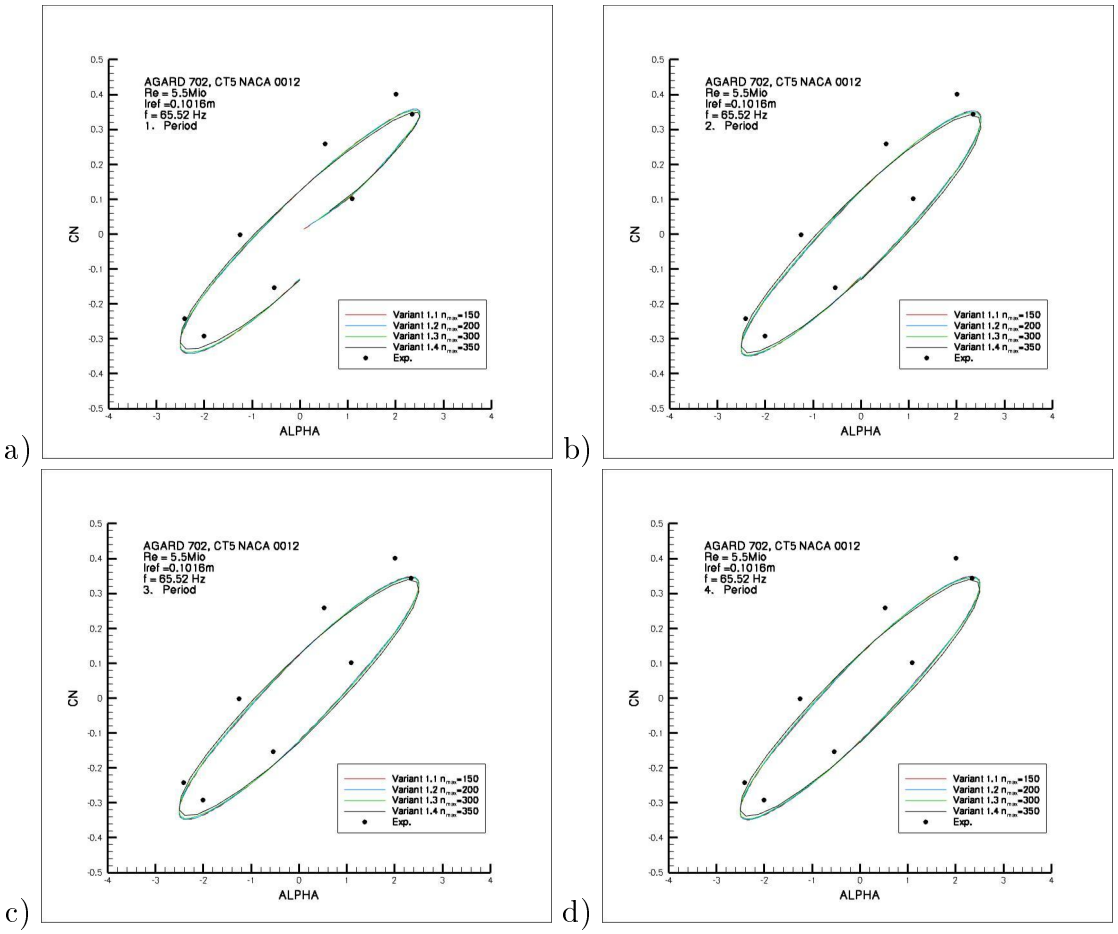

Figure 4.9: C_N-α results for Variants 1.1-1.4 with n_{max}, *a*) 1st cycle, *b*) 2nd cycle, *c*) 3rd cycle, *d*) 4th cycle

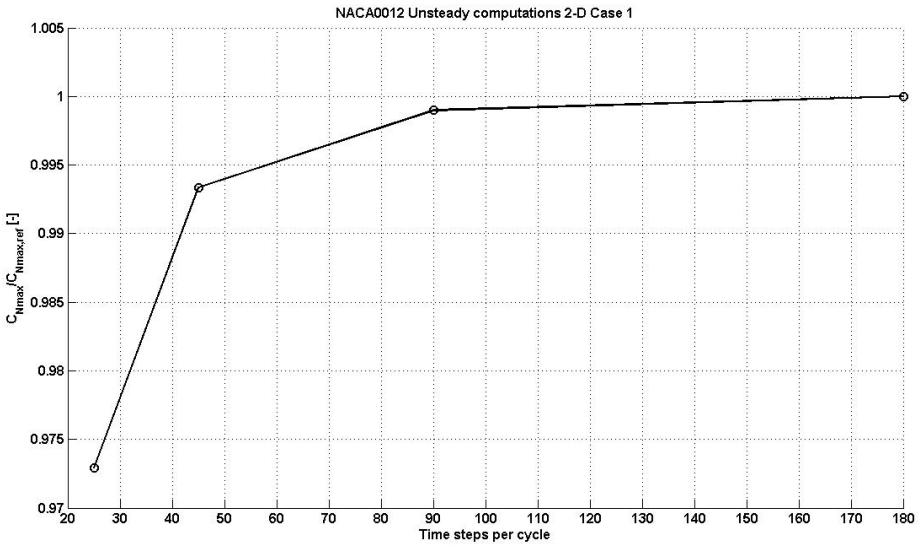

Figure 4.10: C_{Nmax} results for Variants 1.1-1.4 with n_{max}

steps are located closer to the experimental data and Variant 1.4 shows the worst accordance with the experiments. This is observed in Figures 4.11-a and 4.11-b.

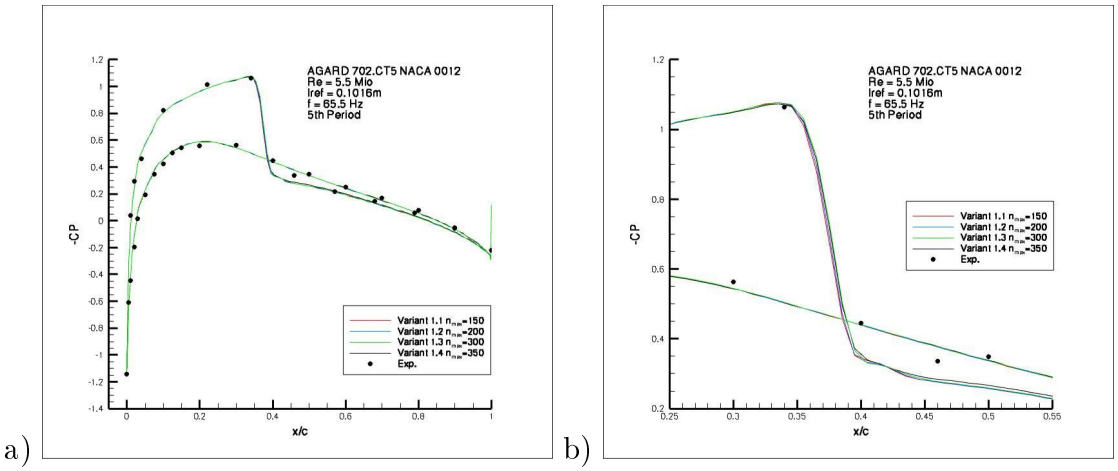

Figure 4.11: a)$-c_P$-distribution Variants 1.1-1.4 with n_{max}, b)Zoom-in on shock region

Now, in a further test for the acceleration of the calculations, the cheapest parameter setting in time is combined with a setting which delivers a better accuracy of the results. Thus, for the initialization of the run, a portion of a *quick* setting is calculated, i.e. Variant 1.4 (black line in Figure 4.12-a), and the rest is performed with an *accurate* setting, i.e. Variant 1.1 (red line in Figure 4.12-a). As in the other calculations, a total of 5 physical cycles are calculated.

With the first variant, an initial approximation of the solution is achieved and initial disturbances are propagated out of the flow field. After this initialization of the flow, the second variant improves the quality of the results giving a better agreement with the reference values (see Fig. 4.12-a). This can also be observed in the residuals history at the transition point from Variant 1.4 to Variant 1.1 in Fig. 4.12-b. The left side in Fig. 4.12-b depicts the residuals from the first variant with a reduction of the density residuals partly just under one order of magnitude (red line in the figure) but with a poor resolution of the periodic development of the lift coefficients (blue line in the figure). On the right side of the figure, comparisons based on Variant 1.1 show a better resolution of the periodic development of the lift coefficients and a larger reduction of the density and turbulence (black line in the figure) residuals.

a) 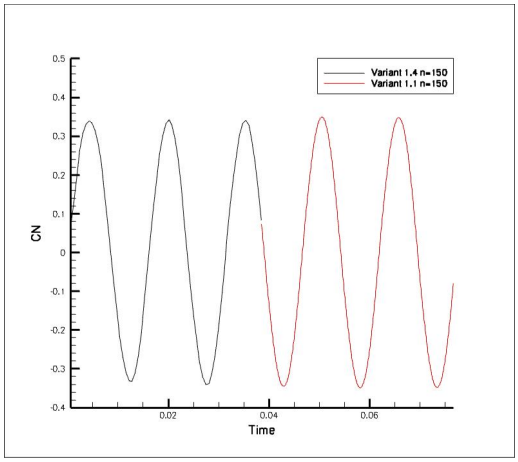

b) 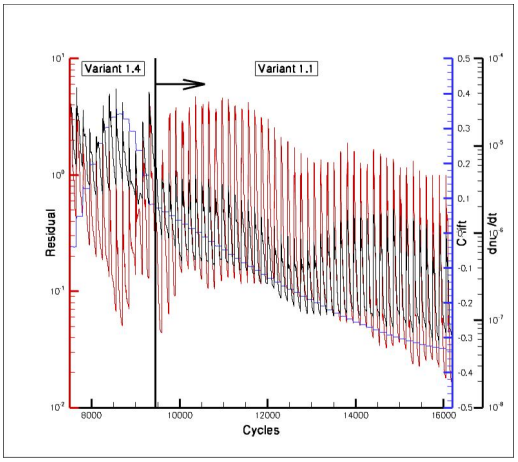

Figure 4.12: a) C_N as function of time for Variant 1.4-1.1 b) Transition of the residuals in Variant 1.4-1.1

With this method, the calculation time can be reduced to almost half of the reference time using a constant time step as in the first variants attempted. Figures 4.13 and 4.14 show the results of this approach. Here the initialization of the run for all the calculations is performed with Variant 1.4 using 150 inner iterations, and it is completed with Variants 1.1 and 1.2 with variation of the inner iterations until a convergence of C_{Nmax} as a function of the inner iterations is achieved.

Figure 4.13, which plots the CPU-time as function of the inner iterations per physical cycle, shows that Variant 1.4-1.1 reduces the calculation time by almost 45% compared with the reference, while Variant 1.4-1.2 by approximately 60%. The assessment of the quality of the results is depicted in Figure 4.14. The C_{Nmax}-values vary approximately 0.08% and 0.18% respectively for Variants 1.4-1.1 and 1.4-1.2 compared with the reference. These deviations of the results are minimal

and confirms that the method delivers better results than using a constant time step, since the time needed for the calculations is notably reduced without affecting the quality of the results.

Nevertheless, this statement should be confirmed with the following 2-D and 3-D cases studied in the present project. For this purpose, the same methodology described in this section is applied for Cases 2-4.

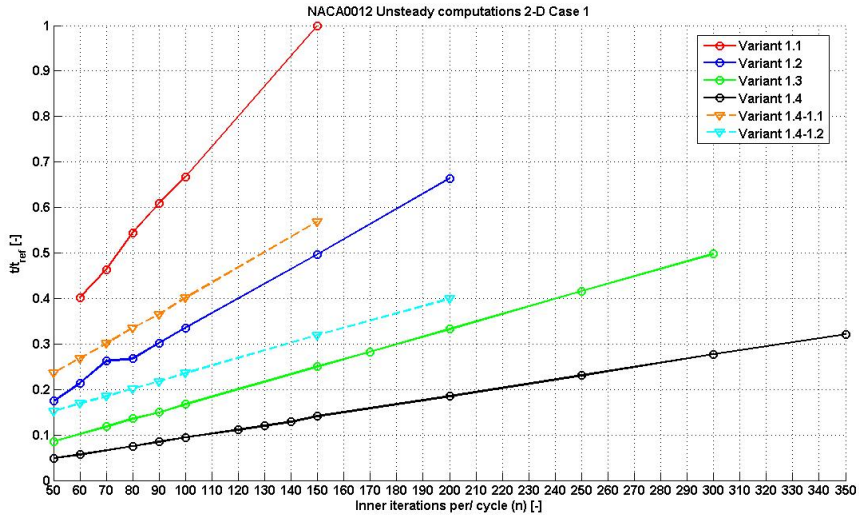

Figure 4.13: CPU-time for Variants 1.4-1.1 and 1.4-1.2

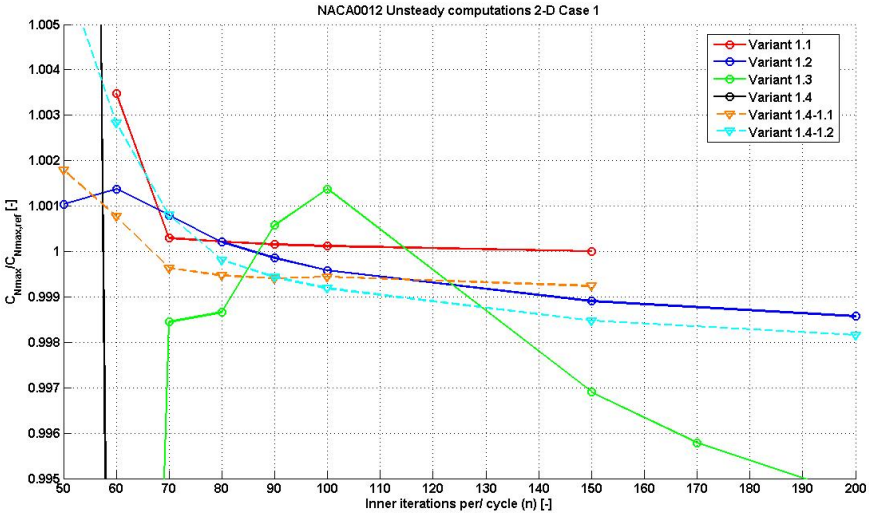

Figure 4.14: C_{Nmax}-values for variants 1.4-11 and 1.4-1.2

4.2 Case 2: Laminar Flow over a Circular Cylinder

The second case analyzed is focused on the unsteady laminar flow over a circular cylinder. The inflow is uniform with a Mach number of 0.2 and a Reynolds number of 150. At this Reynolds number, the flow is essentially laminar with periodic vortex pairs shed from the downstream side of the cylinder.

The physical parameters of the simulation are listed below, as they appear in the DLR Tau-script:

Reference Mach number	0.2
Angle of attack	0.0°
Reynolds number	150
Reference Temperature	277.78 K
Prandtl number	0.72
Sutherland constant	110.4
Sutherland reference viscosity	$1.716 \cdot 10^{-5}$

4.2.1 Grid Generation

The cylinder has a diameter $d = 1.0$ m. The hybrid grid concentrates a structured grid in the vicinity of the wall with quadrilateral elements and triangles outside the boundary layer. A refinement over ten diameters downstream of the body is performed in order to get a good resolution of the expected vortex street in the wake flow. The structured grid has an initial layer thickness of 5.022 mm with 20 prismatic layers and a stretching factor of 1.175. This yields a maximum Y^+- value of 0.3 and a minimum Y^+- value of 0.05 (see Fig. 4.15). For the grid generation, one half of the total grid domain was generated and mirrored along the x axis exploiting the symmetry of the geometry. The complete input files used in *CentaurSoft* for the grid generation are listed in Appendix A.2. The total grid comprehends 24, 572 points.

4.2.2 Numerical Parameters for the Unsteady Simulation

A central scheme is applied for the convective RANS flux discretization, with scalar dissipation for stability using the values for the coefficients $\epsilon^{(2)} = 1/2$ and $\epsilon^{(4)} = 1/64$. Temporal discretization is done using the dual time stepping scheme in combination with a 3 stage Runge-Kutta time integration method. A 3v Multigrid cycle is

a) 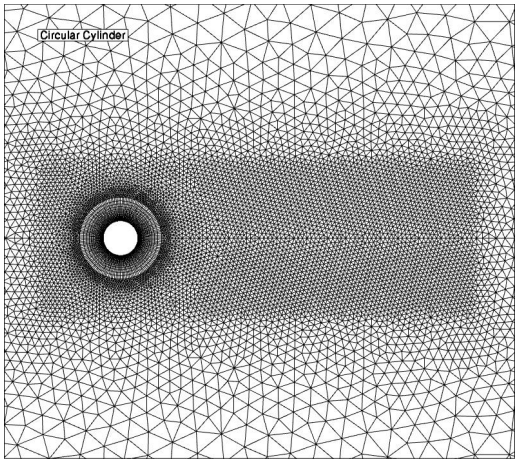

b) 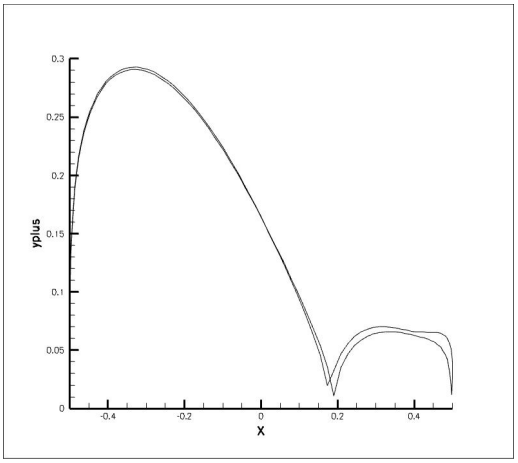

Figure 4.15: a) Cylinder hybrid mesh, b) Y^+ distribution

applied for convergence acceleration and a CFL number of 1.0 is set. The run is performed using the 1-equation turbulence model of Spalart-Allmaras with Edwards modification. The numerical solutions are generated based on the DLR TAU-Code version 2007.1.0. The complete setting of parameters used in TAU for the simulation are listed in Appendix A.2.

Unless otherwise specified, the default parameters are used for the computations. All the calculations were performed on the same Intel Pentium IV Workstation using a 3.00 GHz processor.

4.2.3 Results

For this case, the same strategy is followed as in section 4.1. According to [20], for these flow conditions, the dimensionless frequency of the vortex shedding, called Strouhal number, should be equal to 0.18. With this, the frequency of the periodic shedding vortex street downstream of the cylinder can be calculated with the definition of the Strouhal number

$$Sr = \frac{f \cdot d}{V}. \tag{4.6}$$

With a reference velocity of $V = 66.8284 m/s$, the frequency results to $f = 12.029$ Hz, giving a period $T = 0.08313 s$. In order to have a good accuracy of the results, a time step size of $5 \cdot 10^{-4} s$ is chosen which leads to 166.26 time steps per period, and 100 inner iterations for each time step. To reduce the time needed for the calculation to get the periodic-state solution of the aerodynamic coefficients, an initialization of the flow is performed with a steady calculation. For this, TAU is run using

an explicit 3 stage Runge-Kutta time stepping scheme for 5000 cycles. After the initialization of the flow, 1.5 seconds in physical time are calculated.

Figure 4.16 shows the C_L- and C_D-values which correspond to the lift (black lines in the figure) and drag (red lines in the figure) coefficients respectively as a function of the time. The computations with and without initialization of the flow are compared, and they show a considerable difference in the time needed to get the periodic-state of the flow. It can be observed, that the variant without initialization needs 2.5 seconds until a periodic-state is achieved, while the variant with initialization needs only 0.5 seconds. Fully periodic fluctuations in the force and drag coefficients are obtained after 0.8 seconds. The period between the lift peaks can be extracted as $T = 0.083167$, resulting in a Strouhal number of $Sr = 0.17875$, which differs by about 0.69% from the value specified in [20] for the experimental analysis.

a) 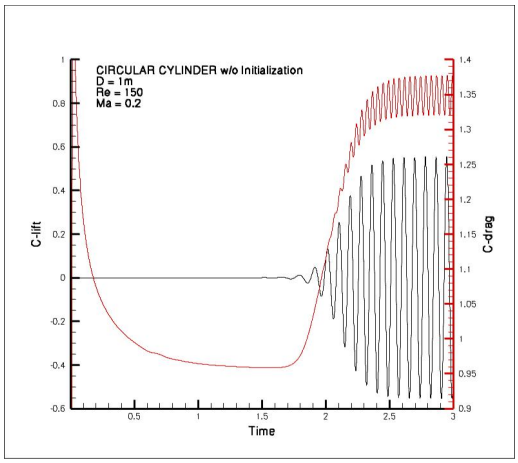

b) 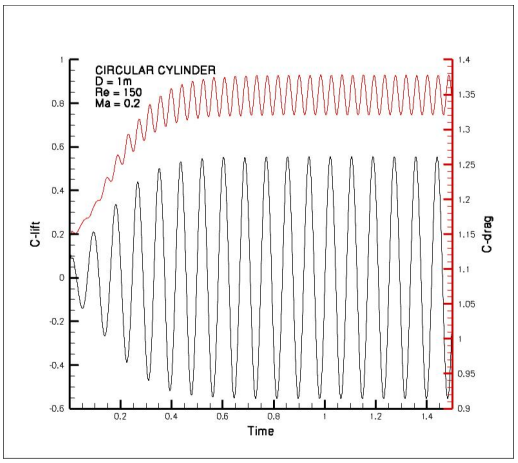

Figure 4.16: Periodic development of the aerodynamic coefficients a) without initialization, b) with initialization of the flow

Figure 4.17-a displays the isotachs after $t = 1.5$ seconds, which show the von Kármán shedding vortex street downstream of the cylinder. Here it can be observed how the boundary layer separates from the surface and becomes highly unstable. This instability emerges as the shear layer vortices shed from both the top and bottom surfaces interact with one another. They shed alternatively from the cylinder and generate a regular vortex pattern in the wake [20].

The boundary layer separates at an angle of separation $\phi_S \approx 98°$ in clockwise direction from the stagnation point located at 0 degrees as shown in Figure 4.17-b. There, it can be observed how the stream lines separate from the surface contour due to the adverse pressure gradients on the downside of the cylinder. At this point, the reverse flow coming from the lower side of the circumference gives rise to a vortex,

whose size is increased still further. Similar phenomena occur at the lower side at an angle of approximately $\phi \approx 215°$ of the circumference at the vortex core position. The vortex detaches shortly afterwards and moves downstream of the body, forming the vortex pattern which move alternately clockwise and counterclockwise as observed in Figure 4.17-a. In the range of dimensionless frequency of the vortex shedding $0.14 < Sr < 0.21$ no experimental information about the angle of separation is available, but it can be assumed to be in a range between $80° < \phi_S < 115°$ according to the information provided in [20]. According to [20], for a flow condition with $Re = 90$, in a laminar flow with stable wake, the separation of the boundary layer occurs at an angle $\phi_S \approx 115°$. For flows with Reynolds number up to 150 in the sub-critical range with instabilities in the vortex street, the separation of the boundary layer is expected at an azimuthal angle $\phi_S \approx 80°$.

a) 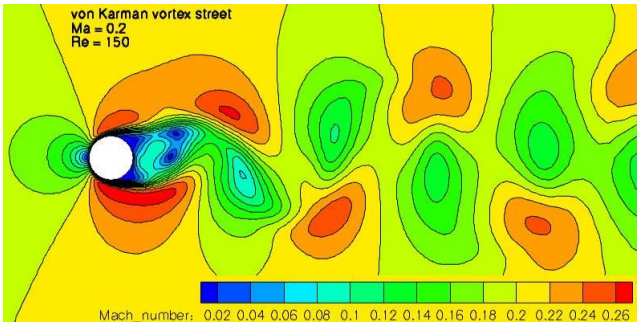

b) 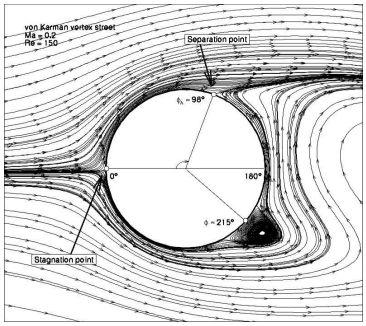

Figure 4.17: a)Mach number contours showing the von Kármán vortex street, b)Stream lines after $t = 1.5$ sec showing the stagnation and separation point around the circular cylinder

As in section 4.1, the residual convergence history is also monitored. The density residuals shown in Figure 4.18 as a black line decrease more than one order of magnitude, while the turbulent residuals shown as a red line, are reduced by almost 5 orders of magnitude. The periodic development of the lift coefficients (blue line in the figure) shows a plateaued distribution with a sufficient convergence of the values for each time step.

Since the residuals fulfill the stability- and accuracy criteria, and the non-dimensional frequency accords reasonably with [20], the results obtained are taken as the point of reference for the present case.

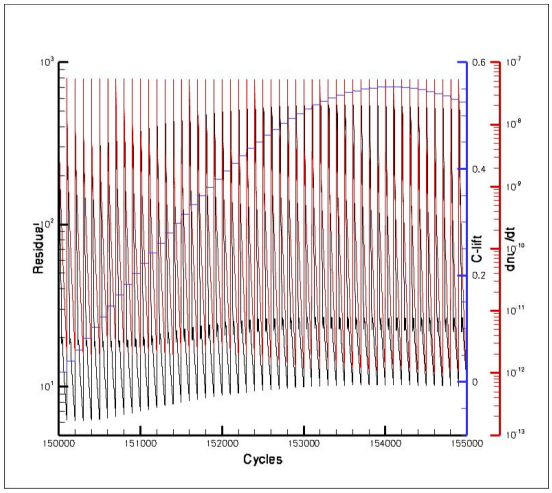

Figure 4.18: Residuals convergence history after $t = 0.75$ sec

Variation of the Relevant Parameters of the Dual Time Step Scheme

In addition to the validation results, 5 more settings of parameters are calculated with variations of the physical time step size per period. These variants are listed in Table 4.2.

The CPU-Time needed for the calculations in this case is much longer than in the first case. To calculate 1.5 seconds, i.e. for the reference variant, with a time step size of 0.0005 seconds and 100 inner iterations per time steps, a total of 300000 iterations need to be performed. This exemplifies the cost needed for each calculation.

	time step size per physical cycle [s]	time steps per physical cycle [-]
Variant 2.1	0.0005	166.26
Variant 2.2	0.001	83.13
Variant 2.3	0.002	41.57
Variant 2.4	0.003	27.71
Variant 2.5	0.004	20.78
Variant 2.6	0.005	16.63

Table 4.2: Setting of parameters performed for Case 2

Figure 4.19 depicts the CPU-Time results as a function of the inner iterations per time step for Variants 2.1 to 2.6. Here, the time for the different variants was normalized by the time $t = 115397.1[s]$ required in Variant 2.1.

As expected, a linear development of the CPU-Time is observed. The cheapest calculation resulted for Variant 2.6 (light blue line in Figure 4.19) which reveals a reduction of 85% of the calculation time compared with the reference setting of

parameters (black line in Figure 4.19) at the settings with the most number of inner iterations.

Despite being the cheapest variant in time, the results obtained in Variant 2.6 show a difference in the C_{Lmax}- values of 10.23% compared with the reference variant, and even a shift in the global distribution of the dynamic coeffcients, resulting in a shift of the vortex shedding frequency. This is observed in Figures 4.20 and 4.21 where the C_{Lmax}- values were normalized by the $C_{Lmax,ref}$- value obtained in Variant 2.1 ($C_{Lmax,ref} = 0.55543$). The differences in the Strouhal number are depicted in Figure 4.22. The Strouhal numbers are normalized by the reference given in the experiments in [20].

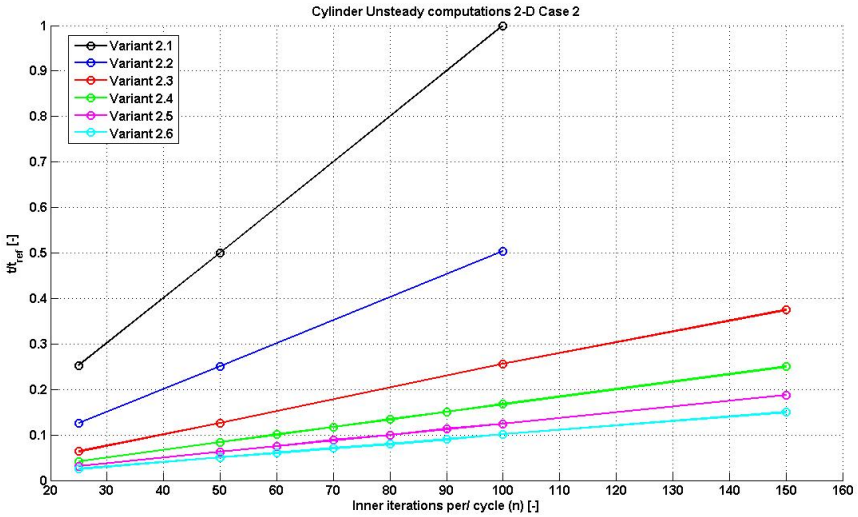

Figure 4.19: CPU- time as function of inner iterations per time step

The same methodology for the acceleration of the unsteady simulations used in section 4.1 is applied. After the initialization of the flow with a steady calculation, 0.75 seconds using the parameters in Variant 2.5 are computed. After this, the rest of the calculation is performed with the parameters of Variants 2.1 and 2.2. As in the initial calculations, a total of 1.5 seconds are simulated.

Figure 4.23-a shows the C_L and C_D coefficients for the complete run performed with Variant 2.5 (left side in the figure) and 2.1 (right side in the figure) with 100 inner iterations. Variant 2.5 approximates the values of the coefficients and accelerates the adaptation of the flow towards the final periodic state. After an initial convergence of the values due to the first variant, the results are improved by running the simulation with the parameters in Variant 2.1. Figure 4.23-b plots the convergence behavior of the initial setting which shows a reduction of the density

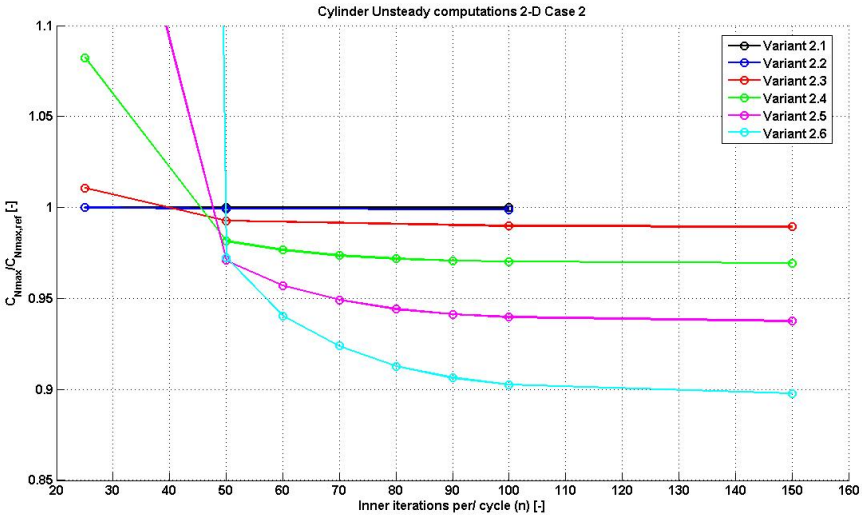

Figure 4.20: C_{Lmax} as function of inner iterations per time step

a)

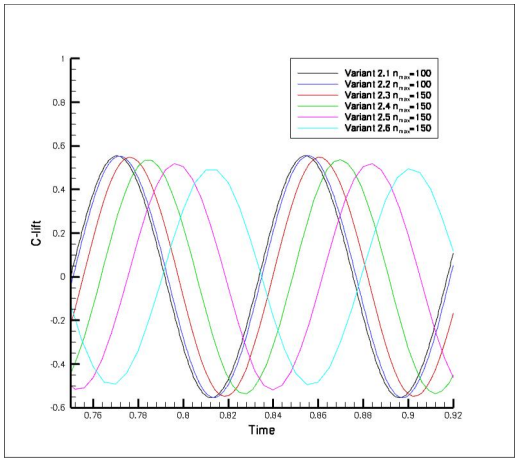

b)

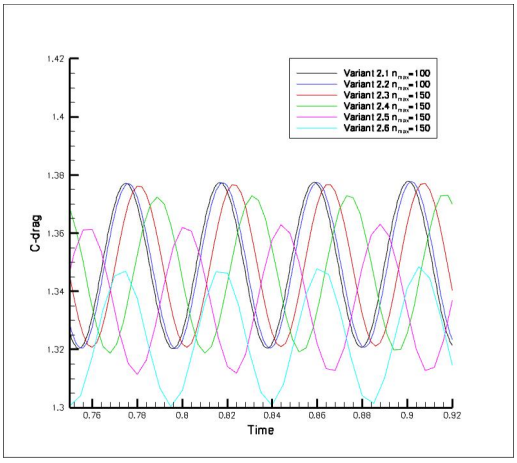

Figure 4.21: a) C_L and b) C_D as function of time at $0.75s \leq t \leq 0.92s$

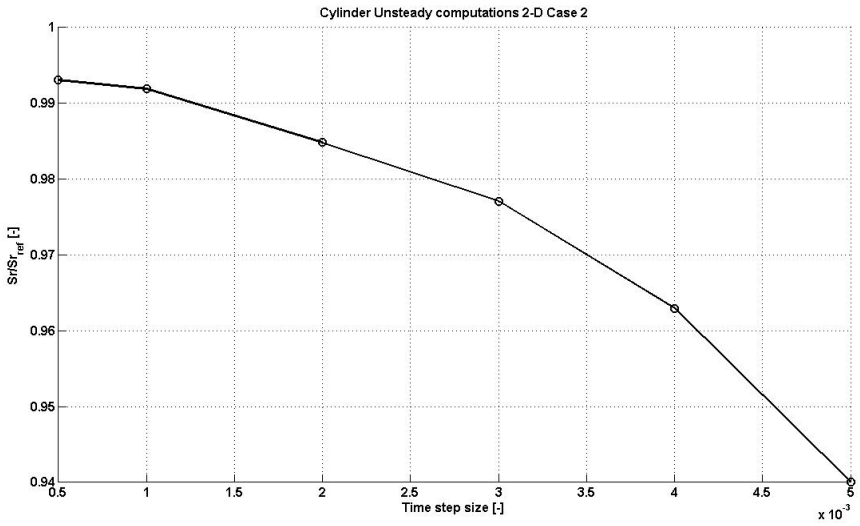

Figure 4.22: Strouhal number as function of time step size

residuals (black line in the figure) of almost one order of magnitude, while Variant 2.5 shows a reduction of almost 2 orders of magnitude for each physical time step Δt.

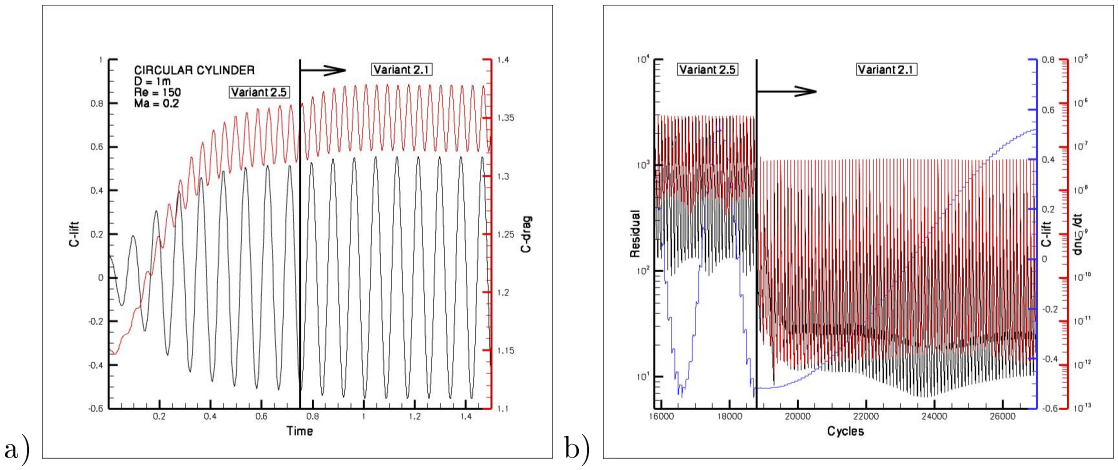

Figure 4.23: a) C_L and C_D as function of time for Variant 2.5-2.1 b) Transition of the residuals in Variant 2.5-2.1

As observed in section 4.1, the CPU-time for the calculation is reduced by using a variable time step through the modification of the parameters from a *quick* to an *accurate* parameter setting. In this case for the Variant 2.5-2.1, the reduction of the CPU-time is approximately 45% with a deviation of C_{Lmax} of approximately $|\Delta C_{Lmax}| = 10^{-04}$ among the settings with constant time step size values and the ones with variable time step size. These results are depicted in Figures 4.24 and 4.25.

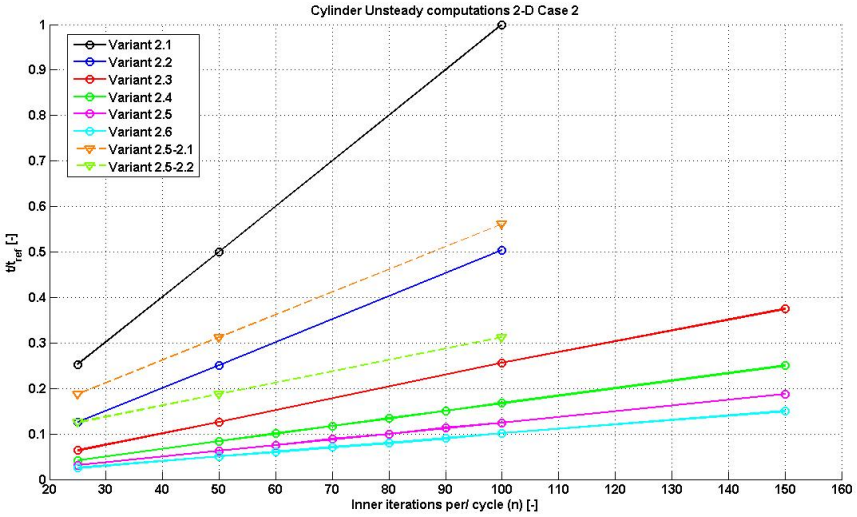

Figure 4.24: CPU-time for Variants 2.5-2.1 and 2.5-2.2

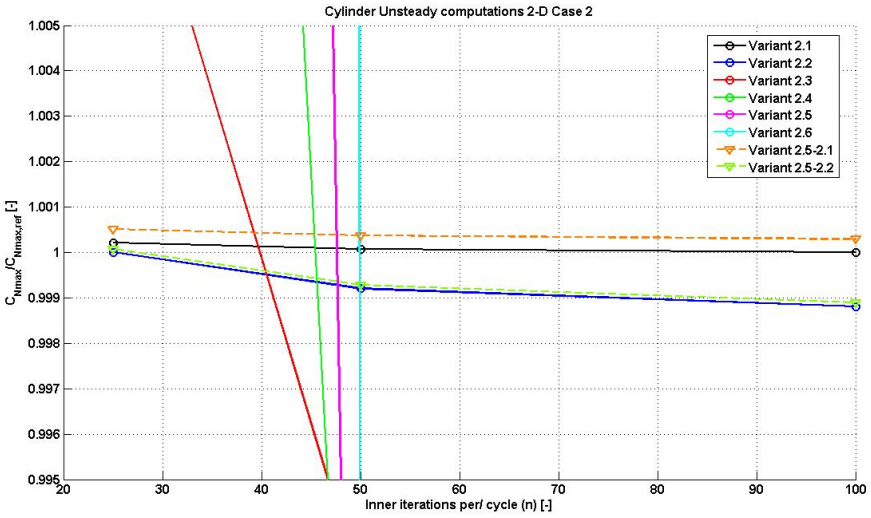

Figure 4.25: C_{Lmax}- values for Variants 2.5-2.1 and 2.5-2.2

With this case, it was confirmed that varying the parameter settings from a *quick* calculation to an *accurate* calculation, by changing the time steps per period and the number of inner iterations, the time needed for the simulations can be reduced by almost 50% compared with the time necessary for the simulations with constant parameter settings without adversely affecting the accuracy of the results. Furthermore, the advantages of an initialization of the flow through a steady simulation were clearly illustrated. The experiences obtained in the 2-D cases will be adopted for the 3-D cases to be examined in Chapter 5.

Chapter 5

3-D Cases

5.1 Case 3: Pitching Oscillation of the DLR-F12 Transport Aircraft Configuration

The first 3-D case investigated is the DLR-F12 wind tunnel model of a transport aircraft configuration of Airbus type (Fuselage, Wing, HTP, VTP) . The case studied is for an oscillatory pitch movement around the axis located at the coordinates [1.04882, 0.0, -0.03029] in a cartesian coordinate system with origin at the model nose (see Figure 5.2). The flow represents a subsonic flow with a reference velocity of $V = 70\text{m/s}$. The oscillatory movement is described by change of the angle of attack α according to Eq. 4.1. The simulation parameters correspond to test conditions described in [12], where an investigation of unsteady dynamic derivatives for transport a/c is performed.

The physical parameters of the simulation are listed below, as they appear in the DLR-Tau script:

Reference Velocity	70 m/s
Angle of attack α_m	0.0°
Fourier coefficient for rotation pitch α_0	4.5°
Frequency f	3 Hz
Reduced frequency for rotation k	0.0680267
Reynolds number	$1.18 \cdot 10^6$
Reference Temperature	293.15 K
Sutherland constant	110.4
Sutherland reference viscosity	$1.716 \cdot 10^{-5}$

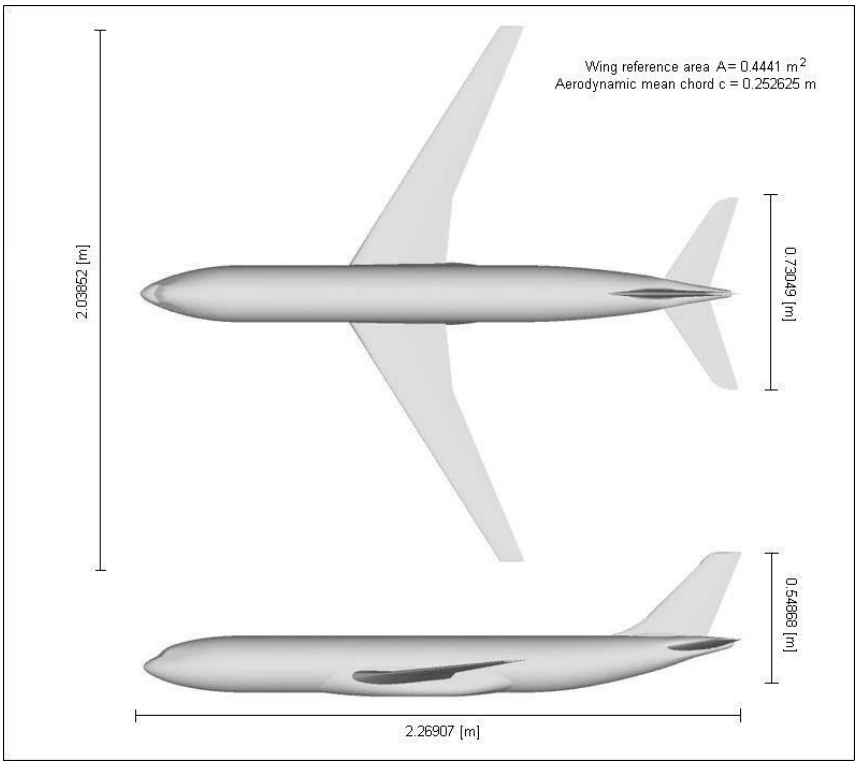

Figure 5.1: DLR-F12 aircraft configuration geometry

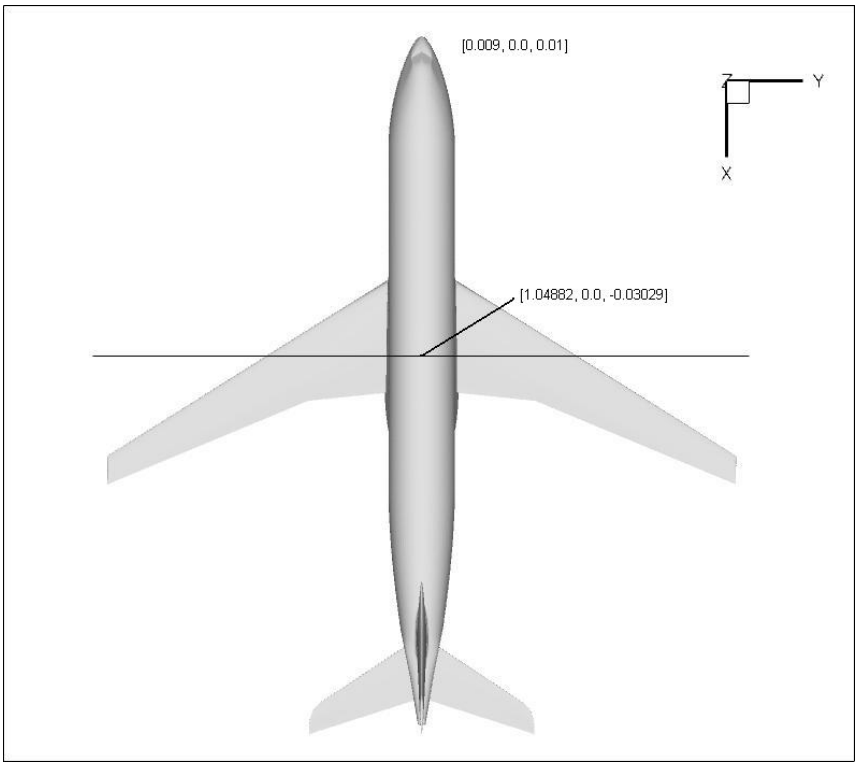

Figure 5.2: DLR-F12 aircraft configuration pitch axis

5.1.1 Grid Generation

The computational model treats half of the aircraft configuration with a symmetry plane along the cartesian coordinates xz. For this case, yaw- and roll motions are not simulated, thus the symmetry assumption should have no major influence on the results obtained. Furthermore with the simulation of only half of the model, a reduction in the dimensions of the grid is achieved, and with it a reduction of the calculation time. The grid generated is a hybrid grid with structured prismatic elements in the vicinity of the wall, and tetrahedral elements outside of the boundary layer. The structured grid has an initial layer thickness of 0.005 mm with 30 prismatic layers and a stretching factor of 1.2. The complete input files used in *CentaurSoft* for the grid generation are listed in Appendix A.3. The total grid has $5,983,556$ computational nodes.

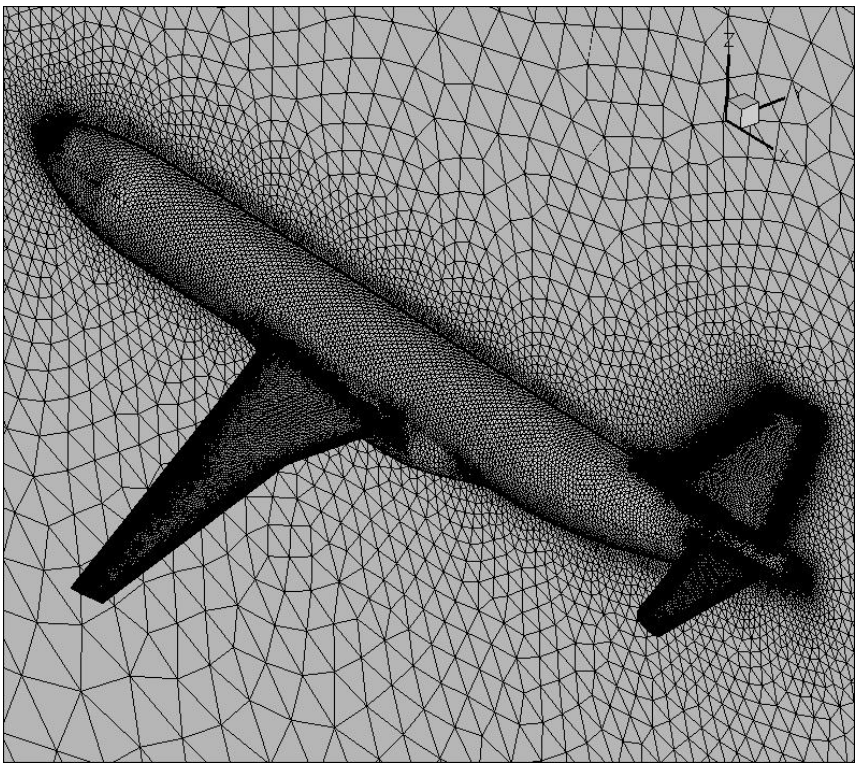

Figure 5.3: DLR-F12 unstructured mesh

For a first validation of the grid and the flow conditions, a steady simulation of the flow was performed to calculate the drag polar for the α-range between $-5°$ and $5°$, with a velocity $V = 70$ m/s and a Reynolds number $Re = 1.18$ Mio. The computation was performed on the DLR HPC-cluster (Gauss) with 24 processors distributed on 12 computational nodes. The cluster consists of 210 computational nodes with a total of 516 processors and 1 Tera-byte main memory resulting in a

performance of 2.5 Tera-FLOPS . The system is based on a Server-Serie Sun Fire V20z system using V20z and X4100 Opteron-Type processors from AMD [33].

The numerical solution was generated using TAU 2007.1.0. The run was performed using the 1-equation turbulence of Spalart-Allmaras with Edwards modification. Spatial discretization is done using a central scheme in combination with a 3 stage Runge-Kutta scheme for time integration. A 3v multigrid cycle is also applied, and a total of 5000 iterations are calculated.

The residuals convergence history depicted in Figure 5.4 shows a full convergence of the relevant aerodynamic coefficients C_L as the red line, and C_D as the blue line after 5000 cycles for the angle $\alpha = 0°$ and approximately 2500 for all other angles of attack. The density residuals shown as a black line in Figure 5.4 also show a good degree of convergence, with a reduction of almost 3 orders of magnitude. The peaks appear due to the restart with a different angle of attack α.

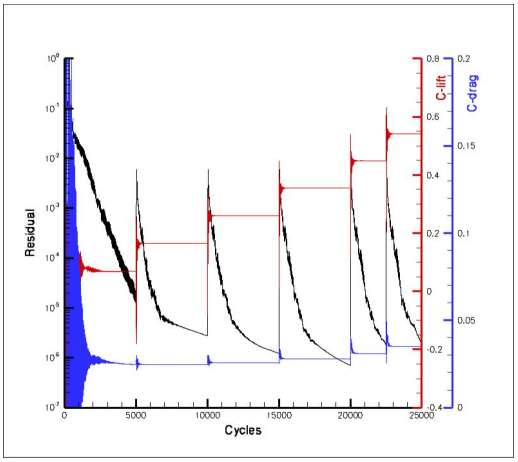

Figure 5.4: Steady convergence history for the range $0° \leq \alpha \leq 5°$

Figures 5.5-a and 5.5-b show the results for the Y^+-contours on a top/bottom view of the model at $\alpha = 0°$. These values represent a range between 0.005 and 2.5, which allows for a good resolution of the flow in the boundary layer at the vicinity of the wall. The lowest Y^+-values (in blue) are observed in the wing-fuselage and HTP-fuselage junctions.

As a small validation of the results, the pressure distribution at the spanwise positions of $\eta = 0.457$ for the wing and at $\eta = 0.171$ for the HTP are extracted for the simulation at $\alpha = 0°$. To get the values η, the position of the cuts in y- direction were normalized by the half wingspan width $b/2 = 1.01926$ m. The position of the cuts is shown in Figures 5.6 and 5.7, where also the pressure coefficient contours at the surface are illustrated. In Figure 5.8 the c_P distribution along the wing and HTP

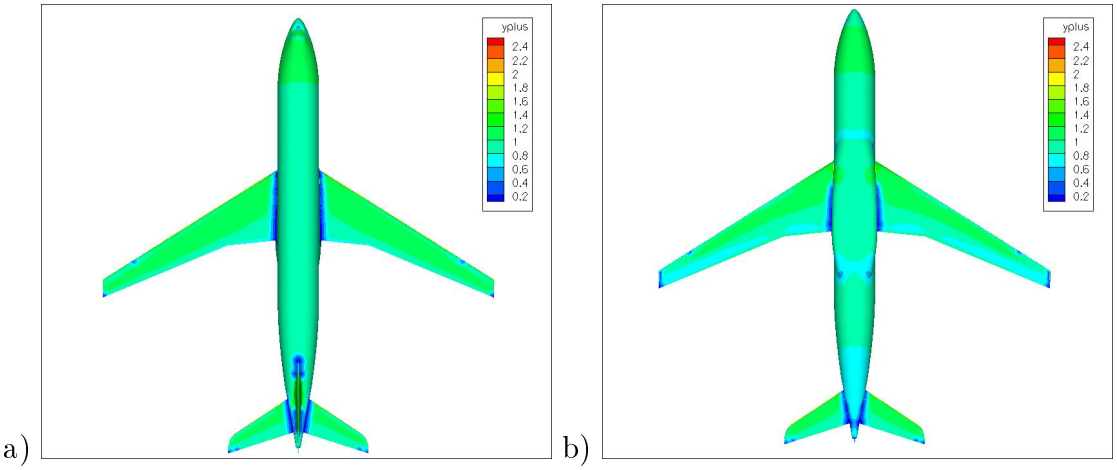

Figure 5.5: Y^+- values top/bottom view, Re=1.18 Mio, V=70 m/s, $\alpha = 0°$

chords are compared with experimental values from WTT data and with previous results obtained in [12]. The results accord reasonably well with the experiments and show nearly no differences with [12].

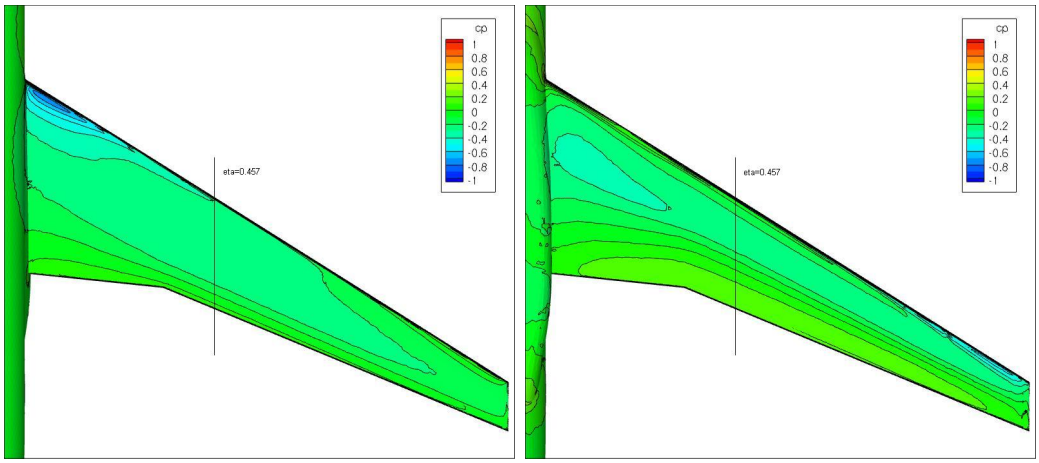

Figure 5.6: c_P contours and position of the cut at $\eta = 0.457$ top/bottom view, Re=1.18 Mio, V=70 m/s, $\alpha = 0°$

The lift and drag polars are depicted in Figure 5.9, where the coefficients are compared with WTT values reported in [12]. The lift coefficients show good accordance with the experiments, however a very slight difference of the gradient $dC_L/d\alpha$ between experiment and simulation is observable. The drag polar shows an under prediction of approximately 20 drag counts (dc=10^{-4}) versus the experiments at $\alpha = 0°$ and almost 100 drag counts for $\alpha \leq -5°$. These deviations between the C_D-values could be reduced by adapting the grid in order to have a better representation of the induced drag at high α-angles (see [4]). Nevertheless, the grid was found to be suitable for the analysis planned on the present study.

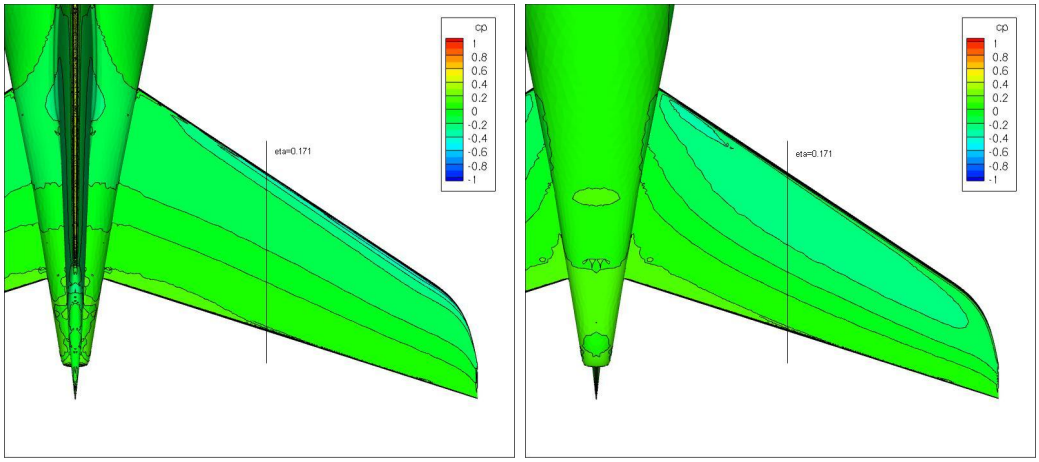

Figure 5.7: c_P contours and position of the cut at $\eta = 0.171$ top/bottom view, Re=1.18 Mio, V=70 m/s, $\alpha = 0°$

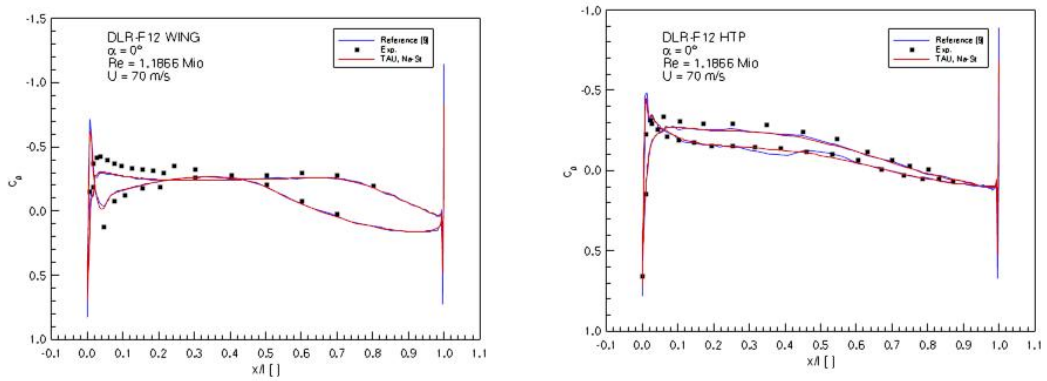

Figure 5.8: DLR-F12 c_P distribution at $\eta = 0.457$ from wing and $\eta = 0.171$ from HTP, Re=1.18 Mio, V=70 m/s, $\alpha = 0°$

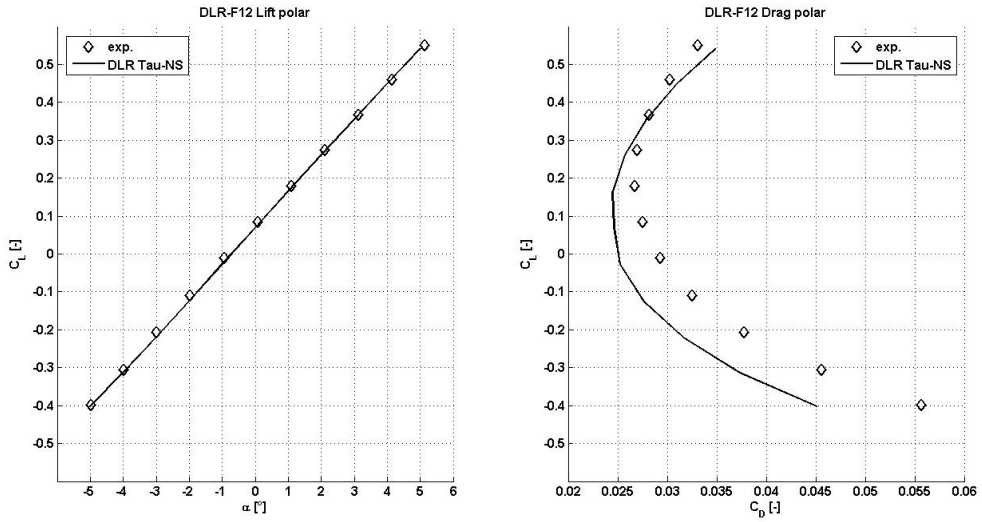

Figure 5.9: DLR-F12 lift and drag polars, Re=1.18 Mio, V=70 m/s

For the unsteady calculations, the steady solution at $\alpha = 0°$ is used as a restart, which serves as an initialization of the flow and should speed up the achievement of a periodic state, as discussed in the previous cases.

5.1.2 Numerical Parameters for the Unsteady Simulation

The purpose of the present investigation, is the acceleration of the simulations by varying the number of physical time steps and the number of inner iterations for each time step. All other numerical parameters are retained unvaried. A central scheme is applied for the convective RANS flux discretization, using matrix dissipation for stability. Temporal discretization is done using the dual time-stepping scheme in combination with a 3 stage Runge-Kutta approach. A 3v multigrid cycle is applied for convergence acceleration and a CFL number of 1.0 for the calculation of the pseudo-time step is set. The run is performed using the 1-equation turbulence model of Spalart-Allmaras with Edwards modification. The numerical solutions are generated based on the DLR TAU-Code version 2007.1.0. The complete setting of parameters used in TAU for the simulation are listed in Appendix A.3.

Unless otherwise specified, the default parameters are used for the computations. All the calculations were performed on the Gauß-cluster with 24 processors distributed in 12 computational nodes.

5.1.3 Results

Because of the dimensions of the grid, the cost of the calculations is higher than in the 2-D cases treated here. For the 3-D cases, the first step is to find a combination of parameters which deliver a good accuracy of the results. The first trial is a variant with the numerical settings mentioned above with 360 time steps per physical period and 150 inner iterations. This variant represents the longest simulation to be performed, and sets the limit for the total number of inner iterations.

An analysis of the results obtained with the first variant, showed that these parameters do not deliver stable results and no accurate representation of the periodic development of the relevant aerodynamic coefficients could be obtained. The number of inner iterations per cycle proved to be too low for an adequate resolution of the periodic coefficient development. The next variant studied was a setup with 180 time steps per period and 300 inner iterations. This parameter setting is equivalent to the previous calculation in terms of total iterations and time. Despite delivering

better results with a better resolution of the coefficients, the simulation becomes unstable around the fourth quarter of the second oscillation period, where especially the periodic C_D development shows big fluctuations. The best results were obtained for a parameter setting with 90 time steps and 600 inner iterations. This number of inner iterations per time step is enough for an overall convergence of the results in each time step.

Table 5.1 and Figure 5.10 show the results obtained for the first three setups of the parameters. In Table 5.1 the parameters for each variant are listed with the respective time needed for the simulation to complete 2 periodic cycles. It can be observed, that despite having the same number of total inner iterations, the times needed for the calculations with the setting in Variants 3.1 and 3.3 differ considerably from Variant 3.2. Figure 5.10 shows the results for the overall C_L (red line), C_D (blue line) and C_{my} (green line) coefficient developments as a function of the number of cycles, obtained through the normalization of the physical time t with the duration of the oscillation period T.

	time steps per physical cycle [-]	inner iterations per time step (n) [-]	CPU-Time after two cycles [s]
Variant 3.1	360	150	916 899.7
Variant 3.2	180	300	882 073.9
Variant 3.3	90	600	912 362

Table 5.1: Setting of parameters for Case 3

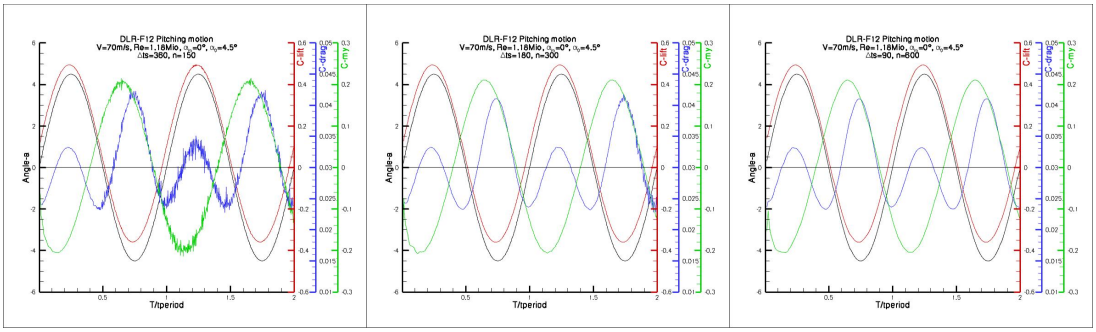

(a) Variant 3.1 (b) Variant 3.2 (c) Variant 3.3

Figure 5.10: Periodic distribution of the aerodynamic coefficients for 3 different parameter settings

Variant 3.3 presents the most stable simulation, since the periodic development of the relevant aerodynamic coefficients shows the fewest erratic oscillations. For these parameter settings, one more physical period was calculated to simulate a total of three physical periods. The results of the simulation show a periodic development

of the relevant force coefficients after 3 physical cycles. Figure 5.11 shows the C_L- and C_m-values which correspond to the lift and pitching moment coefficients plotted as a function of the angle of attack α for each physical cycle.

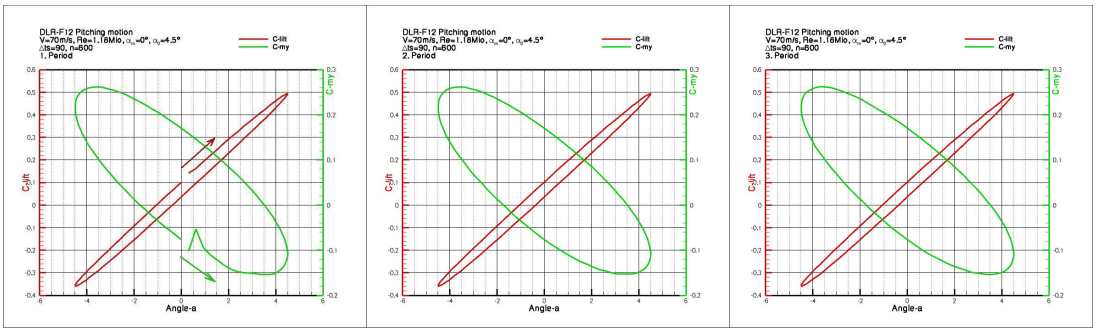

(a) 1st Cycle (b) 2nd Cycle (c) 3rd Cycle

Figure 5.11: $C_L - \alpha$ and $C_m - \alpha$ results for Variant 3.3 after 3 physical cycles

The results obtained were compared with experimental results reported in [12]. For the third physical cycle the computed periodic development of the lift coefficient agrees reasonably well with the experiments in the last half of the cycle and show slightly greater differences in the first half of the cycle. These results are depicted in Figure 5.12, where also the results for the C_D and C_{my} developments are shown. The computed C_{my} evolution agrees with the experiments with slight differences in the amplitude of approximately $|\Delta C_{my}| \approx 0.018$. For this case no experimental information about the periodic behavior of the drag coefficients is available.

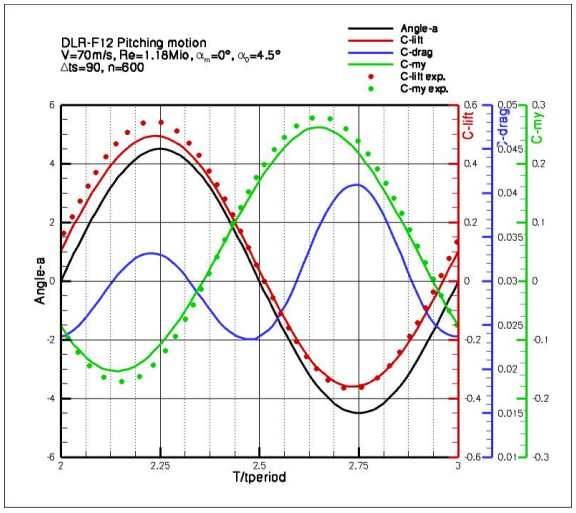

Figure 5.12: DLR-F12 periodic distribution of the aerodynamic coefficients compared with experiments reported in [12]

To ensure that the inner iterations for each physical time step are sufficient, the convergence history of the density and turbulence residuals as function of the number

of inner iterations are checked. Figure 5.13 shows the density residuals as a green line and the turbulence residuals as a black line, as well as the lift convergence history as the red line for the first half of the 2nd period. The residuals are reduced by more than one order of magnitude which ensures a sufficient accuracy of the solution [3]. It can be observed also, that the lift coefficient converges in each physical time step creating the typical plateaued distribution of the aerodynamic coefficients of an unsteady numerical calculation.

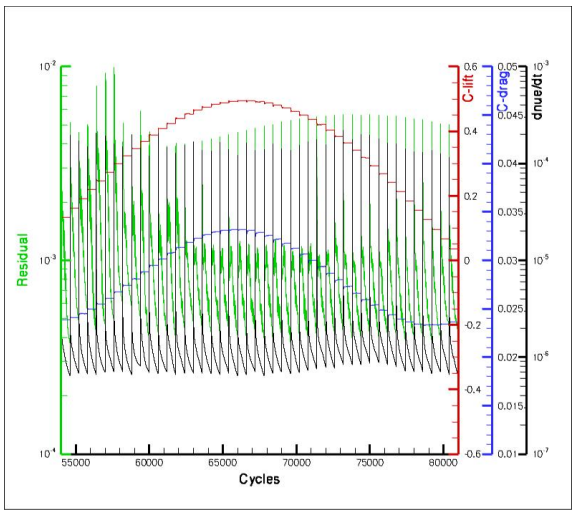

Figure 5.13: DLR-F12 residuals convergence history at the beginning of the 4th Period

For the purpose of the parameter analysis for the acceleration of the simulations with the dual time-stepping scheme, the obtained results with these settings show sufficient accuracy, and can thus be taken as a reference in the present case.

Variation of the Relevant Parameters of the Dual Time Step Scheme

In Cases 1 and 2, it could be demonstrated that the use of variable time steps reduce the time needed for the simulations considerably. For this case, three calculations with *quick* initial parameter settings are performed as a restart from the steady computation. With these parameters, one and a half physical periods are calculated before an *accurate* parameter setting is adopted for the remainder of the simulation through the 3rd physical period. The variants performed for the initialization of the unsteady calculation are listed in Table 5.2.

After the initialization of the unsteady simulation, all the simulation variants listed in Table 5.2 were continued with the parameter setting used in Variant 3.3. The development of the coefficients during the computations with the quick parame-

	time steps per physical cycle [-]	inner iterations per physical cycle [-]
Variant 3.4	90	300
Variant 3.5	45	600
Variant 3.6	45	300

Table 5.2: Setting of parameters for the initialization of the unsteady flow

ter setting show notable erratic fluctuations, in particular for the drag (see Fig.5.14). At 1.5 periodic cycles, the parameters were switched to the ones used in the reference parameter setting. The calculation then requires approximately 0.6 cycles to achieve the force developments obtained in the reference with Variant 3.3. Figure 5.14-a shows the C_L (in red), the C_D (in blue) and the C_{my} (in green) developments as function of the number of periods for Variant 3.4-3.3. In Figure 5.14-b, the values obtained are compared with the reference values shown as the dash-dotted black line for the last 1.5 cycles.

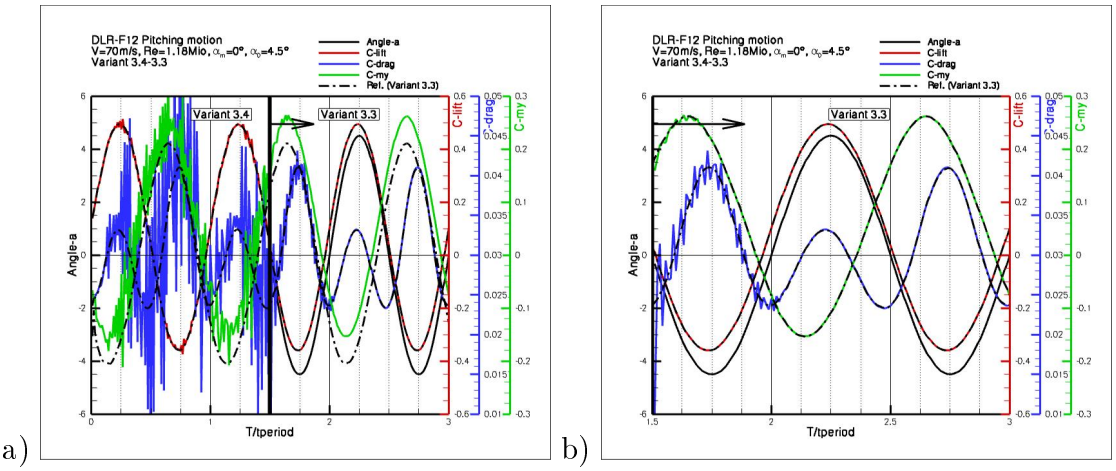

Figure 5.14: DLR-F12 force development with the use of variable time steps

After about 2.125 cycles, the variants with variable time steps, exhibit nearly no difference in the periodic coefficients versus the reference calculation. Figure 5.15 shows the development of C_L and C_{my} as a function of the angle of attack α for Variant 3.4-3.3 (dash-dotted lines in the figure) compared with Variant 3.3 (solid lines in the figure) for each physical cycle.

The advantage of the methodology is observed in Figure 5.16, where the normalized time is plotted as a function of the inner iterations for all the variants performed. The time was normalized by the reference computation time $t = 1362844.2$ seconds. The CPU-time needed to simulate 3 physical periods can be reduced by almost 40% using the Variant 3.6-3.3 combination compared with the reference calculation

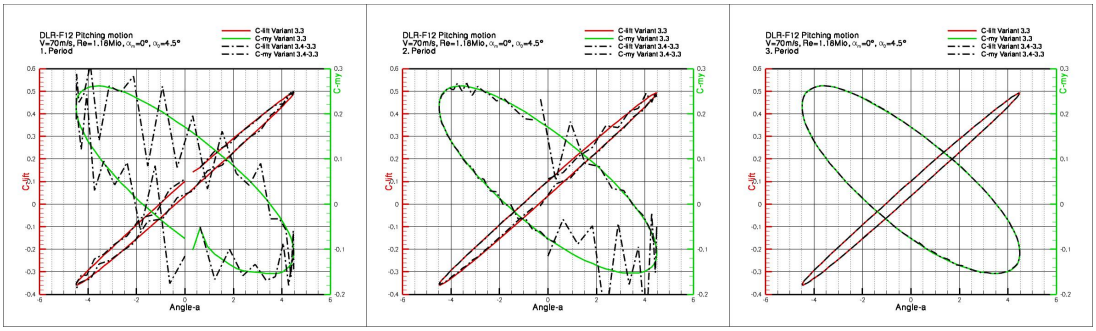

(a) 1st Cycle (b) 2nd Cycle (c) 3rd Cycle

Figure 5.15: $C_L - \alpha$ and $C_m - \alpha$ results for Variant 3.4-3.3 after 3 physical cycles

obtained with Variant 3.3 only.

The assessment of the quality of the result is depicted in Figure 5.17. The resulting maximum values of the relevant aerodynamic coefficients were normalized by the maximum values obtained in the reference calculation and are depicted in Figure 5.17 as a function of the inner iterations per time step. The maximum amplitudes of the lift coefficients plotted on the left in the figure, show the greatest difference of $|\Delta C_{Lmax}| \approx 0.0002$ between Variant 3.5-3.3 and the reference, which represents a deviation of approximately 0.04%. The C_D values show no difference between Var. 3.6-3.3 and Var. 3.4-3.3 which represent a variation of approximately 0.22% compared with the reference values. The maximum deviation of the pitching moment coefficients plotted on the right side in the figure, is observed between Variant 3.5-3.3 and the reference at 0.074%. As it can be observed, the deviations are minimal and can be neglected. This confirms that with the use of variable time steps, a considerable reduction of the CPU-time can be obtained also for more complex configurations as in Case 3. Even having a bad resolution of the representative periodic aerodynamic forces in the initialization of the unsteady simulation, the results can be improved by refining the resolution of the force developments through an accurate parameter setting. Furthermore, the time needed to improve the periodic behavior of the coeffcients after the unsteady-initialization is still lower than computing the full simulation with a constant computationally expensive parameter setting. Now the experiences obtained in the previous cases will be applied to Case 4, which represents the most expensive case to be examined in the present project.

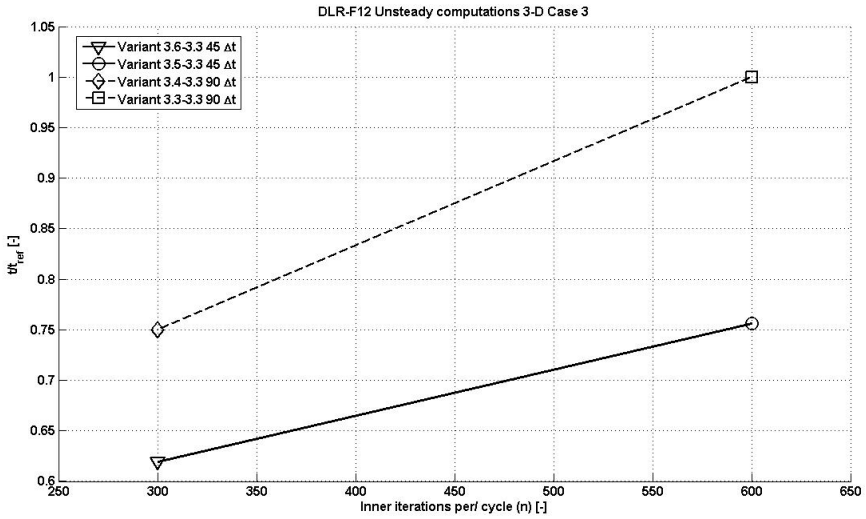

Figure 5.16: DLR-F12 CPU-Time

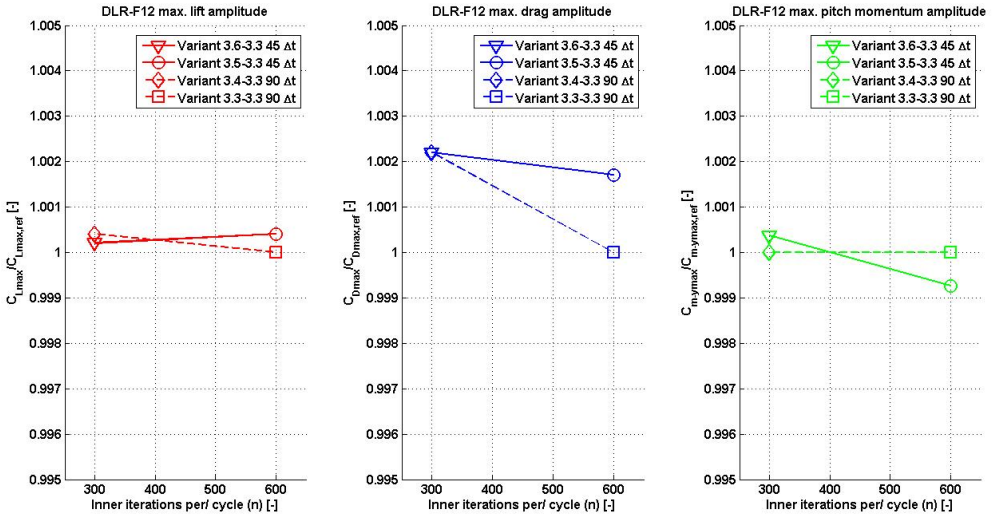

Figure 5.17: DLR-F12 max. coefficient amplitude

5.2 Case 4: Installed AGARD Propeller

The last case to be examined is the simulation of a rotating AGARD propeller installed in tractor configuration on a representative wing section according to the test setup described in [19], where the slipstream aerodynamic effects at low speed conditions were investigated. The geometry represents a propeller configuration with four blades, an axis symmetric nacelle and a generic wing layout with a wing span of about 3.2 propeller diameters. The 1:5 scaled propeller with a diameter d=640 mm is considered to be typical of modern medium speed turboprop commuter aircraft [19]. The propeller rotates with a speed $n = 39900$ [deg/s], which can be expressed in terms of the reduced frequency k defined in Eq. 4.2 as $k = 8.9130$ where c is substituted by the propeller diameter d. This is equal to an advance ratio of $J = 0.70488$, which is defined as

$$J = \frac{U_\infty}{n \cdot d}. \tag{5.1}$$

The configuration was simulated for an angle of attack $\alpha = 10°$. The blade pitch angle at 75% of the blade radius (measured from the propeller center to blade-tip), is set to $\beta_{75} = 29°$. The physical parameters of the simulation are listed below, as they appear in the DLR-Tau script:

Reference Velocity	50 m/s
Angle of attack α_m	10.0°
Reduced frequency for rotation k	8.9138
Propeller rotational speed n	39900 deg/s
Reynolds number	$1.7 \cdot 10^6$
Reference Temperature	276.53 K
Sutherland constant	110.4
Sutherland reference viscosity	$1.7647 \cdot 10^{-5}$

The geometry of the airfoil is taken from the NACA 6-Digit Series (NACA $63_{(10)}$A-012, scaled up NACA 63A-010) with a chord length of $c = 500$ mm. The wingspan is $b = 2060$ mm with constant airfoil section without twist and blending. The nacelle has a length of 985 mm from the blade root to the nacelle end wall. A gap of 1 mm between nacelle and spinner is modeled. Figure 5.18 shows the geometry of the complete configuration.

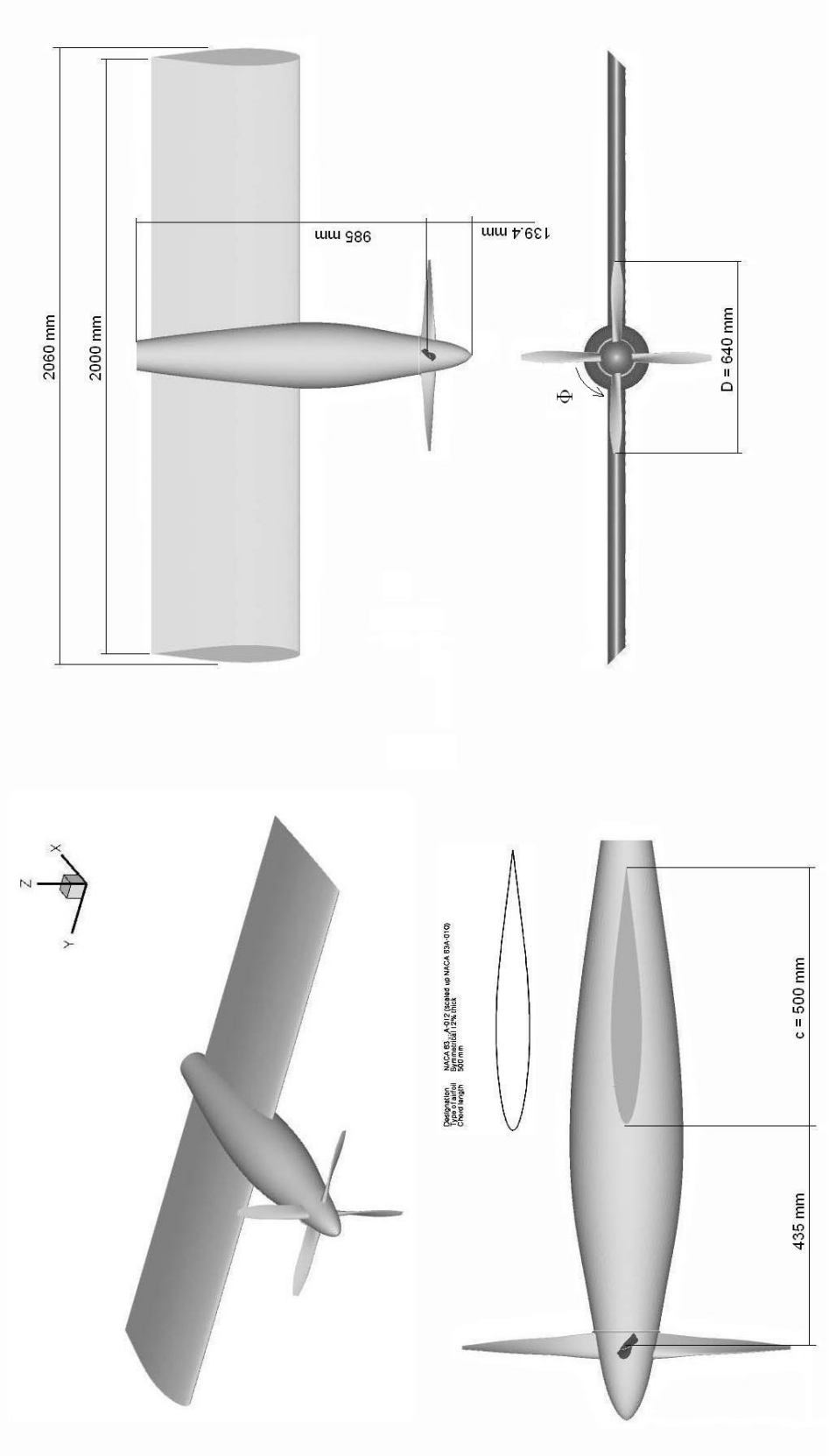

Figure 5.18: AGARD propeller geometry

5.2.1 Grid Generation

Several steps were needed for the AGARD propeller grid generation. Due to the required relative motion between the propeller and the nacelle, the grid is based on the chimera technique. The basic idea is to generate first the grids separately around each geometrical entity in the domain (i.e. the propeller (blades-spinner) separately from nacelle-wing geometries). After that, the grids are combined together in such a way that they overlap each other where they meet [3]. In this way, the first step for the grid generation was to generate the hybrid grid around the nacelle-wing geometries. For this 1st grid the symmetry condition was exploited by only generating a mesh for half of the domain (Figure 5.19-a). This was then duplicated through a mirroring along the xz-plane (Figure 5.19-b). Here, a refinement of the propeller wake over 3.125 propeller diameters downstream of the blade position is performed. The second step for the grid generation was to generate the hybrid grid around a single blade-spinner domain which represents a quarter of the 2nd grid (Figure 5.19-c). After the grid generation with Centaur, the grid was duplicated three times and rotated around the x-axis to complete the four blade-propeller of the 2nd grid (Figure 5.19-d). Finally the two grids were combined together with at least 2 elements in the overlapping region.

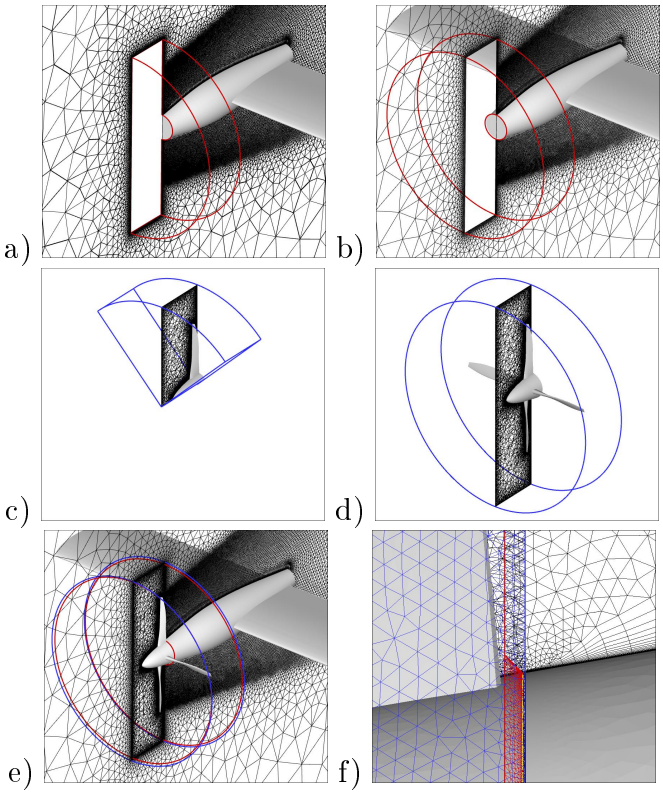

Figure 5.19: AGARD propeller grid generation

The overlapping region was introduced during the creation of the CAD geometry, where a chamfering of the 1st grid boundary towards the surface of the spinner in the 2nd grid was introduced (see Figure 5.19-f). This was done to ensure the nacelle-wing grid extends far enough into the propeller grid block to allow for an adequate overlap region while avoiding possible Chimera interpolation problems near the surfaces of the geometry [24].

The prismatic grid at the vicinity of the wall of block 1 was set up with an initial layer thickness of 0.01 mm using 25 prismatic layers and a stretching factor of 1.3. For block 2 an initial layer thickness of 0.0025 mm, 25 prismatic layers and a stretching factor of 1.275 were used. The nacelle-wing grid block contains $4,802,643$ nodes, while the propeller grid block has $6,307,636$, making for a total of $11,110,279$ computational nodes for the complete grid. The input files used in *CentaurSoft* for the grid generation for both grid blocks are listed in Appendix A.4.

For a first validation of the grid and the flow conditions, a steady simulation of the flow was performed with a velocity of V=50 m/s, a Reynolds number $Re = 1.7 \cdot 10^{06}$ and an angle of attack $\alpha = 10°$. The computation was performed on the DLR CASE-cluster with 48 processors distributed on 12 computational nodes. The cluster consists of 768 computational nodes with a total of 3072 2.6 GHz Dual-Core Opteron processors from AMD [33].

The numerical solution was generated using TAU 2007.1.0. The run was performed using the 1-equation turbulence of Spalart-Allmaras with Edwards modification. Spatial discretization is done using a central scheme in combination with a 3 stage Runge-Kutta scheme for time integration. A 3v multigrid cycle is also applied, and a total of 3000 iterations are calculated.

With these parameters, the Y^+-values vary in a range between 0.01 at the spinner end wall, and 5.34 at the wing leading edge. The minimum Y^+-values at the blade are observed in the middle leading edge zone with 0.021, while the largest are observed in the leading edge tip region. This can be observed in Figure 5.20 which shows a top/bottom view of the Y^+-contours of the steady solution at an angle of attack $\alpha = 10°$.

5.2.2 Numerical Parameters for the Unsteady Simulation

A central scheme is applied for the convective RANS flux discretization, using matrix dissipation for stability. Temporal discretization is done using the dual time-stepping scheme in combination with a 3 stage Runge-Kutta approach. A 3v Multigrid cycle

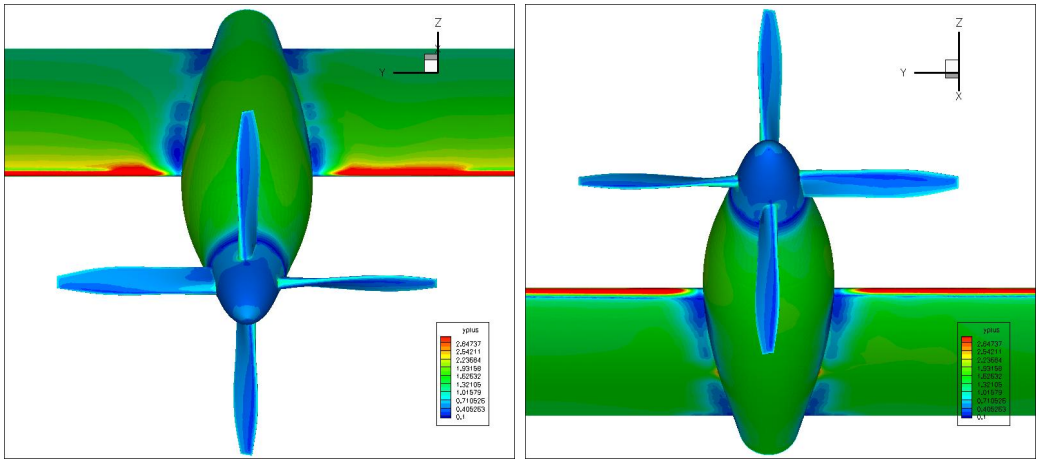

Figure 5.20: AGARD propeller Y^+- values after the steady simulation in a top/bottom view at $\alpha = 10°$

is applied for convergence acceleration and a CFL number of 1.2 for the calculation of the pseudo-time step is set. The run is performed using the 1-equation turbulence model of Spalart-Allmaras with Edwards modification. The numerical solutions are generated based on the DLR TAU-Code version 2007.1.0. The complete setting of parameters used in TAU for the simulation are listed in Appendix A.4.

Unless otherwise specified, the default parameters are used for the computations. All the calculations were performed on the CASE-Cluster with 48 processors distributed on 12 computational nodes.

5.2.3 Results

For the reference simulation, one propeller revolution was resolved with 90 physical time steps, resulting in a rotation of the propeller relative to the nacelle of $4°/\Delta t$ and a physical time step size of $\Delta t = 1.0025 \cdot 10^{-04}$ s with 300 inner iterations for each time step. The same time steps per physical period were applied for the reference variant in Case 3, where it was observed that this number of time steps lead to a good resolution of the periodic force developments. This statement is supported when observing the results obtained in Case 1 and 2, where the simulations with 90 time steps and 83.15 respectively, also showed a good representation of the periodic force developments. In the previous cases, it was also observed that 300 inner iterations for each time step, ensure stability and a good convergence of the coefficient developments with a reduction of the numerical residuals of more than 1 order of magnitude.

The convergence of the computation was monitored using the thrust-coefficient

C_T, as well as the lift- and lateral- force coefficients (C_z and C_y respectively) based on the forces acting on the 4 blades and the spinner including the spinner end wall located in the gap between nacelle and propeller. Figure 5.22 shows the temporal development of the force coefficients as function of the azimuth angle Φ. The azimuth angle Φ refers to a blade position, where the angle $\Phi = 0°$ indicates a blade station extending directly upward from the nacelle [24]. An angle $\Phi = 90°$ indicates a blade position extending out to the left when looking downstream. Figure 5.21 shows the definition of the azimuth angle Φ. The monitoring of the coefficients is evaluated in a rotating coordinate system located at the propeller center.

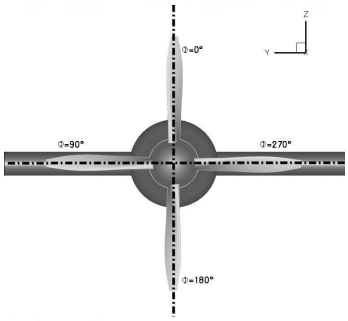

Figure 5.21: Azimuth angle definition

In Figure 5.22, the C_y- and C_z-developments (the blue and green line respectively), show a periodic-state after approximately six propeller revolutions. The coordinate system used for the monitoring, rotates together with the propeller and shows the y- and z- components of the total axial force produced by the propeller rotation. Thus, a sinusoidal evolution of C_y and C_z with equal amplitudes of approximately ± 0.01995 and a shift phase between them is obtained. In contrast, the C_T-development required 22 rotations to achieve a fully periodic state. After 12 rotations the thrust coefficient is seen to increase from which appeared to be a periodic state. Periodicity is then established at a higher thrust coefficient mean value after 5 additional propeller rotations. The total increment of approximately $|\Delta C_T| \approx 0.001$ is attributed to the interaction between the propeller and wing on this particular configuration at $\alpha = 10°$. The simulation needs approximately 17 rotations to fully resolve the complex mutual interaction between the propeller and wing. When the new convergence level is achieved, the thrust coefficient fluctuates in a range of $0.2396 \leq C_T \leq 0.2402$. For the simulation of the required 22 revolutions an effective calculation time of 1100.7 hours was needed, which is equivalent to 45.86 days.

In addition, to check that the number of inner iterations for each physical time step is sufficient, the convergence history of the density residuals as function of the

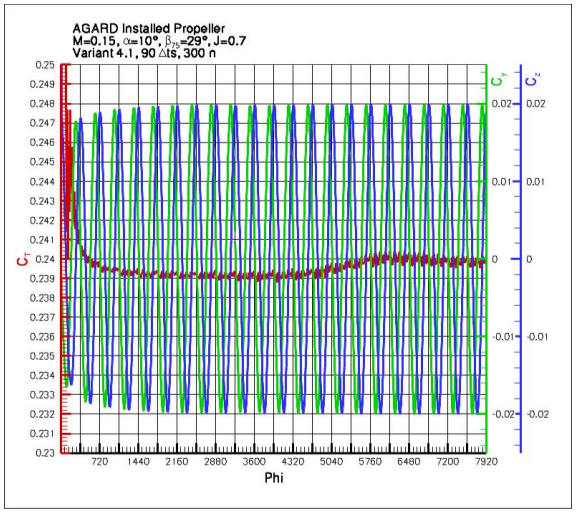

Figure 5.22: AGARD propeller force coefficients development Variant 4.1

number of inner iterations are observed. Figure 5.23 shows the density residuals as a black line, as well as the thrust and lift coefficient history as the red and blue lines respectively for the first half of the 11th propeller revolution. The residuals are reduced by more than two orders of magnitude which ensures a sufficient accuracy of the solution. It can also be observed that the thrust and lift coefficients converge in each physical time step, creating the typical plateaued distribution of aerodynamic coefficients in an unsteady numerical calculation.

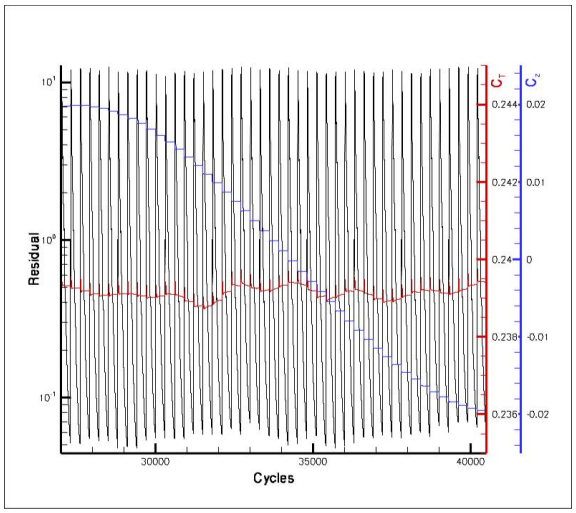

Figure 5.23: AGARD propeller convergence history as a function of the inner iterations per time step

For the last revolution, an analysis of the forces acting on the propeller components is performed using the tool AeroForce [28], developed in the DLR Institute of Aerodynamics and Flow Technology. The forces are evaluated in a non-rotating

and stationary coordinate system located at the propeller center. The results of the analysis are plotted in Figure 5.24. The C_T-, C_z- and C_y-developments plotted in the figure represent the thrust-, lift- and lateral force coefficients as a function of the azimuth angle Φ during a full revolution of the propeller for the different propeller components (blades, spinner and spinner end wall).

The lift component of the blade forces at axial flow (solid blue line in the figure) exhibits a periodic evolution with maximum values of $C_z = -0.01550$ (negative sign due to the z-axis pointing downwards in this coordinate system) at the positions $\Phi = 2°, 92°, 182°, 272°$. According to [24] the maximum values of the lift forces per blade are produced at $\Phi = 90°$, where the maximal relative velocities are achieved due to the vector sum of the free stream velocity components in the plane of rotation and the velocity resulting from the rotation of the propeller at the incidence angle $\alpha = 10°$. The dashed blue line shows the lift forces produced by the blades with consideration of the spinner. The spinner influence increases the lift coefficients by approximately 27.5% ($|\Delta C_z| = 3.6293 \cdot 10^{-03}$), resulting in a periodic development with maximal values of $C_z = -0.01982$ at the same azimuth angles mentioned before. The spinner end wall does not have any influence on the lift forces.

The lateral force component of the blade forces are plotted as solid green line in the figure. The C_y-development shows a periodic development with a phase shift of approximately $\Delta\Phi = 23°$ compared with the lift coefficient curve. In Figure 5.24, the maximum C_y-values are observed at the positions $\Phi = 24°, 114°, 204°, 294°$ with values of $C_y = 4.1193 \cdot 10^{-03}$. The influence of the spinner decreases the lateral force coefficients by approximately 6.97% ($|\Delta C_y| = 2.8729 \cdot 10^{-04}$). The spinner end wall does not influence the lateral force coeffcients.

The thrust component of the blade forces are plotted as solid red line in the figure. The C_T-development shows a periodic development with a phase shift of approximately $\Delta\Phi = 51°$ compared with the lift coefficient curve. The maximum C_T-values are observed at the positions $\Phi = 8°, 98°, 188°, 278°$ with values of $C_T = 0.2377$. The influence of the spinner increases the thrust coefficients by approximately 0.45% ($|\Delta C_T| = 1.0859 \cdot 10^{-03}$). The dynamic pressure produced in the gap region between the propeller and nacelle, increases the thrust coefficients when including the spinner end wall. The coefficients increase by 1.04%, with the difference between the blades only value, and the blades-spinner-spinnerendwall value of $|\Delta C_T| = 2.4897 \cdot 10^{-03}$. The experimental data in [19], reported a thrust coefficient of $C_T = 0.235$ for an advance ratio of $J = 0.699$ for the configuration at $\alpha = 10°$. This value differs from the numerical results by 1.49%, in comparison with the mean value obtained from

the thrust produced by the propeller without considering the end wall influence. In addition in [22], where Euler-simulations of the flow for the same installed-propeller configuration were conducted, the average thrust coefficient, shows an overprediction of 13% compared with the experimental data. These results reflect the impact of the viscous effects acting on the propeller, and the advantages of a NS-simulation versus an Euler-calculation.

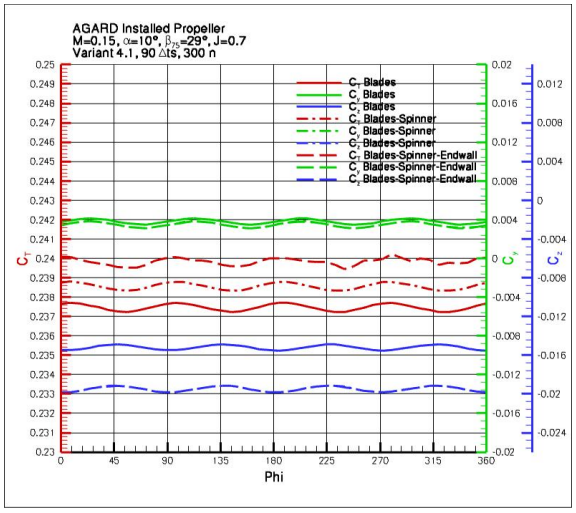

Figure 5.24: AGARD propeller force components

The obtained results with these parameter settings (called Variant 4.1 up to this point) show sufficient accuracy, and can thus be taken as a reference in the present case.

Variation of the Relevant Parameters of the Dual Time Step Scheme

The first action to be taken for the acceleration of the calculation was to begin the unsteady run from a restart after an initialization of the flow through a steady simulation. In Case 2, it was observed that the initialization of the flow accelerates the convergence of the coefficients to a periodic state considerably. In this way the simulation performed for the validation of the grid was taken as a restart for the run, and a new calculation with the same parameters used in Variant 4.1 was performed.

Figure 5.25 plots the time history of the relevant force coefficients. The development of the lift and lateral force coefficients shows a periodic state after six propeller revolutions as occurred in Variant 4.1. However, due to the initialization of the flow with a steady-state solution, the aerodynamic interactions between the propeller and wing are already fully resolved after 15 propeller revolutions. This can be seen in the mean value of the thrust coefficient in Figure 5.25, which is identical to that seen for

Variant 4.1 after 22 propeller revolutions. This represents a reduction of 7 rotations which can be translated into a reduction of the calculation time by approximately 32.91% versus the reference calculation.

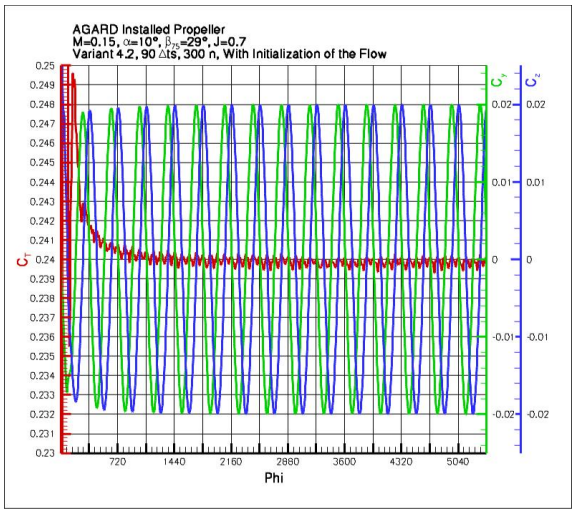

Figure 5.25: AGARD propeller force coefficients development Variant 4.2

Now, as performed in the previous cases, a calculation with *quick* initial parameter settings is performed as a restart from the steady computation. With these parameters, eight propeller revolutions are performed before an *accurate* parameter setting is adopted. Thus, the *quick* parameter setting was performed with 45 physical time steps, resulting in a rotation of the propeller relative to the nacelle of $8°/\Delta t$ and a physical time step size of $\Delta t = 2.005 \cdot 10^{-04}$ s with 300 inner iterations for each time step. After the completion of 8 rotations with the *quick* parameter setting, the parameters were switched to the parameters performed in Variants 4.1 and 4.2 through 15 propeller revolutions.

Figure 5.26 shows the temporal development of the relevant force coefficients as a function of the azimuth angle. In the figure it can be observed that the simulation requires 2 cycles to achieve the thrust development obtained with Variant 4.2 after the *accurate* parameter setting is adopted. The lift and lateral force coefficient developments present practically no difference with the the developments observed in the reference case. After 10 cycles the force developments of Variant 4.2 and 4.3 show good accordance and almost no difference in the temporal evolution of the forces. The time needed for this Variant was of 554.36 hours, which represents a reduction of 49.63% compared with the reference in Variant 4.1, and 25% compared with Variant 4.2.

The results obtained for the last propeller revolution for each Variant (22nd rota-

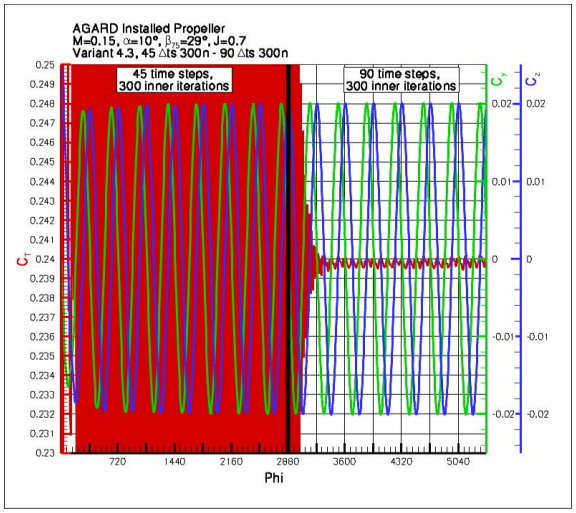

Figure 5.26: AGARD propeller force coefficients development Variant 4.3

tion of Variant 4.1 and the 15th of Variants 4.2-4.3) were extracted and compared. The diagram in Figure 5.27 shows the lift and lateral force coefficients as a function of the azimuth angle for all the variants during the final propeller revolution, where nearly no difference among the different setups can be observed. Since it was observed that the spinner end wall does not influence the C_y and C_z developments, only the blades-spinner-developments are compared. Only minor differences among the variants can be found, which confirms the good accuracy of the results. The maximum difference of the C_y-developments is observed between Variant 4.1 and Variant 4.2 with 0.2104%, considering the influence of blades and spinner. The maximum differences of the C_z-developments are also found between Variant 4.1 and Variant 4.2 with 0.0444%.

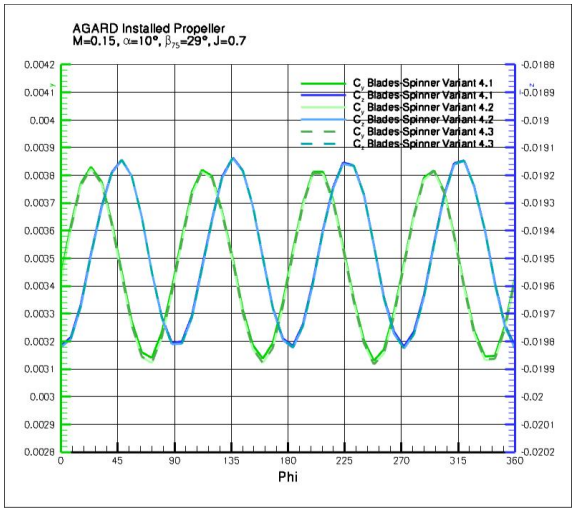

Figure 5.27: AGARD propeller lift- and lateral force coefficients for Variants 4.1-4.3

In Figure 5.28 the thrust development as a function of the azimuth angle for the different variants is plotted. The diagram in the figure shows the development during a complete revolution. Again, the maximum differences are observed between Variant 4.1 and 4.2 with 0.0224% for the blades-spinner-curve.

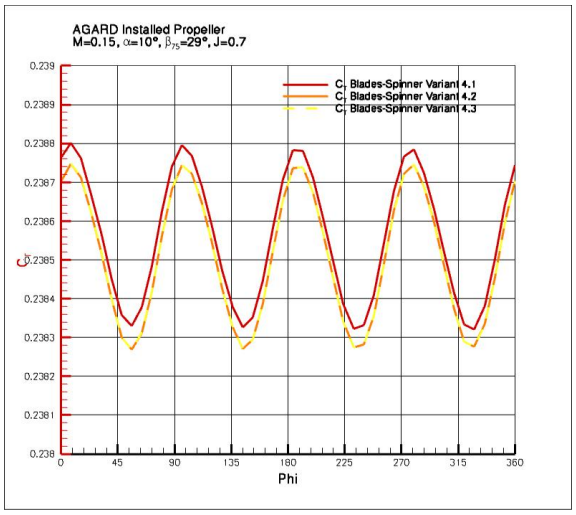

Figure 5.28: AGARD propeller thrust coefficients for Variants 4.1-4.3

These results confirm the findings obtained in Cases 1-3, and thus the methodology used here for the acceleration of unsteady simulations is found to be applicable for a wide range of different configurations.

Perspective

P.1 Cauchy Convergence Criterion

The DLR Tau-Code offers the option of a Cauchy convergence criterion for the determination of the number of inner iterations to be performed in each time step. If this function is activated, then the inner iterations are stopped if the relative changes in drag and lift coefficients during a certain number of previous inner iterations specified by the number of samples for the Cauchy convergence are smaller than this tolerance value, i.e., if

$$\epsilon = \frac{\left|c_l^n - c_l^{n-k}\right|}{|c_l^n|} \leq total\_lift \tag{5.2}$$

for all $k = 1, ...n\_sample\_inner$. Here the upper index denotes the inner pseudo time step. The number of samples gives the number of previous inner iterations that are considered to check whether Cauchy convergence of the integral coefficients of lift and drag has been reached.

With this criterion, the time for the calculations can be reduced, since the number of inner iterations varies for each time step until the criteria are fulfilled, possibly avoiding unnecessary additional iterations. As an introduction, which could lead to further investigations of this method, three setting of parameters were calculated using the Cauchy convergence criteria. Using the same physical and numerical parameters as in section 4.1 Variant 1.1, three simulations were performed with a variation of the relative drag and lift changes ϵ. The variations attempted were with the values $\epsilon = 1 \cdot 10^{-6}$, $1 \cdot 10^{-5}$, $1 \cdot 10^{-4}$, each with 20 samples for the convergence verification. The tolerance of the criterion is increased if the relative change is also increased, but with the consequence of having a sensitivity to unstable behaviors in the calculation. A recommended value in the DLR Tau User guide for relative lift and drag coefficients is $1 \cdot 10^6$. Using this tolerance, the advantage of the method is

very limited, since the minimal number of inner iterations needed for each time step is close to the 150 inner iterations for almost each time step, which confirms the accuracy in the convergence of the results obtained in the reference simulation in Case 1. For this reason coarser values were investigated, showing that the time for the calculations can be reduced, but with the tendency of getting unstable behavior. Figure 5.29 shows CPU-Time as a function of the relative C_L and C_D changes ϵ. The values were normalized by the time obtained for the reference calculation in section 4.1. Here it can be observed that using the recommended value given in [7], the computation time is reduced by approximately 4% compared with the reference in Case 1. Furthermore, with a value $\epsilon = 1 \cdot 10^{-4}$ the time can be reduced by almost 50%.

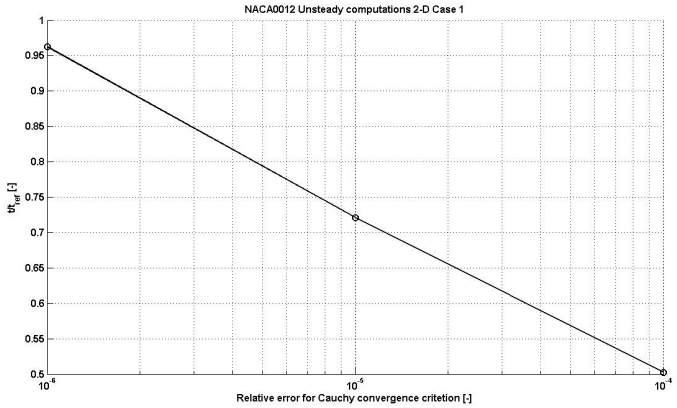

Figure 5.29: CPU-time with the use for the Cauchy convergence criterion with variation of the relative error for convergence

The values obtained for the periodic lift coefficient distribution are depicted in Figure 5.30. The Figure depicts the periodic C_L-values as a function of the physical time. Here it can be observed, that the results obtained for the coefficients do not vary dramatically by varying the Cauchy convergence criteria. The C_{Lmax}-values obtained in the last physical cycle were extracted and normalized by the reference values in Case 1, and finally plotted as function of the relative coefficient changes for Cauchy convergence criterion as shown in Figure 5.31. The largest discrepancy of the coefficients is found for the simulation with $\epsilon = 1 \cdot 10^{-6}$, showing a difference of $5.6 \cdot 10^{-4}$ compared with the reference, which still represents a negligible difference.

The results obtained with the Cauchy convergence criterion provide an insight into the method, which might lead to further investigations of the dual time-stepping scheme using these criteria for more complex configurations.

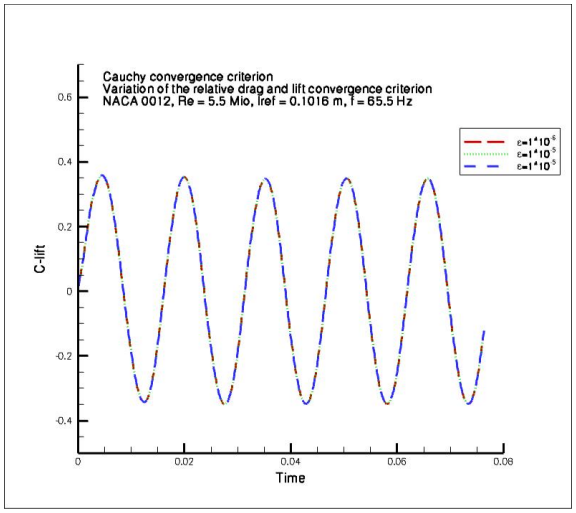

Figure 5.30: CPU-time with the use for the Cauchy convergence criterion with variation of the relative error for convergence

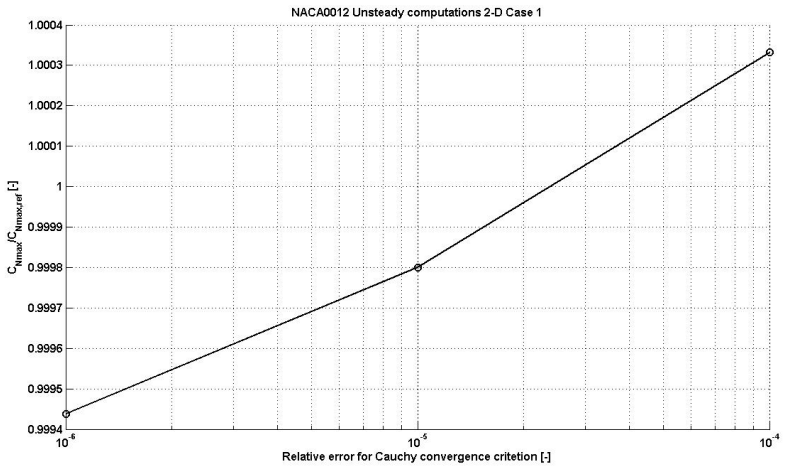

Figure 5.31: C_{Nmax}-values with the use for the Cauchy convergence criterion with variation of the relative error for convergence

Conclusions

Through the cases studied in the present project, a methodology for the acceleration of unsteady simulations was developed and validated.

The main conclusion drawn from the 2-D cases studied here, is that the use of a time steps variation from a rough resolution of the temporal development of the relevant forces (*quick* parameter settings) to a finer resolution (*accurate* parameter settings), decreases the cost of the simulations without having a major impact on the accuracy of the results. Thus, the time needed for the calculations can be reduced by almost 50% with negligible deviations of the results versus the reference calculation with the use of a constant time step. The experiences obtained from the 2-D cases were applied to the 3-D cases, obtaining similar results which validate the methodology.

The cases studied, especially Cases 2 and 4 showed the advantages of the initialization of the flow through a steady calculation before the simulation of the unsteady flow is started. For these cases it was clearly shown that the steady simulation, which can be performed in a relatively short time (3000-5000 iterations), enables a much quicker attainment of a periodic state in the subsequent time-accurate computations leading to a clear reduction in computational cost.

For the acceleration of unsteady simulations it is thus recommendable to run a steady computation of the flow as a restart before the unsteady simulation is performed. After the steady simulation is completed, a first unsteady computation should be performed with parameters which lead to a quick simulation of the first physical periods (i.e. 25-45 time steps per period with 150-300 inner iterations). The quick simulation may not necessarily deliver the required accuracy, but allows for a quicker propagation of the initial flow disturbances out of the computational domain and a more rapid establishment of at least an approximation of the unsteady flow fields. After 2-5 physical cycles with the *quick* parameter settings are performed, the parameters should be switched to a setup that delivers the required resolution of the temporal development of the relevant aerodynamic phenomena (i.e. 90-180 time

steps per period with 150-300 inner iterations). In the present study approximately 0.75-1.5 cycles were required to obtain fully periodic and sufficiently accurate aerodynamic forces using this subsequent accurate parameter setting. This approach of employing a variation of the time-step size from the *quick* to the *accurate* settings leads to a significant reduction in the computation time

Although the Cauchy convergence criterion option still needs to be improved for a wider applicability (i.e. use of changes in drag and lift instead of relative changes in drag and lift coefficients for the tolerance ϵ evaluation) to the calculation of the entire diversity of challenges in the aerospace industry, further investigations of the dual time-stepping scheme using these criteria for more complex configurations should be performed.

Bibliography

[1] Abbas, Safdar: *"'A Third Order Accurate Semi-Implicit Runge-Kutta method for the Compressible Navier-Stokes Equations"'*; Master Thesis, DLR-Braunschweig; DE, 2007.

[2] Anderson, John D.: *"'Computational Fluid Dynamics, The basics with applications"'*; McGraw-Hill, Inc.; New York, USA, 1995.

[3] Blazek, J.: *"'Computational Fluid Dynamics: principles and applications"'*; Elsevier Science Ltd; Kidlington, Oxford, UK, 2001.

[4] Brodersen, O., Stuermer, A.: *"'Drag Prediction of Engine-Airframe interference effects using unstructured Navier-Stokes calculations"'*; AIAA 2001-2414, 19th AIAA Applied Aerodynamics Conferences; Anaheim CA, USA, 2001.

[5] Cebeci, T., Shao, J. P., et al.: *"'Computational Fluid Dynamics for Engineers"'*; Horizons Publishing Inc.; Long Beach CA, USA, 2005.

[6] Deutsches Zentrum für Luft- und Raumfahrt e.V., *"'Technical Documentation of the DLR TAU-Code"'*; Institute of Aerodynamics and Flow Technology; Technical Report; DLR-Braunschweig, DE, 2005.

[7] Deutsches Zentrum für Luft- und Raumfahrt e.V., *"'TAU-Code User guide"'*, Release 2007.1.0; Institute of Aerodynamics and Flow Technology; DLR-Braunschweig, DE, 2007.

[8] Group for Aeronautical Research and Technology in Europe: *"'GARTEUR AD (AG38) Time Accurate Methods"'*; Technical Report No. FOI RH 057 SE, Stockholm; SE, 2006.

[9] Edwards, J.R., Chandra, S.: *"'Comparison of Eddy Viscosity-Transport Turbulence Models for Three-Dimensional, Shock-Separated Flowfields"'*; AIAA Journal, Vol.34, No. 4; April 1996.

[10] Ferziger, Peric: *"'Computational Methods for Fluid Dynamics"'*; Springer, 3.Auflage; New York, USA, 2001.

[11] Flatscher, T.: *"'Strömung um einen Zylinder"'*; Berechnung turbulenter Strömungen mit Computerprogrammen LVA Nr. 319.020; Institut für Strömungsmechanik und Wärmeübertragung, TU Wien; Wien, AT, 2005.

[12] Huebner, A.: *"Experimental and Numerical Investigations of Unsteady Aerodynamic Derivatives for Transport Aircraft Configurations"*; AIAA-2007-1076; 45th AIAA Aerospace Sciences Meeting and Exhibit; Reno, NV, USA; 2007

[13] Jameson, A.: *"'Time Dependent Calculations Using Multigrid, with Applications to Unsteady Flows Past Airfoils and Wings"'*; AIAA 10th Computational Fluid Dynamics Conference; AIAA Report No. 91-1596; Honolulu, HI, USA, 1991.

[14] Jameson, A., et al. : *"'Numerical Solution of the Euler Equations by Finite Volume Methods Using Runge-Kutta Time Stepping Schemes"'*; AIAA 14th Fluid and Plasma Dynamics Conference; AIAA Report No. 81-1259; Palo Alto, California, USA, 1981.

[15] Klenner, J., Becker, K., Cross, M., Kroll, N.: *Future Simulation Concept"'*; CEAS-2007-105, 1st European Air and Space Conference; Berlin, DE, 2007.

[16] Kroll, N., Fassbender, J.K.: *"MEGAFLOW - Numerical Flow Simulation for Aircraft Design"; Notes on Numerical Fluid Dynamics and Multidisciplinary Design*; Volume 89; Springer; 2005.

[17] Mavriplis. D. J., Darmofal, D., Keyes, D., Turner, M.: *"Petaflops Opportunities for the NASA Fundamental Aeronautics Program"*; AIAA-2007-4084; 18th AIAA Computational Fluid Dynamics Conference; Miami, FL, USA; 2007

[18] NATO Advisory Group for Aerospace Research and Development: *"'Compendium of Unsteady Aerodynamic Measurements"'*; AGARD Report No. 702; London, UK, 1982.

[19] Samuelsson, I.: *"'Low Speed Wind Tunnel Investigation of Propeller Slipstream Aerodynamic Effects on Different Nacelle/Wing Combinations Part 1"'*; FFA TN 1987-22; SE, 1987.

[20] Schlichting, H.: *"'Boundary Layer Theory"'*; McGraw-Hill Series in Mechanical Engineering, 6th Edition; USA, 1968.

[21] Schuette, A., Einarsson, G., Raichle, A., Schoening, B., Orlt, M., Neumann, J., Arnold, W., Monnich, W., Forkert, T.: *"Numerical Simulation of Maneuvering Aircraft by Aerodynamic, Flight Mechanics and Structural Mechanics Coupling"*; AIAA-2007-1070; 45th AIAA Aerospace Sciences Meeting and Exhibit; Reno, NV, USA; 2007.

[22] Stuermer, A.: *"CFD Validation of Unsteady Installed Propeller Flows using the DLR TAU-Code"*; CEAS-2007-104; 1st European Air and Space Conference; Berlin, Germany; 2007.

[23] Stuermer, A.: *"Validation of an Unstructured Chimera Grid Approach for the Simulation of Propeller Flows"*; AIAA 2004-5289; 22nd Applied Aerodynamics Conference and Exhibit; Providence, RI, USA; 2004.

[24] Stuermer, A.: *"Unsteady Euler Computations of an isolated Propeller using the DLR TAU-Code"*; DLR Institute of Aerodynamics and Flow Technology, IB 124-2004/21; Braunschweig, DE; 2004.

[25] Spalart, P.R., Allmaras, S.R.: *"'A One-Equations Turbulence Model for aerodynamic Flows"'*; AIAA Report No. 92-0439, 1992.

[26] Thomas, P.D., Lombard, C.K.: *"'Geometric Conservation Law and its application to Flow Computations on Movng Grids"'*; AIAA Journal 17; 1979.

[27] Turkel E.: *"'Improving the accuracy of central difference schemes"'*, in D. L. Dwoyer, M. Y. Hussaini, and R. G. Voigt, editors, Numerical Methods in Fluid Dynamics, volume 323 of Lecture Notes in Physics; Berlin Springer Verlag; DE, 1989.

[28] Wild, J.: *"'AeroForce: Thrust/Drag Bookkeeping and Aerodynamic Force Breakdown over component"'*; DLR Institute of Aerodynamics and Flow Technology; Technical Report AIDATA WP4.1; Braunschweig, DE; 1999.

[29] Wulf, Peter: CFD-Vorlesungsmanuskript, HAW-Hamburg, DE, 2007.

[30] http://geolab.larc.nasa.gov/APPS/YPlus/

[31] http:// www.centaursoft.com

[32] http://www.cfd-online.com

[33] http://www.dlr.de

[34] http://www.grc.nasa.gov/WWW/wind/valid/lamcyl/lam_cyl.html

[35] http://www.imech.tu-chemnitz.de/mpf/PartFlow.3D/Von_Karman/Von_Karman.html

Appendices

A.1 Case 1

***Centaur* input files**

Surface parameter file (*.sin)

```
1               !  Output Level(0-none, 1-normal, 2-detailed)
0               !  Desired number of surface triangles (0=off)
1.8             !  Stretching ratio (1.5-2.1)
1.0             !  Scaling parameter (0.25-4.0)
F               !  Use constant spacing
38.184          !  Initial/Constant spacing value
10              !  Length Scale in absence of any features
1.591           !  Minimum Length scale for analytic curvature clustering
T               !  Activate interpanel curvature clustering
100.  8.        !  Angle and factor for interpanel curvature clustering
100.            !  Factor for analytic curvature clustering interior to panels
2.              !  Factor for proximity clustering
2.              !  Factor for CAD clustering
```

Prisms parameter file (*.pin)

```
1               !  Output Level (0-none, 1-normal, 2-detailed)
F               !  Read in prismatic gap/cavity detection file (T/F)
0.4             !  Proportion of gaps to be filled by tets (0.2 - 0.8)
0               !  No.  of passes for extending cavity area (0-4)
T               !  Automatic curve pullback activation(T/F)
100.  0.33      !  Min.  angle(degrees) at curve for activation; ratio
20.0            !  Ramp angle(deg)- growth rate on final layer (5-30)
32              !  No.  of prismatic layers to be generated (5-30)
0.0115          !  Initial layer thickness (case dependent)
1.2             !  Stretching factor (1.1-1.5)
T               !  Chop prismatic layers (T/F)
0.0025          !  Minimum layer thickness (case dependent)
```

Tetrahedral parameter file (*.tin)

```
1              !  Output Level(0-none, 1-normal, 2-detailed)
F              !  Restarting (T/F)?
1.9            !  Stretching ratio (1.5-2.1)
1.0            !  Scaling parameter (0.25-4.0)
T              !  Limit maximum tetrahedral size
2500           !  Maximum tet.  length scale (if limit is True)
0.8            !  Thickness matching ratio(0.-1.)
2.0            !  Tet./prism interface ratio(1.-3.)
5              !  Tet.  Grid Quality (1-lowest - 10-highest)
```

DLR Tau-Code parameter setting

```
----------------------------------------
BOUNDARY MAPPING:
----------------------------------------
Markers:                                    1
Type:                                       farfield
Name:                                       Farfield
Angle alpha (degree):                       0.0
Vortex correction (0/1):                    0
Chord length:                               1
Mach number:                                0.755
block end
-------------------------
Markers:                                    2
Type:                                       viscous wall
Subtype:                                    turbulent
Name:                                       SS
Write surface data (0/1):                   1
Cutting plane allowed (0/1):                1
Monitor forces (0/1):                       1
block end
--------------
Markers:                                    3
Type:                                       viscous wall
Subtype:                                    turbulent
Name:                                       PS
Write surface data (0/1):                   1
Cutting plane allowed (0/1):                1
Monitor forces (0/1):                       1
block end
--------------
Markers:                                    4
Type:                                       viscous wall
Subtype:                                    turbulent
Name:                                       LE
Write surface data (0/1):                   1
Cutting plane allowed (0/1):                1
Monitor forces (0/1):                       1
block end
--------------
Markers:                                    5
Type:                                       symmetry plane
Name:                                       Side1
Write surface data (0/1):                   1
```

```
Cutting plane allowed (0/1):                          1
Monitor forces (0/1):                                 1
block end
--------------
Markers:                                              6
Type:                                                 symmetry plane
Name:                                                 Side2
Write surface data (0/1):                             1
Cutting plane allowed (0/1):                          1
Monitor forces (0/1):                                 1
block end
--------------
---------------------------------------
REQUIRED PARAMETERS
---------------------------------------
Boundary mapping filename:                            naca0012.para
Primary grid filename:                                naca0012.tau
Reference Mach number:                                0.755
---------------------------------------
IO
---------------------------------------
Grid/Solution ------------------:                     -
Grid prefix:                                          naca0012.dualgrid
Output files prefix:                                  naca0012.sol
Restart-data prefix:                                  (none)
Chimera grid info filename:                           chimgridinfo
Controls --------------------:                        -
Automatic parameter update (0/1):                     1
Write pointdata dimensionless (0/1):                  0
---------------------------------------
MOVING GRID
---------------------------------------
Type of grid movement:                                rigid
Motion description filename:                          (thisfile)
Motion hierarchy filename:                            (thisfile)
Geometric conservation law (0/1):                     0
Number of time steps per period:                      180
Evaluate forces and moments at node:                  block_1
Extended motion monitoring (0/1):                     1
Node name:                                            block_1
Node reference frame:                                 inertial
Node controls grid block:                             1
Node motion description id:                           block_1
hdf end
-------------------------
Motion description id:                                block_1
Type of movement:                                     periodic
Origin of local coordinate system:                    0.0 0.0 0.0
Degree of Fourier series for rotation:                1
Reduced frequency for rotation:                       0 0.1628 0
Reduced frequency reference length:                   0.1016 0.1016 0.1016
Fourier coefficients for rotation (sin) pitch:  0.0 2.51
mdf end
-------------------------
---------------------------
PREPROCESSING
---------------------------
```

```
Output level:                                    100
Cache-coloring (0/max_faces in color):           50
Compute/store wall distances:                    0
Number of multigrid levels:                      3
Partitioning ------------------:                 -
Number of primary grid domains:                  1
Number of domains:                               1
Type of partitioning (name):                     private
Additionals -------------------:                 -
Compute exact whirlflux (0/1):                   1
Compute lusgs mapping (0/1):                     1
2D offset vector (0 / x=1,y=2,z=3):              2
---------------------------------------
SOLVER->GENERAL
---------------------------------------
Convective RANS flux discretization type:        central
Order of basic equations (1/2):                  2
Order of additional equations (1/2):             2
Increase memory (0/1):                           1
--Timestepping Start/Stop -----------:           -
Output period:                                   45
Maximal time step number:                        5000
Minimum residual:                                1e-10
Project time steps (0/1):                        1
--MG----------------------:                      -
MG description filename:                         3v
--MG-Smoothing ------------------:               -
Residual smoother:                               Point_explicit
Correction smoother:                             Point_explicit
Interpolate corrections (0/1):                   0
Correction smooth epsilon:                       0.2
Residual smooth epsilon:                         0.2002
Correction smoothing steps:                      2
Residual smoothing steps:                        2
Smoothing relaxation steps:                      2
--MG Start up ------------------:                -
SG start up steps (fine grid):                   0
Multigrid start level:                           1
Maximal time step number (coarse grids):         50
Minimum residual (coarse grids):                 0.0001
--Monitoring -------------------:                -
Monitor history (0/1):                           1
Residual monitoring type (0/1):                  1
Monitor history (0/1):                           1
--Dual time -------------------:                 -
Unsteady time stepping:                          dual
Unsteady show pseudo time steps (0/1):           1
Unsteady physical time steps:                    900
Minimum number of inner iterations per time step:  50
Unsteady inner iterations per time step:         150
Unsteady implicit scheme order:                  2
Unsteady extrapolation order:                    1
Variable timestepping (0/1/2):                   0
Timestep data filename:                          (none)
Compute DES solution(0/1):                       0
DES constant:                                    0.65
--References -------------------:                -
```

```
Reference Mach number:                                0.755
Reference temperature:                                288.15
Prandtl number:                                       0.72
Gas constant gamma:                                   1.4
Gas constant R:                                       287.1
--Transport coefficients ------------:                -
Reynolds number:                                      5.5e6
Reynolds length:                                      0.1016
Prandtl number:                                       0.72
Sutherland constant:                                  110.4
Sutherland reference viscosity:                       1.716e-05
Sutherland reference temperature:                     273
--Geometry -------------------:                       -
Grid scale:                                           1
Reference relation area:                              0
Reference length (pitching momentum):                 0.1016
Reference length (rolling/yawing momentum):           1
Origin coordinate x:                                  0
Origin coordinate y:                                  0
Origin coordinate z:                                  0
---------------------------------------
SOLVER->DISSIPATION: SCALAR
---------------------------------------
Central dissipation scheme:                           Scalar_dissipation
2nd order dissipation coefficient:                    0.5
Inverse 4th order dissipation coefficient:            64
---------------------------------------
SOLVER->TIME-STEPPING: RUNGE-KUTTA
---------------------------------------
Relaxation solver:                                    Runge_Kutta
Number of Runge-Kutta stages:                         3
CFL number:                                           1.8
CFL number (coarse grids):                            1.8
---------------------------------------
SOLVER->PRECONDITIONING
---------------------------------------
Preconditioning (0/1/2):                              0
Cut-off value:                                        2
---------------------------------------
SOLVER->TURBULENCE: SPALART-ALLMARAS
---------------------------------------
Monitoring values:  Residual_Max-res_X-max-res_Z-max-res_dnue/dt_C-lift
              _C-drag_C-my_Max-y+_Max-eddyv_Angle-a
Monitoring significant figures:                       4_4_4_4_4_9_9_9_4_4_4
--Turbulence -------------------:                     -
Turbulence model version:                             SAE
Turb.  Prandtl number:                                0.9
Ratio mue-t/mue-l:                                    0.1
Maximum limit mue-t/mue-l:                            20000
Turbulent intensity:                                  0.001
Reference bl-thickness:                               1e+22
Maximum turbulence production/destruction:            20
Turbulence equations use multigrid (0/1):             1
Positivity scheme:                                    0
EARSM expansion order:                                1
Rotational correction (0/1):                          0
Rotational correction model:                          0
```

```
Work space for rotational correction smoother (0/1):  0
Smooth rotational correction eps:                          1e-05
Number of Smoothing steps for rotcorr:                     0
----------------------------------------
EXTRA FIELD POINTDATA OUTPUT
----------------------------------------
Field output description file:                             naca0012.para
Field output values:  xyzgeod_temp_Ptot_mach_vort_vxyzgeod_wxyz_vxyzmoving
Field output period:                                       45
----------------------------------------
SURFACE OUTPUT
----------------------------------------
Surface output description file:                           naca0012.para
Surface output files prefix:                               surf
Surface output values:  xyzgeod_xyz_rho_cp_v_mach_vort_yplus_vxyzgeod_wxyz
             _vxyzmoving
Surface output period:                                     45
----------------------------------------
TAU2PLT
----------------------------------------
Bounding Box ------------------:                           -
Volume element options -------------:                      -
Volume data output (0/1):                                  1
Element types for zone:                                    (none)
One zone for all volume elements:                          0
Surface element options -------------:                     -
Surface data output (0/1):                                 1
Output Control -----------------:                          -
Output format:                                             tecplot
Ascii (0/1):                                               0
Precision :                                                9
Title of output file:                                      (none)
----------------------------------------
UPDATES
----------------------------------------
```

A.2 Case 2

***Centaur* input files**

Surface parameter file (`*.sin`)

```
1              !  Output Level(0-none, 1-normal, 2-detailed)
0              !  Desired number of surface triangles (0=off)
1.5            !  Stretching ratio (1.5-2.1)
1.0            !  Scaling parameter (0.25-4.0)
F              !  Use constant spacing
628.119        !  Initial/Constant spacing value
1256.24        !  Length Scale in absence of any features
26.1716        !  Minimum Length scale for analytic curvature clustering
T              !  Activate interpanel curvature clustering
100.  8.       !  Angle and factor for interpanel curvature clustering
160.           !  Factor for analytic curvature clustering interior to panels
```

```
2.              !  Factor for proximity clustering
2.              !  Factor for CAD clustering
```

Prisms parameter file (*.pin)

```
1               !  Output Level (0-none, 1-normal, 2-detailed)
F               !  Read in prismatic gap/cavity detection file (T/F)
0.4             !  Proportion of gaps to be filled by tets (0.2 - 0.8)
0               !  No.  of passes for extending cavity area (0-4)
F               !  Automatic curve pullback activation(T/F)
100.  0.33      !  Min.  angle(degrees) at curve for activation; ratio
10.0            !  Ramp angle(deg)- growth rate on final layer (5-30)
20              !  No.  of prismatic layers to be generated (5-30)
10.044          !  Initial layer thickness (case dependent)
1.175           !  Stretching factor (1.1-1.5)
T               !  Chop prismatic layers (T/F)
0.2088          !  Minimum layer thickness (case dependent)
```

Tetrahedral parameter file (*.tin)

```
1               !  Output Level(0-none, 1-normal, 2-detailed)
F               !  Restarting (T/F)?
1.8             !  Stretching ratio (1.5-2.1)
1.0             !  Scaling parameter (0.25-4.0)
T               !  Limit maximum tetrahedral size
100000.0        !  Maximum tet.  length scale (if limit is True)
0.8             !  Thickness matching ratio(0.-1.)
2.0             !  Tet./prism interface ratio(1.-3.)
5               !  Tet.  Grid Quality (1-lowest - 10-highest)
```

DLR Tau-Code parameter setting

```
----------------------------------------
BOUNDARY MAPPING:
----------------------------------------
Markers:                                        1
Type:                                           farfield
Name:                                           Farfield
Angle alpha (degree):                           0.0
Vortex correction (0/1):                        0
Chord length:                                   1
Mach number:                                    0.2
block end
-------------------------
Markers:                                        2
Type:                                           viscous wall
Subtype:                                        laminar
Name:                                           Cylinder
Write surface data (0/1):                       1
```

```
Cutting plane allowed (0/1):                    1
Monitor forces (0/1):                           1
block end
--------------
Markers:                                        4
Type:                                           symmetry plane
Name:                                           Side1
Write surface data (0/1):                       1
Cutting plane allowed (0/1):                    1
Monitor forces (0/1):                           1
block end
--------------
Markers:                                        5
Type:                                           symmetry plane
Name:                                           Side2
Write surface data (0/1):                       1
Cutting plane allowed (0/1):                    1
Monitor forces (0/1):                           1
block end
--------------
---------------------------------------
REQUIRED PARAMETERS
---------------------------------------
Boundary mapping filename:                      cylinder180.para
Primary grid filename:                          cylinder180.tau
Reference Mach number:                          0.2
---------------------------------------
IO
---------------------------------------
Grid/Solution ------------------:               -
Grid prefix:                                    cylinder180.dualgrid
Output files prefix:                            cylinder180.sol
Restart-data prefix:                            (none)
Chimera grid info filename:                     chimgridinfo
Controls --------------------:                  -
Automatic parameter update (0/1):               1
Write pointdata dimensionless (0/1):            0
---------------------------
PREPROCESSING
---------------------------
Output level:                                   100
Cache-coloring (0/max_faces in color):          50
Compute/store wall distances:                   0
Number of multigrid levels:                     3
Partitioning ------------------:                -
Number of primary grid domains:                 1
Number of domains:                              1
Type of partitioning (name):                    private
Additionals -------------------:                -
Compute exact whirlflux (0/1):                  1
Compute lusgs mapping (0/1):                    1
2D offset vector (0 / x=1,y=2,z=3):             2
---------------------------------------
SOLVER->GENERAL
---------------------------------------
Convective RANS flux discretization type:       central
Order of basic equations (1/2):                 2
```

```
Order of additional equations (1/2):                    2
Increase memory (0/1):                                  1
--Timestepping Start/Stop -----------:                  -
Output period:                                          3000
Maximal time step number:                               5000
Minimum residual:                                       1e-10
Project time steps (0/1):                               1
--MG----------------------:                             -
MG description filename:                                3v
--MG-Smoothing ------------------:                      -
Residual smoother:                                      Point_explicit
Correction smoother:                                    Point_explicit
Interpolate corrections (0/1):                          0
Correction smooth epsilon:                              0.2
Residual smooth epsilon:                                0.2002
Correction smoothing steps:                             2
Residual smoothing steps:                               2
Smoothing relaxation steps:                             2
--MG Start up ------------------:                       -
SG start up steps (fine grid):                          0
Multigrid start level:                                  1
Maximal time step number (coarse grids):                50
Minimum residual (coarse grids):                        0.0001
--Monitoring -------------------:                       -
Monitor history (0/1):                                  1
Residual monitoring type (0/1):                         1
Monitor history (0/1):                                  1
--Dual time -------------------:                        -
Unsteady time stepping:                                 dual
Unsteady show pseudo time steps (0/1):                  1
Unsteady physical time step size:                       5.0e-004
Unsteady physical time steps:                           3000
Minimum number of inner iterations per time step:       50
Unsteady inner iterations per time step:                100
Unsteady implicit scheme order:                         2
Unsteady extrapolation order:                           1
Variable timestepping (0/1/2):                          0
Timestep data filename:                                 (none)
Compute DES solution(0/1):                              0
DES constant:                                           0.65
--References -------------------:                       -
Reference Mach number:                                  0.2
Reference temperature:                                  277.78
Prandtl number:                                         0.72
Gas constant gamma:                                     1.4
Gas constant R:                                         287.1
--Transport coefficients ------------:                  -
Reynolds number:                                        150
Reynolds length:                                        1
Prandtl number:                                         0.72
Sutherland constant:                                    110.4
Sutherland reference viscosity:                         1.716e-05
Sutherland reference temperature:                       273
--Geometry --------------------:                        -
Grid scale:                                             1
Reference relation area:                                0
Reference length (pitching momentum):                   1
```

```
Reference length (rolling/yawing momentum):             1
Origin coordinate x:                                    0
Origin coordinate y:                                    0
Origin coordinate z:                                    0
---------------------------------------
SOLVER->DISSIPATION: SCALAR
---------------------------------------
Central dissipation scheme:                             Scalar_dissipation
2nd order dissipation coefficient:                      0.5
Inverse 4th order dissipation coefficient:              64
---------------------------------------
SOLVER->TIME-STEPPING: RUNGE-KUTTA
---------------------------------------
Relaxation solver:                                      Runge_Kutta
Number of Runge-Kutta stages:                           3
CFL number:                                             1.0
CFL number (coarse grids):                              1.0
---------------------------------------
SOLVER->PRECONDITIONING
---------------------------------------
Preconditioning (0/1/2):                                0
Cut-off value:                                          2
---------------------------------------
SOLVER->TURBULENCE: SPALART-ALLMARAS
---------------------------------------
Monitoring values:  Residual_Max-res_X-max-res_Z-max-res_dnue/dt
              _C-lift_C-drag_C-my_Max-eddyv
Monitoring significant figures:                         4_4_4_4_4_9_9_9_4_4_4
--Turbulence ------------------:                       -
Turbulence model version:                               SAE
Turb.  Prandtl number:                                  0.9
Ratio mue-t/mue-l:                                      0.1
Maximum limit mue-t/mue-l:                              20000
Turbulent intensity:                                    0.001
Reference bl-thickness:                                 1e+22
Maximum turbulence production/destruction:              20
Turbulence equations use multigrid (0/1):               1
Positivity scheme:                                      0
EARSM expansion order:                                  1
Rotational correction (0/1):                            0
Rotational correction model:                            0
Work space for rotational correction smoother (0/1):0
Smooth rotational correction eps:                       1e-05
Number of Smoothing steps for rotcorr:                  0
---------------------------------------
EXTRA FIELD POINTDATA OUTPUT
---------------------------------------
Field output description file:                          cylinder180.para
Field output values:                                    Ptot_mach_vort_wxyz
Field output period:                                    3000
---------------------------------------
SURFACE OUTPUT
---------------------------------------
Surface output description file:                        cylinder180.para
Surface output files prefix:                            surf
Surface output values:                                  xyz_rho_cp_v_mach_vort_yplus_wxyz
Surface output period:                                  3000
```

```
---------------------------------------
TAU2PLT
---------------------------------------
Bounding Box ------------------:                    -
Volume element options -------------:               -
Volume data output (0/1):                           1
Element types for zone:                             (none)
One zone for all volume elements:                   0
Surface element options -------------:              -
Surface data output (0/1):                          1
Output Control -----------------:                   -
Output format:                                      tecplot
Ascii (0/1):                                        0
Precision :                                         9
Title of output file:                               (none)
---------------------------------------
UPDATES
---------------------------------------
```

A.3 Case 3

***Centaur* input files**

Surface parameter file (`*.sin`)

```
1              !  Output Level(0-none, 1-normal, 2-detailed)
0              !  Desired number of surface triangles (0=off)
1.8            !  Stretching ratio (1.5-2.1)
1.0            !  Scaling parameter (0.25-4.0)
F              !  Use constant spacing
35             !  Initial/Constant spacing value
70             !  Length Scale in absence of any features
1.25           !  Minimum Length scale for analytic curvature clustering
T              !  Activate interpanel curvature clustering
100.  8.       !  Angle and factor for interpanel curvature clustering
15.            !  Factor for analytic curvature clustering interior to panels
2.             !  Factor for proximity clustering
1.             !  Factor for CAD clustering
```

Prisms parameter file (`*.pin`)

```
1              !  Output Level (0-none, 1-normal, 2-detailed)
F              !  Read in prismatic gap/cavity detection file (T/F)
0.4            !  Proportion of gaps to be filled by tets (0.2 - 0.8)
0              !  No.  of passes for extending cavity area (0-4)
T              !  Automatic curve pullback activation(T/F)
100.  0.33     !  Min.  angle(degrees) at curve for activation; ratio
7.0            !  Ramp angle(deg)- growth rate on final layer (5-30)
30             !  No.  of prismatic layers to be generated (5-30)
0.005          !  Initial layer thickness (case dependent)
```

```
1.2             !  Stretching factor (1.1-1.5)
T               !  Chop prismatic layers (T/F)
0.0005          !  Minimum layer thickness (case dependent)
```

Tetrahedral parameter file (*.tin)

```
1               !  Output Level(0-none, 1-normal, 2-detailed)
F               !  Restarting (T/F)?
1.8             !  Stretching ratio (1.5-2.1)
1.1             !  Scaling parameter (0.25-4.0)
F               !  Limit maximum tetrahedral size
800             !  Maximum tet.  length scale (if limit is True)
0.5             !  Thickness matching ratio(0.-1.)
1.3             !  Tet./prism interface ratio(1.-3.)
5               !  Tet.  Grid Quality (1-lowest - 10-highest)
```

DLR Tau-Code parameter setting

```
----------------------------------------
BOUNDARY MAPPING
----------------------------------------
Markers:                                        1
Type:                                           viscous wall
Subtype:                                        turbulent
Name:                                           Surface-Fuselage
Write surface data (0/1):                       1
Monitor forces (0/1):                           1
Structured layer refinement (0/1):              0
block end
--------------
Markers:                                        2
Type:                                           farfield
Name:                                           far
Angle alpha (degree):                           0
Angle beta (degree):                            0
Vortex correction (0/1):                        0
block end
--------------
Markers:                                        3
Type:                                           symmetry plane
Name:                                           sym
Write surface data (0/1):                       1
Monitor forces (0/1):                           1
block end
--------------
Markers:                                        4
Type:                                           viscous wall
Subtype:                                        turbulent
Name:                                           FUSELNOSE
Write surface data (0/1):                       1
Monitor forces (0/1):                           1
Structured layer refinement (0/1):              0
```

```
block end
--------------
Markers:                                          5
Type:                                             viscous wall
Subtype:                                          turbulent
Name:                                             Surface-Wing
Write surface data (0/1):                         1
Monitor forces (0/1):                             1
Structured layer refinement (0/1):                0
block end
--------------
Markers:                                          6
Type:                                             viscous wall
Subtype:                                          turbulent
Name:                                             Surface-HTP
Write surface data (0/1):                         1
Monitor forces (0/1):                             1
Structured layer refinement (0/1):                0
block end
--------------
Markers:                                          7
Type:                                             viscous wall
Subtype:                                          turbulent
Name:                                             Surface-VTP
Write surface data (0/1):                         1
Monitor forces (0/1):                             1
Structured layer refinement (0/1):                0
block end
--------------
---------------------------------------
REQUIRED PARAMETERS
---------------------------------------
Boundary mapping filename:                        (thisfile)
Primary grid filename:                            dlrf12hm.tau
Reference velocity:                               70
---------------------------------------
IO
---------------------------------------
--Grid/Solution ----------------:                 -
Grid prefix:                                      dlrf12hm.dualgrid
Output files prefix:                              dlrf12hm.sol
Restart-data prefix:                              (none)
Chimera grid info filename:                       chimgridinfo
--Controls --------------------:                 -
Automatic parameter update (0/1):                 1
Write pointdata dimensionless (0/1):              0
Reference system of forces and moments (tau/ln9300):  ln9300
---------------------------------------
MOVING GRID
---------------------------------------
Type of grid movement:                            rigid
Motion description filename:                      (thisfile)
Motion hierarchy filename:                        (thisfile)
Geometric conservation law (0/1):                 0
Number of time steps per period:                  90
Evaluate forces and moments at node:              block_1
Extended motion monitoring (0/1):                 1
```

```
Initialize deformation (0/1):                          0
Flutter parameters description filename:               (none)
Extern motion filename:                                (none)
Node name:                                             block_1
Node reference frame:                                  inertial
Node controls grid block:                              1
Node motion description id:                            block_1
hdf end
-------------------------
Motion description id:                                 block_1
Type of movement:                                      periodic
Degree of polynomial for rotation:                     1
Origin of local coordinate system:                     1.048816832 0.0 -0.030285319
Degree of Fourier series for rotation:                 1
Reduced frequency for rotation:                        0 0.0680267 0
Reduced frequency reference length:                    0.252625 0.252625 0.252625
Fourier coefficients for rotation (cos) pitch:  0.0 0.0
Fourier coefficients for rotation (sin) pitch:  0.0 4.5
mdf end
-------------------------
---------------------------------------
PREPROCESSING
---------------------------------------
Read partitioning filename:                            (none)
Write graph filename:                                  (none)
Preprocessing for incompressible solver (0/1):  0
Number of blocks:                                      1
Cache-coloring (0/max_faces in color):                 200000
Number of multigrid levels:                            3
Point fusing reward:                                   1.2
Structured grid coarsening:                            0
Sharp edge angle (degrees):                            0
--Partitioning -----------------:                      -
Number of primary grid domains:                        24
Number of domains:                                     24
Type of partitioning (name):                           private
--Additionals ------------------:                      -
2D offset vector (0 / x=1,y=2,z=3):                    0
Compute exact whirlflux (0/1):                         1
Compute exact surface(0/1):                            1
Bandwidth optimisation (0/1):                          0
Compute/store wall distances:                          50
Control volume edge weight (0/1):                      1
Change boundary control volumes (0/1):                 0
Output level:                                          5
Parameter-Update:                                      1
Compute DES scale(0/1):                                0
Periodic translation vector:                           0 0 0
Periodic angle:                                        0
Periodic epsilon value:                                1e-2
--Extensions -------------------:                      -
Preprocessing for incompressible solver (0/1):  0
Correct metric for boundary control volumes (0/1):  0
Project boundary control volumes coordinates (0/1):0
Translation factor for shifted boundary points:  1
Compute parent faces (0/1):                            0
---------------------------------------
```

```
SOLVER->GENERAL
---------------------------------------
--Viscous --------------------:                  -
Viscous calculation (0/1):                       1
--Flux---------------------:                     -
Convective RANS flux discretization type:        central
Order of basic equations (1/2):                  2
Order of additional equations (1/2):             2
Increase memory (0/1):                           1
Fix negative values (0/1):                       0
Viscous flux type TSL/Full (0/1):                1
Hold static velocity field (0/1):                0
Set mixed upwind/central inviscid fluxes (0/1):  0
Compute exact whirlflux (0/1):                   0
--Limiter --------------------:                  -
Limiter freezing convergence:                    0
--Timestepping Start/Stop -----------:           -
Output period:                                   180
Maximal time step number:                        5000
Minimum residual:                                1e-10
Project time steps (0/1):                        1
Accumulate queue time (0/1):                     0
Matching period:                                 150
--MG----------------------:                      -
MG description filename:                         3v
--MG-Smoothing -----------------:                -
Residual smoother:                               Point_explicit
Correction smoother:                             Point_explicit
Interpolate corrections (0/1):                   0
Correction smooth epsilon:                       0.2
Residual smooth epsilon:                         0.2002
Correction smoothing steps:                      2
Residual smoothing steps:                        2
Smoothing relaxation steps:                      2
No smoothing near shocks (0/1):                  0
--MG Start up -----------------:                 -
SG start up steps (fine grid):                   250
Multigrid start level:                           1
Maximal time step number (coarse grids):         50
Minimum residual (coarse grids):                 0.0001
--Monitoring -------------------:                -
Monitor history (0/1):                           1
Residual monitoring type (0/1):                  0
--References -------------------:                -
Reference velocity:                              70
Reference temperature:                           293.15
Prandtl number:                                  0.72
Gas constant gamma:                              1.4
Gas constant R:                                  287
--Transport coefficients ------------:           -
Reynolds number:                                 1.1866e+6
Reynolds length:                                 0.252625
Prandtl number:                                  0.72
Gas constant gamma:                              1.4
Sutherland constant:                             110.4
Sutherland reference viscosity:                  1.716e-05
Sutherland reference temperature:                293.15
```

```
--Geometry -------------------:                          -
Grid scale:                                              1
Reference relation area:                                 0.22207
Reference length (pitching momentum):                    0.252625
Reference length (rolling/yawing momentum):              0.252625
Origin coordinate x:                                     1.048816832
Origin coordinate y:                                     0
Origin coordinate z:                                     -0.030285319
---------------------------------------
SOLVER->DISSIPATION: MATRIX
---------------------------------------
Central dissipation scheme:                              Matrix_dissipation
Matrix dissipation terms coefficient:                    1
Minimum artificial dissipation for acoustic waves:  0.2
Minimum artificial dissipation for velocity:  0.2
Reconstruction of gradients:                             Green_Gauss
---------------------------------------
SOLVER->TIME-STEPPING: DUAL TIME
---------------------------------------
--Dual time -------------------:                         -
Unsteady time stepping:                                  dual
Unsteady show pseudo time steps (0/1):                   1
Unsteady physical time steps:                            23
Minimum number of inner iterations per time step:  50
Unsteady inner iterations per time step:                 600
Unsteady implicit scheme order:                          2
Unsteady extrapolation order:                            1
Variable timestepping (0/1/2):                           0
Timestep data filename:                                  (none)
Compute DES solution(0/1):                               0
DES constant:                                            0.65
Unsteady residual type (0/1):                            1
---------------------------------------
SOLVER->TIME-STEPPING: RUNGE-KUTTA
---------------------------------------
Relaxation solver:                                       Runge_Kutta
Number of Runge-Kutta stages:                            3
CFL number:                                              1.0
CFL number (coarse grids):                               1.0
---------------------------------------
SOLVER->PRECONDITIONING
---------------------------------------
Preconditioning (0/1/2):                                 0
Cut-off value:                                           2
---------------------------------------
SOLVER->TURBULENCE: SPALART-ALLMARAS
---------------------------------------
Monitoring values:  Residual_Max-res_X-max-res_Y-max-res_Z-max-res_dnue/dt
             _T/tperiod_C-drag_C-lift_C-my_Fx_Fy_Fz_Mx_My_Mz_Phi_Psi_Xi_Angle-a
--Turbulence ------------------:                         -
Turbulence model version:                                SAE
Turb.  Prandtl number:                                   0.9
Ratio mue-t/mue-l:                                       0.1
Maximum limit mue-t/mue-l:                               20000
Turbulent intensity:                                     0.001
Reference bl-thickness:                                  1e+22
Maximum turbulence production/destruction:               20
```

```
Turbulence equations use multigrid (0/1):                1
Positivity scheme:                                       0
EARSM expansion order:                                   1
Rotational correction (0/1):                             0
Rotational correction model:                             0
Work space for rotational correction smoother (0/1):  0
Smooth rotational correction eps:                        1e-05
Number of Smoothing steps for rotcorr:                   0
---------------------------------------
EXTRA FIELD POINTDATA OUTPUT
---------------------------------------
Field output description file:                           (thisfile)
Field output values:                                     cp_mach_vort_xyzgeod_Ptot
             _cf_yplus
Field output period:                                     180
---------------------------------------
SURFACE OUTPUT
---------------------------------------
Surface output description file:                         (thisfile)
Surface output values:                                   xyz_vxyzaero_xyzgeod_rho_p
             _cp_Ptot_cf_cfxyz_yplus
Surface output period:                                   180
---------------------------------------
CUT PLANE OUTPUT
---------------------------------------
Plane output description file:                           (thisfile)
Plane output values:                                     xyz_rho_p_cp_Ptot
Plane output period:                                     180
Number of planes:                                        3
Boundary type (euler/ns):                                ns
Plane support x:                                         0 0 0
Plane support y:                                         0.01 0.1712 0.4578
Plane support z:                                         0 0 0
Plane normal x:                                          0 0 0
Plane normal y:                                          1 1 1
Plane normal z:                                          0 0 0
---------------------------------------
TAU2PLT
---------------------------------------
--Output Control ----------------:                       -
Output format:                                           tecplot
Ascii (0/1):                                             0
Precision :                                              9
Title of output file:                                    (none)
---------------------------------------
UPDATES
---------------------------------------
```

A.4 Case 4

***Centaur* input files propeller-spinner block**

Surface parameter file (`*.sin`)

```
2               !  Output Level(0-none, 1-normal, 2-detailed)
0               !  Desired number of surface triangles (0=off)
1.8             !  Stretching ratio (1.5-2.1)
1.0             !  Scaling parameter (0.25-4.0)
F               !  Use constant spacing
4.68277         !  Initial/Constant spacing value
9.36553         !  Length Scale in absence of any features
0.05            !  Minimum Length scale for curvature clustering
T               !  Activate interpanel curvature clustering
100.  8.        !  Angle and factor for interpanel curvature clustering
36.             !  Factor for curvature clustering interior to panels
2.              !  Factor for proximity clustering
2.              !  Factor for CAD clustering
```

Prisms parameter file (`*.pin`)

```
2               !  Output Level (0-none, 1-normal, 2-detailed)
F               !  Read in prismatic gap/cavity detection file (T/F)
0.4             !  Proportion of gaps to be filled by tets (0.2 - 0.8)
0               !  No.  of passes for extending cavity area (0-4)
T               !  Automatic curve pullback activation(T/F)
100.  0.33      !  Min.  angle(degrees) at curve for activation; ratio
20.0            !  Ramp angle(deg)- growth rate on final layer (5-30)
25              !  No.  of prismatic layers to be generated (5-30)
0.0025          !  Initial marching step (case dependent)
1.275           !  Stretching factor (1.1-1.5)
T               !  Chop prismatic layers (T/F)
0.001           !  Minimum nominal marching step (case dependent)
```

Tetrahedral parameter file (`*.tin`)

```
2               !  Output Level(0-none, 1-normal, 2-detailed)
F               !  Restarting (T/F)?
2.0             !  Stretching ratio (1.5-2.1)
0.85            !  Scaling parameter (0.25-4.0)
F               !  Limit maximum tetrahedral size
98.1738         !  Maximum tet.  length scale (if limit is True)
0.85            !  Thickness matching ratio(0.-1.)
1.6             !  Tet./prism interface ratio(1.-3.)
5               !  Tet.  Grid Quality (1-lowest - 10-highest)
```

***Centaur* input files wing-nacelle block**

Surface parameter file (`*.sin`)

```
2               !  Output Level(0-none, 1-normal, 2-detailed)
```

```
0               !  Desired number of surface triangles (0=off)
1.8             !  Stretching ratio (1.5-2.1)
1.0             !  Scaling parameter (0.25-4.0)
F               !  Use constant spacing
9.57403         !  Initial/Constant spacing value
19.1481         !  Length Scale in absence of any features
0.398918        !  Minimum Length scale for analytic curvature clustering
T               !  Activate interpanel curvature clustering
100.  8.        !  Angle and factor for interpanel curvature clustering
40.             !  Factor for curvature clustering interior to panels
2.              !  Factor for proximity clustering
2.              !  Factor for CAD clustering
```

Prisms parameter file (*.pin)

```
2               !  Output Level (0-none, 1-normal, 2-detailed)
F               !  Read in prismatic gap/cavity detection file (T/F)
0.4             !  Proportion of gaps to be filled by tets (0.2 - 0.8)
0               !  No.  of passes for extending cavity area (0-4)
T               !  Automatic curve pullback activation(T/F)
100.  0.33      !  Min.  angle(degrees) at curve for activation; ratio
20.0            !  Ramp angle(deg)- growth rate on final layer (5-30)
25              !  No.  of prismatic layers to be generated (5-30)
0.01            !  Initial marching step (case dependent)
1.3             !  Stretching factor (1.1-1.5)
T               !  Chop prismatic layers (T/F)
0.001           !  Minimum nominal marching step (case dependent)
```

Tetrahedral parameter file (*.tin)

```
2               !  Output Level(0-none, 1-normal, 2-detailed)
F               !  Restarting (T/F)?
2.0             !  Stretching ratio (1.5-2.1)
0.85            !  Scaling parameter (0.25-4.0)
F               !  Limit maximum tetrahedral size
7853.66         !  Maximum tet.  length scale (if limit is True)
0.85            !  Thickness matching ratio(0.-1.)
1.6             !  Tet./prism interface ratio(1.-3.)
5               !  Tet.  Grid Quality (1-lowest - 10-highest)
```

DLR Tau-Code parameter setting

```
----------------------------------------
BOUNDARY MAPPING BLOCK 1:  Farfield
----------------------------------------
Markers:                                        2,3,4
Chimera block:                                  1
Type:                                           farfield
Name:                                           farfield
Angle alpha (degree):                           10
```

```
Angle beta (degree):                    0
Vortex correction (0/1):                0
Chord length:                           1
Temperature :                           276.53
Mach number :                           0.15
block end
-------------------------
Markers:                                5, 6, 7, 8, 9
Chimera block:                          1
Type:                                   chimera
Name:                                   nacelle_chimera
block end
-------------------------
Markers:                                10
Chimera block:                          1
Type:                                   viscous wall
Subtype:                                turbulent
Name:                                   nacelle_endwall
Write surface data (0/1):               1
Cutting plane allowed (0/1):            0
Monitor forces (0/1):                   0
block end
-------------------------
Markers:                                11
Chimera block:                          1
Type:                                   viscous wall
Subtype:                                turbulent
Name:                                   nacelle
Write surface data (0/1):               1
Cutting plane allowed (0/1):            0
Monitor forces (0/1):                   0
block end
-------------------------
Markers:                                12
Chimera block:                          1
Type:                                   viscous wall
Subtype:                                turbulent
Name:                                   nacelle_endplane
Write surface data (0/1):               1
Cutting plane allowed (0/1):            0
Monitor forces (0/1):                   0
block end
-------------------------
Markers:                                13
Type:                                   viscous wall
Subtype:                                turbulent
Name:                                   wing_te
Write surface data (0/1):               1
Cutting plane allowed (0/1):            0
Monitor forces (0/1):                   0
block end
--------------
Markers:                                14
Type:                                   viscous wall
Subtype:                                turbulent
Name:                                   wing_ps
Write surface data (0/1):               1
```

```
Cutting plane allowed (0/1):                    0
Monitor forces (0/1):                           0
block end
--------------
Markers:                                        15
Type:                                           viscous wall
Subtype:                                        turbulent
Name:                                           wing_le
Write surface data (0/1):                       1
Cutting plane allowed (0/1):                    0
Monitor forces (0/1):                           0
block end
--------------
Markers:                                        16
Type:                                           viscous wall
Subtype:                                        turbulent
Name:                                           wing_ss
Write surface data (0/1):                       1
Cutting plane allowed (0/1):                    0
Monitor forces (0/1):                           0
block end
--------------
Markers:                                        17
Type:                                           viscous wall
Subtype:                                        turbulent
Name:                                           wing_tip
Write surface data (0/1):                       1
Cutting plane allowed (0/1):                    0
Monitor forces (0/1):                           0
block end
--------------
---------------------------------------
BOUNDARY MAPPING BLOCK 2:  Prop
---------------------------------------
Markers:                                        18, 19, 20
Chimera block:                                  2
Type:                                           chimera
Name:                                           prop_chimera
block end
-------------------------
Markers:                                        21
Type:                                           viscous wall
Subtype:                                        turbulent
Name:                                           spinner
Write surface data (0/1):                       1
Cutting plane allowed (0/1):                    0
Monitor forces (0/1):                           1
block end
--------------
Markers:                                        22
Type:                                           viscous wall
Subtype:                                        turbulent
Name:                                           spinner_endwall
Write surface data (0/1):                       1
Cutting plane allowed (0/1):                    0
Monitor forces (0/1):                           1
block end
```

```
--------------
Markers:                                23
Type:                                   viscous wall
Subtype:                                turbulent
Name:                                   bld_te_r
Write surface data (0/1):               1
Cutting plane allowed (0/1):            0
Monitor forces (0/1):                   1
block end
--------------
Markers:                                24
Type:                                   viscous wall
Subtype:                                turbulent
Name:                                   bld_te_m
Write surface data (0/1):               1
Cutting plane allowed (0/1):            0
Monitor forces (0/1):                   1
block end
--------------
Markers:                                25
Type:                                   viscous wall
Subtype:                                turbulent
Name:                                   bld_te_t
Write surface data (0/1):               1
Cutting plane allowed (0/1):            0
Monitor forces (0/1):                   1
block end
--------------
Markers:                                26
Type:                                   viscous wall
Subtype:                                turbulent
Name:                                   bld_ps
Write surface data (0/1):               1
Cutting plane allowed (0/1):            0
Monitor forces (0/1):                   1
block end
--------------
Markers:                                27
Type:                                   viscous wall
Subtype:                                turbulent
Name:                                   bld_le_r
Write surface data (0/1):               1
Cutting plane allowed (0/1):            0
Monitor forces (0/1):                   1
block end
--------------
Markers:                                28
Type:                                   viscous wall
Subtype:                                turbulent
Name:                                   bld_le_m
Write surface data (0/1):               1
Cutting plane allowed (0/1):            0
Monitor forces (0/1):                   1
block end
--------------
Markers:                                29
Type:                                   viscous wall
```

```
Subtype:                                    turbulent
Name:                                       bld_le_t
Write surface data (0/1):                   1
Cutting plane allowed (0/1):                0
Monitor forces (0/1):                       1
block end
--------------
Markers:                                    30
Type:                                       viscous wall
Subtype:                                    turbulent
Name:                                       bld_ss
Write surface data (0/1):                   1
Cutting plane allowed (0/1):                0
Monitor forces (0/1):                       1
block end
--------------
Markers:                                    31
Type:                                       viscous wall
Subtype:                                    turbulent
Name:                                       bld_tip
Write surface data (0/1):                   1
Cutting plane allowed (0/1):                0
Monitor forces (0/1):                       1
block end
--------------
---------------------------------------
REQUIRED PARAMETERS
---------------------------------------
Boundary mapping filename:                  agardprop.para
Primary grid filename:                      agardprop.tau
Reference Mach number:                      0.15
---------------------------------------
IO
---------------------------------------
--Grid/Solution ----------------:           -
Grid prefix:                                agardprop.dualgrid
Output files prefix:                        agardprop.sol
Restart-data prefix:                        (none)
Chimera grid info filename:                 chimgridinfo
--Controls -------------------:             -
Automatic parameter update (0/1):           1
Write pointdata dimensionless (0/1):        0
---------------------------------------
MOVING GRID
---------------------------------------
Type of grid movement:                      rigid
Motion description filename:                (thisfile)
Motion hierarchy filename:                  (thisfile)
Geometric conservation law (0/1):           0
Number of time steps per period:            90
Evaluate forces and moments at node:        block_2
Extended motion monitoring (0/1):           1
Node name:                                  block_1
Node reference frame:                       inertial
Node controls grid block:                   1
Node motion description id:                 block_1
hdf end
```

```
-------------------------
Node name:                                    block_2
Node reference frame:                         block_1
Node controls grid block:                     2
Node motion description id:                   block_2
hdf end
-------------------------
Motion description id:                        block_1
Type of movement:                             static
Origin of local coordinate system:            0.0 0.0 0.0
Degree of polynomial for rotation:            0
Polynomial coefficients for rotation roll:    0 0
mdf end
-------------------------
Motion description id:                        block_2
Type of movement:                             rotate
Degree of polynomial for rotation:            1
Origin of local coordinate system:            0.0 0.0 0.0
Hinge - specify vector:                       -1 0 0
Hinge - reduced frequency for rotation:       8.913799989847377101
Hinge - reduced frequency reference length:   0.64
mdf end
-------------------------
---------------------------------------
PREPROCESSING
---------------------------------------
Output level:                                 50
Cache-coloring (0/max_faces in color):        200000
Compute/store wall distances:                 0
Number of multigrid levels:                   3
--Partitioning -----------------:             -
Number of primary grid domains:               96
Number of domains:                            96
Type of partitioning (name):                  private
--Additionals ------------------:             -
2D offset vector (0 / x=1,y=2,z=3):           0
Compute exact whirlflux (0/1):                1
Compute exact surface(0/1):                   1
Bandwidth optimisation (0/1):                 0
---------------------------------------
SOLVER->GENERAL
---------------------------------------
Convective RANS flux discretization type:     central
Order of basic equations (1/2):               2
Order of additional equations (1/2):          2
Increase memory (0/1):                        1
--Timestepping Start/Stop -----------:        -
Output period:                                45
Maximal time step number:                     3000
Minimum residual:                             1e-10
Project time steps (0/1):                     1
Accumulate queue time (0/1):                  0
--MG----------------------:                   -
MG description filename:                      3v
--MG-Smoothing -----------------:             -
Residual smoother:                            Point_explicit
Correction smoother:                          Point_explicit
```

```
Interpolate corrections (0/1):                          0
Correction smooth epsilon:                              0.2
Residual smooth epsilon:                                0.2002
Correction smoothing steps:                             2
Residual smoothing steps:                               2
Smoothing relaxation steps:                             2
--MG Start up -----------------:                        -
SG start up steps (fine grid):                          250
Multigrid start level:                                  1
Maximal time step number (coarse grids):                50
Minimum residual (coarse grids):                        0.0001
--Monitoring ------------------:                        -
Monitor history (0/1):                                  1
Residual monitoring type (0/1):                         1
Monitor history (0/1):                                  1
--References ------------------:                        -
Reference Mach number:                                  0.15
Reference temperature:                                  276.53
Prandtl number:                                         0.72
Gas constant gamma:                                     1.4
--Transport coefficients ------------:                  -
Reynolds number:                                        1.7e6
Reynolds length:                                        0.5
Prandtl number:                                         0.72
Gas constant gamma:                                     1.4
Sutherland constant:                                    110.4
Sutherland reference viscosity:                         1.7647e-05
Sutherland reference temperature:                       276.53
--Geometry --------------------:                        -
Grid scale:                                             1
Reference relation area:                                1
Reference length (pitching momentum):                   1
Reference length (rolling/yawing momentum):             1
Origin coordinate x:                                    0
Origin coordinate y:                                    0
Origin coordinate z:                                    0
---------------------------------------
SOLVER->DISSIPATION: MATRIX
---------------------------------------
Central dissipation scheme:                             Matrix_dissipation
Matrix dissipation terms coefficient:                   1
Minimum artificial dissipation for acoustic waves:      0.33
Minimum artificial dissipation for velocity:            0.33
Reconstruction of gradients:                            Green_Gauss
---------------------------------------
SOLVER->TIME-STEPPING: DUAL TIME
---------------------------------------
--Dual time -------------------:                        -
Unsteady time stepping:                                 dual
Unsteady show pseudo time steps (0/1):                  1
Unsteady physical time steps:                           45
Minimum number of inner iterations per time step:       50
Unsteady inner iterations per time step:                300
Unsteady implicit scheme order:                         2
Unsteady extrapolation order:                           1
Variable timestepping (0/1/2):                          0
Timestep data filename:                                 (none)
```

```
Compute DES solution(0/1):                              0
DES constant:                                           0.65
---------------------------------------
SOLVER->TIME-STEPPING: RUNGE-KUTTA
---------------------------------------
Relaxation solver:                                      Runge_Kutta
Number of Runge-Kutta stages:                           3
CFL number:                                             1.2
CFL number (coarse grids):                              1.2
---------------------------------------
SOLVER->PRECONDITIONING
---------------------------------------
Preconditioning (0/1/2):                                0
Cut-off value:                                          2
---------------------------------------
SOLVER->TURBULENCE: SPALART-ALLMARAS
---------------------------------------
Monitoring values:  Residual_Max-res_X-max-res_Y-max-res_Z-max-res_dnue/dt_C-lift
              _C-drag_C-sidef_C-mx_C-my_C-mz_Max-y+_Max-eddyv_Fx_Fy_Fz
Monitoring significant figures:                         4_4_4_4_4_4_9_9_9_9_9_4_4_9_9_9
--Turbulence ------------------:                       -
Turbulence model version:                               SAE
Turb.  Prandtl number:                                  0.9
Ratio mue-t/mue-l:                                      0.1
Maximum limit mue-t/mue-l:                              20000
Turbulent intensity:                                    0.001
Reference bl-thickness:                                 1e+22
Maximum turbulence production/destruction:              20
Turbulence equations use multigrid (0/1):               1
Positivity scheme:                                      0
EARSM expansion order:                                  1
Rotational correction (0/1):                            0
Rotational correction model:                            0
Work space for rotational correction smoother (0/1):    0
Smooth rotational correction eps:                       1e-05
Number of Smoothing steps for rotcorr:                  0
---------------------------------------
EXTRA FIELD POINTDATA OUTPUT
---------------------------------------
Field output description file:                          agardprop.para
Field output values:  gidx_xyz_rho_v_p_cp_mach_Ptot_yplus_xyzgeod_vxyzgeod
              _wxyz_vxyzmoving
Field output period:                                    45
---------------------------------------
SURFACE OUTPUT
---------------------------------------
Surface output description file:                        agardprop.para
Surface output values:  gidx_xyz_rho_v_p_cp_temp_mach_Ptot_cf_cfxyz_yplus_xyzgeod
              _vxyzgeod_wxyz_vxyzmoving_cfxyzgeod
Surface output period:                                  45
---------------------------------------
TAU2PLT
---------------------------------------
--Volume element options ------------:                 -
Volume data output (0/1):                               1
Element types for zone:                                 (none)
One zone for all volume elements:                       0
```

```
Specify tetrahedral list:                          (none)
Specify phyramide list:                            (none)
Specify prism list:                                (none)
Specify hexaeder list:                             (none)
--Surface element options ------------:            -
Surface data output (0/1):                         1
Create surface zone for surface element:           (none)
Create one boundary:                               0
Create surface zone for triangular elements:       (none)
Create surface zone for quadrilateral elements:    (none)
--Output Control ----------------:                  -
Output format:                                     tecplot
Ascii (0/1):                                       0
Precision :                                        9
Title of output file:                              (none)
---------------------------------------
UPDATES
---------------------------------------
```